# THE EFFECTS OF PROCESS PARAMETERS ON THE PROPERTIES OF RESIN TRANSFER MOLDED COMPOSITES

by

Robert John Demaree

Thesis submitted to the Faculty of the

Virginia Polytechnic Institute and State University

in partial fulfillment of the requirements for the degree of

MASTER OF SCIENCE

in

Materials Science and Engineering

APPROVED:

Dr. Alfred C. Loos, Chairman

Dr. Ronald G. Kander

Dr. Brian J. Love

January, 1996
Blacksburg, Virginia

# THE EFFECTS OF PROCESS PARAMETERS ON THE PROPERTIES OF RESIN TRANSFER MOLDED COMPOSITES

by
Robert John Demaree

Dr. Alfred C. Loos, Chairman
Department of Materials Science and Engineering

(ABSTRACT)

A series of composite panels were fabricated by resin transfer molding (RTM), varying materials and process conditions. Reinforcements used included a fiberglass woven material, and AS-4 carbon in both sized and unsized plain weave fabrics. Vinyl ester, epoxy, and cyanate ester resins were pressure injected into these fabrics. The epoxy panels were processed with varying injection temperatures and pressures.

A density based technique was used to measure the fiber volume fraction and void content of the composite panels. Optical photomicrographs were used to verify the accuracy of the void calculations. Mechanical tests included compression strength, inplane and interlaminar shear strengths, and impact. Compression after impact tests were performed and compared to undamaged compression strengths.

The compression, inplane shear, and interlaminar shear strengths of the epoxy composites were higher than the vinyl ester composites. Similarly, cyanate ester systems with similar reinforcements outperformed the epoxy composites in these tests. In impact testing, the graphite fabric/ epoxy resin composite retained the lowest portion of original strength after impact. The cyante esters retained the most strength, but vinyl ester

composites suffered less damage. Vinyl ester composites made with unsized carbon fibers performed better in interlaminar shear, and in impact tests, than those with sized fibers. The variation of injection temperature had little effect on either void content or strength of the epoxy composites. Increases in injection pressure did produce a higher void content in epoxy laminates, but no significant change in strength was observed.

# Acknowledgements

The author would like to thank Dr. A. C. Loos, committee chairman, for his patience, support and perseverance, throughout the graduate program, but particularly in the last two months. Thanks are also due to the committee members, Dr. R. G. Kander and Dr. B. J. Love, for much patience and support over the past two years.

This research was supported by the National Science Foundation, Science and Technology Center for High Performance Adhesives and Composites, and by McDonnell Douglas Aerospace under the Affordable Polymeric Composite Materials Synthesis and Processing Program. This financial support was greatly appreciated.

In addition to those previously mentioned, the author would like to acknowledge the support and advice of several persons whose assistance was invaluable. Thanks are due to A. V. Rau for help with processing of panels and development of the test matrix. K. E. Verghese provided assistance with equipment and processing. The author would also like to thank Dr. W. P. H. Tsang for his help in running many of the mechanical tests, and B. Simonds for help with the others.

Finally, the author would like to thank his family and friends who provided incredible support and encouragement during this ordeal.

# Table of Contents

# List of Figures

# List of Tables

# Chapter 1: Introduction

## 1.1 Introduction to RTM

In recent years, mounting concerns of production speed and cost have led to a tremendous interest in low cost, highly automated production processes such as resin transfer molding (RTM) for the manufacture of fiber-reinforced composites. RTM is a process where a dry fiber preform, contained in a sealed mold, is injected with resin under pressure and consolidated in the mold. The preform can be assembled ahead of time from a variety of stacked, stitched or woven fibers. These preforms can be manufactured automatically on a large scale. A small amount of human labor is then required to prepare and load the mold for injection. Development of RTM has opened areas of opportunity for structural applications previously reserved for autoclave-cured prepreg composites. Advances in weaving and braiding have led to composites utilizing more types of fibers, with lower porosities. As a result, a good understanding of materials selection and process parameter effects on RTM is critical in the production of a quality part. For example, a proven RTM process for a fiberglass composite with a given resin system can be inadequate for use on a similar graphite part. Also, higher structural loading in graphite parts makes the elimination of voids more critical.

Resin transfer molding is by no means a new process. RTM has been used for many years to produce high-volume, very low cost composites. Traditionally, these structures are made with low-cost fiberglass matte or coarse-weave rovings. Fiber volume fractions were typically very low compared to autoclave-cured tapes, between 10-30 per cent. Injection would usually be accomplished with inexpensive unsaturated polyester resins. The resulting parts were commonly used for nonstructural or lightly loaded applications at or near room temperature. As such, a complete understanding of the process was not essential. A very narrow range of materials were in use, and for most applications, a certain void content was considered tolerable. High preform permeabilities made injection quick, and the resins would cure with little or no temperature elevation.

Recently, RTM has expanded into new arenas. Many contractors are considering resin transfer molding for aircraft primary and secondary structures. Emphasis is shifting from glass to higher modulus graphite fibers. At the same time, volume fractions from RTM are increasing to levels competitive with autoclave composites, often as high as 60 per cent or above. Preform designers are also adding more stitching and layer-to-layer reinforcements to fulfill demands for more automated processes and higher interlaminar strength. The major effect of these changes is a drastic change in permeability. The preform permeabilities are generally much lower, but now also depend very much on direction and microstructure (stitches, etc.) Traditional low-cost resins used for RTM lack performance at high temperatures, or are more susceptible to environmental factors.

Some manufacturers wish to use high-performance or special purpose resins for RTM. Many of these resins are highly viscous or even solid at room temperature, so they must be heated for injection. Injection of some resins into dense preforms may cause voids and large air pockets. The type of resin, type and form of reinforcement, and injection parameters can affect the quality and speed with which a composite can be infiltrated. **(1)**

## 1.2 Related Research

Carroll and Cochran **(2)** looked at panels made from woven fiberglass and epoxy at differing fiber volume fractions, $v_f$. Panels were made at 51%, 56%, and 68% volume fractions, and specimens from these panels subjected to compression, tension, and interlaminar shear testing. Tensile strength increased with volume fraction as would be expected, but compression strength showed almost no change with increasing volume fraction. Interlaminar shear strengths increased slightly with the increasing $v_f$, but this change was within the experimental variance. Normalizing the data with respect to fiber volume fraction distorted the results. Optical micrograph studies of the three panels also indicated a higher concentration of voids in the high volume fraction panels. The voids were also much larger in the 56% and 68% panels than in the 51% panel.

The void content of a particular composite specimen is of paramount interest in resin transfer molding. Voids of varying sizes can be formed during resin infiltration, due to uneven flow through the preform or mechanical entrapment of bubbles in the resin. Voids in the finished composite can normally be classified either as microvoids or macrovoids. Microvoids are small air pockets which exist in the tow, between individual fibers. Larger macrovoids generally form outside the fiber bundle, and can be of considerable size, even visible with the naked eye. These larger voids often form in a layer at the ply interface.

Several methods have been employed to measure voids in a composite. By and large these involve direct visual measurement of void area on a cross section. Aside from manual analysis of photomicrographs, several image analysis techniques have been developed to increase speed and accuracy of these measurements. **(3) (4)** Haque et al. were able to use ultrasonic C-scan to detect and measure voids **(5)**, while Ghiorse **(6)** used both image analysis and acid digestion. For this investigation, a density-based approach, similar to ASTM D2734 - 91 **(7)**, has been used. This approach considers the differences between measured and apparent fiber volume fractions, and will be discussed in detail in Chapter 2.

Void content has been shown to affect the matrix-dominated performance of graphite and fiberglass composites. A study conducted by Ghiorse **(6)** looked at the variation of interlaminar shear strength (short beam shear) and four point flexural strength of graphite/ epoxy composites having void contents up to 5%. The interlaminar

shear strength decreased with increasing void volume. A similar, though less pronounced, drop in flexural strength and modulus was noted across the range of void volumes. Flexural properties also suffered more scatter than the short beam shear results. These results clearly show the effect of voids on composite performance. However, this study was conducted on prepreg tape composites, and the methods of varying void volume were not reported. More void performance data must be gathered on composites made by resin transfer molding.

Haque et al. **(5)** performed mechanical tests on graphite/ epoxy RTM laminates having differing void contents. Comparing a nearly void-free panel with a panel containing 5% voids, a reduction in compression strength of about 35% was observed, while tensile strength changed by less than 10%. Interlaminar shear was also shown to be more susceptible to voids than in-plane shear strengths. In fact, in-plane shear properties changed by only 6% between the void-free and the high void panels, while interlaminar shear strength suffered about a 25% drop.

Some researchers have developed methods to reduce or remove voids from RTM injections. Hwang et al. **(8)** developed a two step RTM injection scheme to help reduce mechanical entrapment. Injections were carried out using vinyl ester resin and a woven fiberglass cloth. The mold was originally set to provide a very low volume fraction, about 38%. Resin is injected under vacuum assistance (fully evacuated mold) and flows smoothly through the preform. When a predetermined weight of resin has been injected, the ports are closed and the mold compacted to the desired final volume fraction. The

final volume is equal to the combined calculated volumes of the preform and resin. The resulting panels should have a low void content.

Another approach is suggested by Stabler et al. **(9)** In their investigation of carbon/epoxy injection, they found that properly degassing the resin before infiltration will reduce the final void volume significantly. They also performed tests in which the mold was vibrated at a controlled frequency during infiltration. With use of the proper frequency, this vibration was seen to dislodge mechanically trapped air and wash away bubbles.

The engineer working in RTM today has an intrinsic need to understand the factors affecting the outcome of resin injection. The success of any RTM injection can vary by changing the resin temperature, injection pressure, or by altering some element of the injection scheme, such as the addition of vacuum assistance. High fiber volume fraction preforms used today are difficult to infiltrate. The resin must have a low enough viscosity to fully impregnate the part, but must have the necessary cured properties to maintain the designed strength. High performance resins can be heated to reduce their viscosity, but may gel before full infiltration if injection temperature is not carefully selected. Heating the resin may also speed up infiltration times, but the effect of temperature on part quality is not well understood. In addition, some resins may not spread on some fiber types. In modern stitched preforms, which may contain carbon, glass, and Kevlar fibers, this can be a very important consideration.

Good flow through a fiber preform requires a reasonable surface compatibility

between fiber and resin. This can be a problem when using vinyl ester resins, a type originally developed to be used with fiberglass, with high strength carbon fibers. A number of researchers have studied the effects of fiber and sizing on resin flow. Palmese and Karbhari **(10)** looked at the flow of Derakane 411-C50 resin through a long, thin glass tube containing carbon fiber tows. The resin was pumped into the tube by a pressure pot under a pressure of 20 psig. Both sized and unsized AS-4 fibers were used, and the volumetric flow rate was calculated from the mass flow rate, measured by weighing resin exiting the far end of the tube. Results of tests conducted at several fiber volume fractions indicated that microflow through the unsized tows was significantly higher than flow through sized fiber tows.

Another study by Dahlbäck and Lundström **(11)** looked at transient resin spreading on fiber bundles. Their study used several E-glass, S-glass, and carbon fibers, with epoxy and vinyl ester resins. A drop of liquid was placed on a fiber bundle and allowed to spread. A video camera and computer analyzer measured the drop's height, width and contact angle over time. Their results show that vinyl ester spreads more quickly on the glass fibers, particularly E-glass, than on carbon fibers. The vinyl ester also spreads more slowly on carbon than the epoxy.

The geometry of an injection can have a large effect on the final quality of an RTM part. Even in the manufacture of a flat plate, port location can affect void content and fill time immensely. In flat panels, one of four injection schemes is commonly used. Line-to-line injection is often considered to be the simplest method, with resin flowing

under pressure from a fill channel on one side of the part to an exit channel on the far side. In theory, a one-dimensional flow front will result, with the front location following D'arcy's Law. In practice, however, the flow next to the wall will proceed toward the exit vent more quickly than that in the center, a phenomenon known as "channeling". Large voids can easily develop in the center of the preform. Some researchers have developed computer simulations to model this edge flow. Hammani et al. **(12)** modeled a thin gap between the preform edge and the mold wall, leading to preferential flow. By varying parameters such as the width of this gap and varying transverse flow, the model was fit to experimental results. Leek et al. (**13**) prepared a model which assumes such a gap in only a few plies, giving the preform nearest the wall a lower volume fraction. Both researchers back up their models with visually measured results by infiltrating a fiberglass preform with oil or some other nonreactive liquid.

The remaining three injection strategies are center port injection, peripheral injection, and corner injection. Each of these injection schemes is complicated by the geometry. Instead of a constant one-dimensional flow through the preform, the flow patterns are two-dimensional and can vary significantly with the permeability of the reinforcement. In addition, woven fabrics may have permeabilities which vary with direction in the material. Woven fabrics usually have defined an orthogonal coordinate system based on the specific weave geometry. The principal in-plane coordinates are referred to as "warp" and "fill", and a permeability can be specified for warp and fill directions. The warp direction of a woven fabric is the direction in which the fabric is

woven and then placed on the roll. Fill direction tows are shuttled back and forth between the warp tows. Specific fabrics may have much lower permeabilities in one or the other direction. The result can be an elliptical flow front, which can also result in incomplete mold filling if fabric orientation is not carefully chosen. Salem and Parnas **(14)** have shown that in-plane permeabilities can vary significantly between warp and fill. Principal permeabilities also may not lie directly along the warp or fill directions. In their study of an 8-harness satin weave fabric, center port injected with corn syrup, the principal permeabilities were off-axis by about 15°, corresponding to the crimp angle of the fabric.

RTM research involving woven fabrics is still relatively new. A number of investigators have studied the effects of above conditions on nonwoven fiberglass mattes. Many papers cited here **(3) (4) (15) (16) (17)** used panels manufactured with continuous strand mat preforms. Several have studied coarsely-woven fiberglass fabrics. These coarse fabrics are often processed to low volume fraction, and typically use unsaturated polyester or vinyl ester matrices. Work by Carroll and Cochran **(18)** looks at the effects of fiberglass preform weave. They studied the infiltration of plain weave, satin weave, and uniweave preforms to assess the relative ease of injection and properties of each fabric type. They conclude that weave patterns with less out-of-plane travel (such as satin weave or uniweave fabrics) restrict macroscopic flow paths and are therefore more difficult to inject. Plain weave panels contain more overlapping tows and crimp areas, which provide these macroscopic flow paths. Even at much higher volume fractions,

resins infiltrated plain weave fabrics more quickly than lower volume fraction satin weaves.

Karbhari et al. **(15)** produced a number of laminates with both center port and corner injection strategies. The materials were Derakane 411-C50 and two continuous strand fiberglass mattes. The inplane permeabilities of these preforms is likely to be the same, regardless of orientation. Several other process variables were studied as well, such as tool temperature and injection pressure. The resulting laminates were tested in tension and in flexure. The corner-injected panels appeared to perform better in flexure, while tension tests favored center-injected panels.

Other researchers have looked at using more than one fill port to quickly manufacture composite panels with low void content. Work by Hamada, Ikegawa and Meakawa **(3)** looks at both the center injection and line-to-line injection schemes. They acknowledge the edge difficulties associated with line injection, and their results indicate that lower concentrations of voids exist in panels made by center injection. Voids are measured by image analysis of cross-sections viewed with a microscope. They propose that using both center and line injection systems together will reduce the final void content even further. However, fairly high void contents are still found in the regions where the two flow fronts meet.

Chan and Morgan **(19)** propose another multiple-port method to infiltrate large parts. They argue that using a series of ports located along the length of the part will speed injection time by reducing the distance from the resin source to the flow front.

D'arcy's law states that the flow rate will vary directly with permeability and pressure gradient. Shorter distances between higher pressure (inlet) and lower pressure (flow front) increase the gradient and flow rate. By waiting until after the flow front has passed each port before opening it, entrapped voids associated with two converging flow fronts can be avoided.

Injection temperature is perhaps the most important parameter for controlling process time. A rise in temperature will both decrease the initial viscosity of a resin, and speed up its reaction rate. Although a given resin may flow more quickly at a higher temperature, it is also more likely to gel before the preform is fully infiltrated. The effects of varying the resin viscosity on infiltration and void formation are not well known. Several researchers have investigated the effects of temperature and viscosity on RTM composite properties, often in combination with other factors.

Karbhari et al. **(15)** studied the effects of varying a number of injection parameters on the properties of glass/ epoxy laminates. These included corner vs. center injection, high or low injection pressure, and ambient or elevated mold temperature. Panels were tested in four point flexure and open hole tension. In general, process parameters which improved open hole tension performance were detrimental to flexure, and vice versa. Center injection with low viscosity and pressure appeared to favor open hole tension specimens, while corner injection with higher viscosity and pressure resulted in higher flexure strengths.

Kuttenkueler and Grenestedt **(20)** studied various process parameters in the

production of graphite/ epoxy RTM laminates. They used a five harness satin weave fabric in combination with two epoxy resins. The panels were fabricated under constant pressure and were peripherally injected. Each resin was used to make panels with different injection pressures, vacuum pressures, injection temperatures and cure cycles. Each of these parameters had a high and low setting, and a series of panels were manufactured using each of these settings. The laminates were subjected to unnotched tension, open hole compression, and open hole tension tests. The results showed no significant changes in mechanical properties with changing process conditions. Mode I and mode II fracture toughnesses were measured with double cantilever beam (DCB) and end-notched flexure (ENF) tests, respectively. Results of the Double Cantilever Beam tests were widely scattered. They found significantly less variation in the mode II fracture tests than in mode I tests, but both $G_{IC}$ and $G_{IIC}$ appeared to be insensitive to process conditions. The final void content of the panels was not measured.

Hayward and Harris **(17)** examined process parameters on RTM panels made with a number of reinforcements and resins. Included in the study were a fiberglass unidirectional reinforcement, plain weave cloths, continuous strand mats, and a 5-harness satin carbon fabric. The laminates were manufactured by resin transfer molding with a constant pressure system using center port injection. Specimens cut from these panels were tested in tension, four point flexure, and short beam shear. Specimens taken from across the injection length, and showed no variation in properties. An increase in injection pressure was seen to slightly decrease the flexure strength of the glass

composites, but did not appear to affect short beam properties. Small temperature variations (~20°C) produced no significant changes in properties. They also looked at two resins with different viscosities injected into preforms having different (40% and 55%) volume fractions. In the 40% fiber volume fraction composite, the higher viscosity resin produced a panel with lower void content. In the 55% fiber volume fraction case, the lower viscosity resin was better able to fully wet the preform and produced fewer voids.

Several researchers have studied the effects of injection rate on composite properties. Injection rate for a constant pressure system is determined by the pressure at the resin source, usually a heated pressure pot. Other RTM injection systems may use constant displacement pumps, which can provide a steady volume flow of resin. Stabler et al. **(9)** looked at injection pressures between 30 and 50 psi, and found no differences in void content or laminate mechanical performance. Other researchers **(20), (15)** have also looked at varying injection pressure, but have come to mixed conclusions.

A topic related to the injection pressure is that of vacuum assistance. Vacuum assistance generally appears to reduce void content and improve laminate quality. Lundström, Gebart and Lundemo **(4)** studied the effect of vacuum assistance on the void content of RTM panels. They manufactured a series of panels with varying amounts of vacuum at the outlet, and a constant pressure differential between inlet and outlet. They conclude that bubbles formed under vacuum-assisted RTM contain air at a lower pressure. These bubbles then collapse when the vacuum is released. The effect is a

lower void content, and smaller voids on average, with vacuum assistance. Most other researchers are in agreement that void content drops and laminate quality increases when vacuum assistance is used. Hayward and Harris **(17)** showed the positive influence of vacuum by comparing short beam shear strengths and flexural properties of RTM composites with and without vacuum assistance. In all cases, the addition of vacuum improved the performance. These tests were conducted with three glass and one carbon preform, using epoxy and polyester resins. Graphite/ epoxy RTM panels made at 55% volume fraction with vacuum assistance showed performance comparable to similar prepreg composites.

### 1.3 Objectives of this Research

In this investigation, a series of composite panels was manufactured in an attempt to understand the effects of material selection and process parameters on resin transfer molded composites. Both graphite and fiberglass preforms, injected with three common resin systems, were considered. A detailed discussion of these materials can be found in Chapter 2. Panels utilizing different materials were injected using similar process conditions, and panels of similar materials were made under differing conditions. Process conditions considered include injection temperature, injection pressure, and injection geometry.

Close study of literature related to RTM processing indicates a few areas where research is weak. Resin transfer molding is historically a manufacturing method for low-performance parts, and literature studies follow this profile. Most investigators use inexpensive resins and low fiber volume fraction fiberglass preforms. Many use high-permeability, low performance fiberglass matte materials. By comparison, literature on high fiber volume fraction fiberglass and graphite woven materials is rather sparse. Many researchers have studied a wide variety of parameters such as injection temperature or pressure , but often used only two data points instead of a range. Many studies have speculated that particular fibers and resins would be incompatible such as sized graphite and vinyl ester, but no information appears to be available on attempts to build composites with these materials. Although a few researchers have studied the effects of voids in the composite, few have looked at the effects of materials selection or process conditions on the void content. Others did not consider void content at all, but compared process conditions with corresponding mechanical test results. This research seeks to fill in some of these gaps, using several materials to study the manufacture of high performance, high fiber volume fraction composites.

A series of tests must be selected to serve as a measurement of laminate quality. These will consist of both physical (nondestructive) measurements and mechanical (destructive) testing. Physical measurements and observations include fiber volume fraction and void determination, and micrograph studies. Mechanical tests conducted include compression, compression after impact, interlaminar shear, in-plane shear and

four point flexure.

Fiber volume fraction is a universal measurement of composite quality. Since resin transfer molding makes use of a closed mold, fiber volume fractions can be easily controlled. The panels under consideration here had final fiber volume fractions in the range of 53-56% for fiberglass panels, and 58-61% for graphite panels. Two independent assessments of fiber volume fraction were used in this investigation and will be discussed in Chapter 2. Another important tool in this investigation is a method of void measurement. Although many void measurement methods are available, a technique is needed which is quick, reliable, and non-destructive to the specimen. A density-based calculation for composite void fraction is presented in Chapter 2 and will be validated by photographic evidence in Chapter 4.

# Chapter 2: Experimental Procedures

## 2.1 Equipment

The panels used in this investigation were made in an aluminum mold containing a 152 mm square (6" x 6") cavity. A photograph of the mold can be found in Figure 2.1. The assembled mold consists of three parts. The bottom plate is used as a bearing surface in the press. Two different bottom plates are used in this study: a flat plate used for 6.3 mm (¼ inch) thick panels, and a plate with a 3.2 mm (0.125 in) step for 3.2 mm (⅛ inch) thick panels. An aluminum frame in the center contains the preform, and is equipped with two side ports and o-ring channels for the top and bottom surfaces. The top part of the mold, referred to as a "plunger", consists of an aluminum block which fits the mold cavity and a surrounding flange. Pressure on the plunger compacts the fiber preform, reaching full compaction when its flange comes into contact with an o-ring on the frame. A hole drilled in the center of the plunger serves as a center injection port. A top bearing plate contains a channel, to allow access to the center port.

One of the features of this mold is the resin port layout. With the three available gate locations, the mold can be used for line-to-line, center port, or peripheral injection. For line-source to line-sink panels, only the two side ports in the frame are used. The preform is cut so that an empty channel about 3.2 mm (0.125 in) wide is left open on

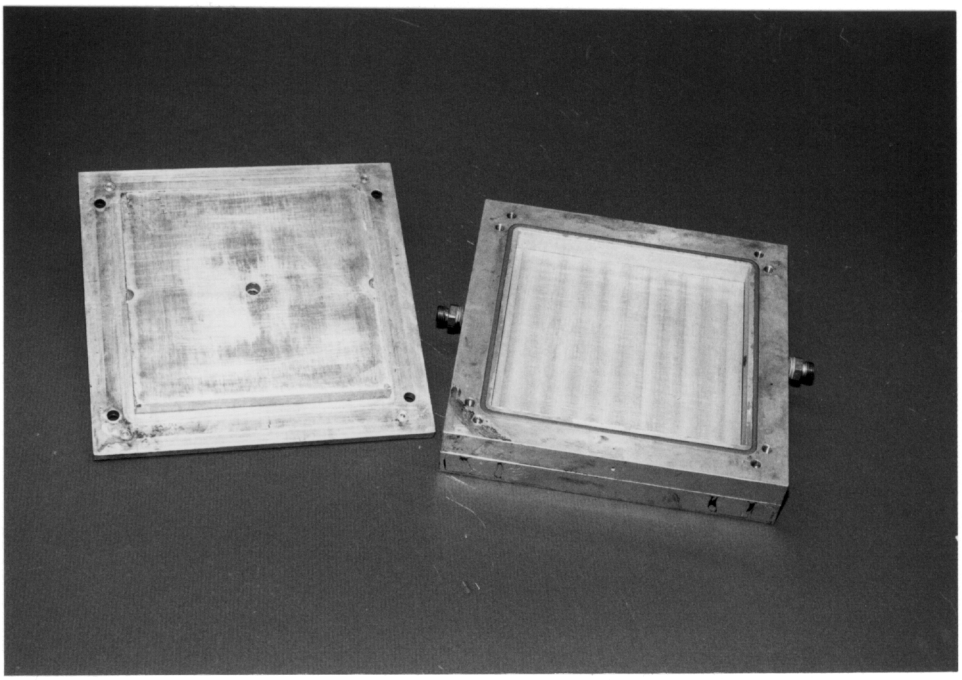

**Figure 2.1: Photograph of the aluminum mold used to manufacture RTM composites.**

opposite ends of the mold. Resin from the source port fills one channel, then the preform, and finally the far channel before flowing out of the exit port. In the center injection scheme, resin enters the preform from the center port in the top of the mold, fills the preform, and exits from the side ports. In a peripheral injection scheme, the preform would be cut to allow a channel on all sides. The resin enters from the sides, first filling the channels, then infiltrating the preform and exiting from the center port. For very viscous resin systems, the mold can be used to manufacture panels by the Resin Film Infusion Technique. In Resin Film Infusion, a film containing the proper amount of resin is cast in the bottom of the mold. The resin flows into a preform, placed atop the film, under the application of heat and pressure. Although all four of these infiltration strategies were tried, the injection data presented here were made with the center port injection scheme. A photograph of three successfully injected center-port panels is shown in Figure 2.2.

All RTM panels manufactured in this study were made in a computer-controlled hot press at Virginia Tech. This press is connected to an IBM PC AT, with independent closed-loop PID control of each heated platen. The computer control allows precise control of platen temperatures, heating and cooling rates, and hold times. The press is cooled by compressed air above 100°C, and by water below 98°C. This programmed control system assures that all panels made with a particular resin system undergo the same cure cycle. A photograph of this hot press system is displayed in Figure 2.3.


**Figure 2.2: Photograph of typical RTM Composite Panels.**

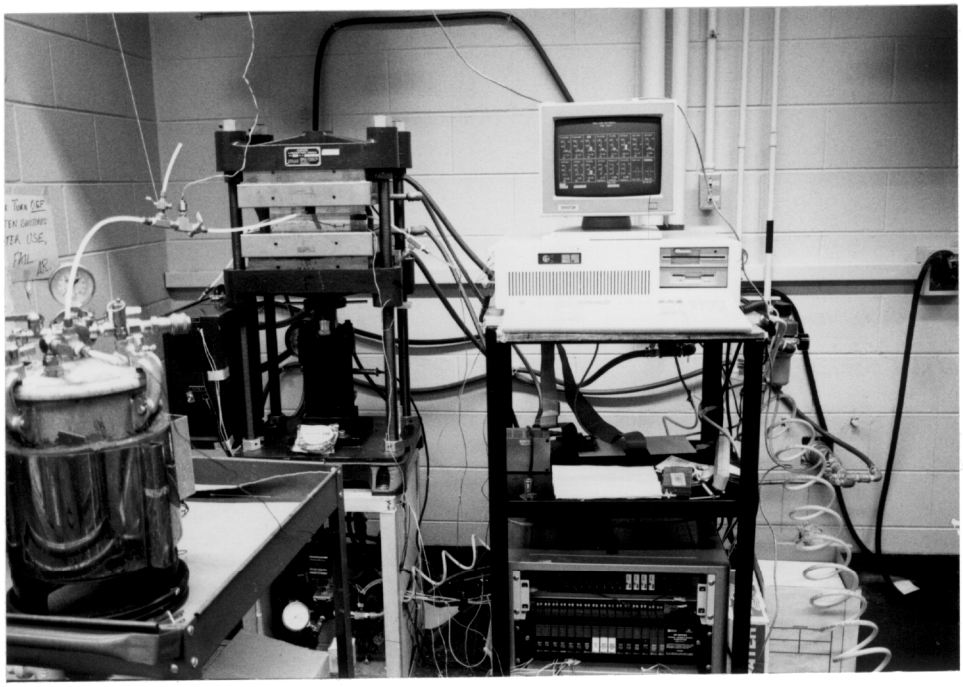

**Figure 2.3: Photograph of Computer Controlled Hot Press and RTM Injection Setup.**

The panels manufactured for this investigation were injected under constant-pressure conditions with a pressure pot. The aluminum pressure pot used allows control of pressure and is wrapped in a blanket heater for elevated temperature injections. The resin for a particular panel can be placed in a smaller container, typically a glass mason jar, and placed in the center of the pressure pot. Since the pot's walls are heated, the jar will be partially immersed in heat transfer oil. A metal tube carries resin from the jar to the outlet in the pressure pot's lid. The pressure pot has a maximum service pressure of about 750 kPa, or 110 psi, at room temperature. Figure 2.4 shows a schematic of the pressure-injection RTM setup, showing the mold, pressure pot and lines carrying resin to the preform.

Between the pressure pot and mold, the resin is carried by 3 mm PTFE tubes interconnecting a series of stainless steel and brass fittings. A typical injection setup for center injection with a heated resin is shown in Figure 2.5. A thermocouple fitting is located just outside the pot, to read resin pot temperature. Further downstream, the resin meets a pair of brass tee-fittings, which hold the pressure transducer and bleed valve. The bleed valve allows air to escape from the lines when the pot is first pressurized. Once resin begins to exit, the valve is closed for the duration of the injection run. At the far end of this large fitting is the inlet valve, which leads directly to the inlet port at the top of the mold. These fittings, along with the pressure transducer, can be seen on the left side of Figure 2.5. Typically, heating tape, not shown in Figure 2.5, is wrapped around the tubing and fittings between the mold and pressure pot, and kept at or 5°C

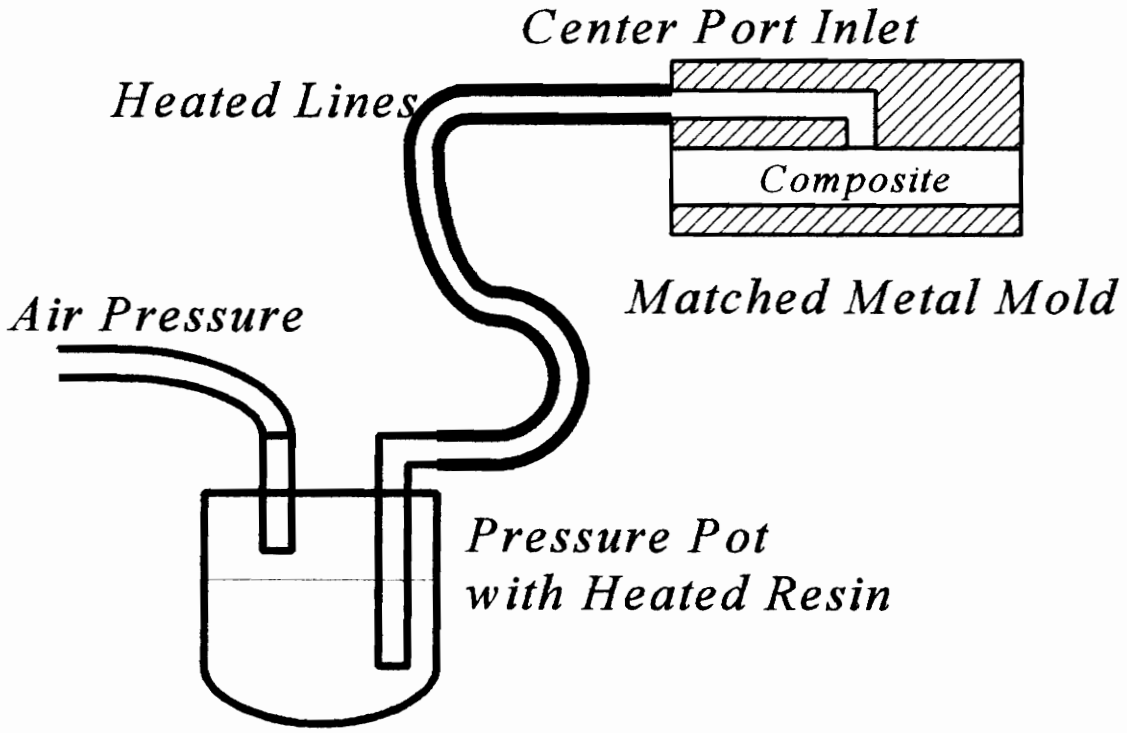


**Figure 2.4: Schematic of the Pressure Injection RTM Setup**

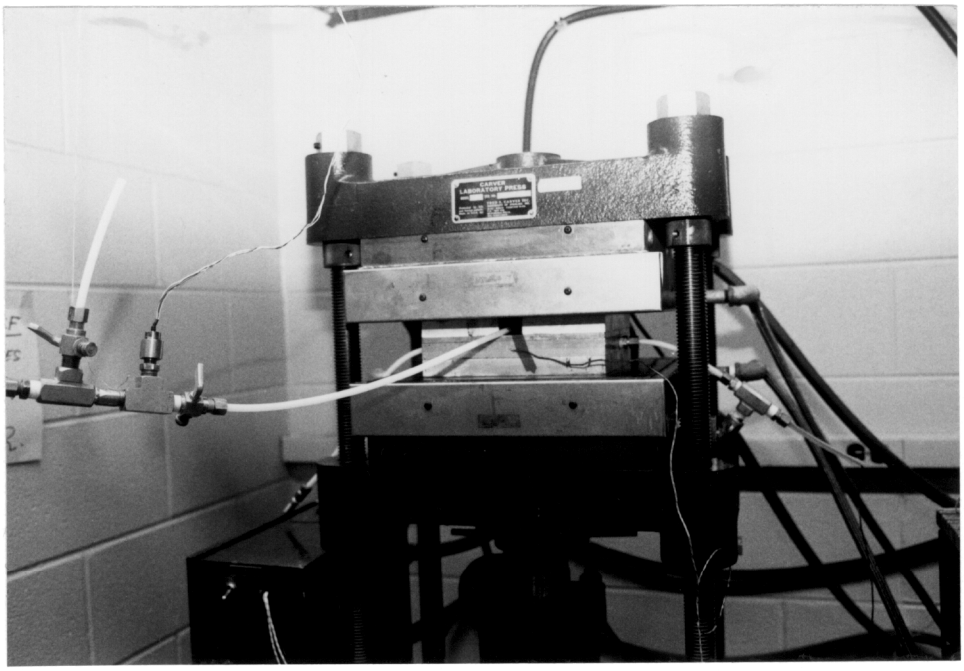

**Figure 2.5: Photograph of Pressure Injection RTM Setup.**

above the desired injection temperature. Additional fittings and lines are attached to the mold's exit ports. A fitting at one side exit port contains a valve leading to a vacuum pump. At the other exit is a thermocouple fitting used to detect the presence of heated resin, and a resin bleed valve if needed.

A data acquisition system, an integral part of the computer process control, was also used during the manufacture of all panels. This system keeps track of the platen temperatures, up to five thermocouples in the mold and lines, and pressures in the injection line and on the platens. Data from the mold inlet pressure transducer are used to accurately set injection pressure. The thermocouple signals can also be tied to the program. For example, a hold of specified length can be programmed to begin only after the mold has reached a certain temperature. Acquisition times can be altered by the operator to correspond with critical times of injection. During the cure phase, data would only need to be recorded every minute or two. At the beginning of injection, the data is recorded at the system's fastest acquisition rate of one data point every two seconds. This helps track the pressure drop and spike associated with the resin valve opening, and the flowfront reaching the preform. An intermediate time can then be chosen to record data during infiltration, ending with the outlet thermocouple recording resin exiting the mold.

## 2.2 Materials

Several resin systems were used in this investigation. They consisted of one vinyl ester system (Dow Derakane 441-400), one epoxy system (Shell RSL-1895) and one cyanate ester system (AroCy B10). The Derakane 441-400 is a low styrene content version of a common bisphenol-based vinyl ester resin system. This and other Derakane resin formulations are common to resin transfer molding, and are popular resins in RTM research. Derakane 441-400 is catalyzed with 1% by weight benzoyl peroxide and 0.2% t-butyl perbonzoate. Shell Chemical Company's RSL-1895 is a research epoxy resin developed specifically for Resin Transfer Molding applications. RSL-1895 has good flow properties at elevated temperatures, and a long pot life. It is cured with 33% by weight of amine-based Shell Curing Agent W.

In addition to these common resin systems, new high temperature resins are becoming more common in low-cost applications like RTM. Stockton **(21)** has successfully fabricated graphite RTM composites with cyanate esters and bismaleimides with up to 60% fiber volume fraction. One of these new cyanate ester systems, AroCy B10, was also used in this investigation. AroCy B10 is a low molecular weight monomer, and is a crystalline solid at room temperature. When heated, the resin melts to become a very low viscosity liquid.**(22)** Thermoplastic-toughened variations of this cyanate ester system containing poly(arylene ether sulfone) have been synthesized at Virginia Tech. **(23)** Several of these have been successfully applied in resin transfer

molding processes, and are used in several panels here. RTM laminates, utilizing various matrices, were manufactured to determine the effects of resin systems and their interactions with the fabric preforms considered here.

The panels manufactured in this investigation contained one of three types of fiber reinforcement. The first was an E-glass style 162 plain weave fabric. Panels were made of this fiberglass fabric with the vinyl ester and epoxy systems. A plain weave graphite fabric of Hercules AS-4 fibers, with a common epoxy-compatible sizing ("W" sizing), was also used. This fabric was used to manufacture RTM panels with all resin systems considered here. This fabric was composed of 3k bundles, woven at 12 tows per inch. An identical plain weave of unsized AS-4 graphite fabric, sometimes referred to as AU-4, was used to manufacture panels with the vinyl ester resin system. The two graphite fibers were used to study the effect of the fiber interface on graphite/ vinyl ester composites. All tests conducted on composites made of Derakane 441-400 with sized graphite were duplicated with a laminate of Derakane 441-400 and unsized graphite.

## 2.3 RTM Processing

This section discusses the procedures involved in the fabrication of a composite panel by Resin Transfer Molding. Included are procedures for preparing the mold, resin and fabric preform, and problems associated with two common injection approaches.

### 2.3.1 Panel Fabrication Procedures

Typically the first step in the manufacture of an RTM panel is to prepare the mold and preform. The frame must be affixed to the proper bottom plate, depending on the desired panel thickness. All parts of the mold will be release coated using Miller Stephenson Chemical Co.'s Release Agent MS-122N. The fabric is to be cut to fit the mold closely in one dimension, and to leave a 3 mm, or ⅛ inch channel on the sides of the mold facing the resin ports. For this mold the preform dimensions work out to about 152 mm by 146 mm, or 6.0" x 5.75". It is important here to choose the orientation of the preform properly. The direction of lowest permeability should be across the short dimension of the preform. This helps ensure that the entire preform infiltrates before resin reaches the exit gate. If the preform were oriented in the other direction, resin might reach the exit well before reaching the corners. This would leave large voids and dry areas. The number of plies in the preform was chosen to give a compacted fiber volume fraction of about 60%.

After the mold is loaded and closed, fittings appropriate for the panel were assembled. A different set of fittings would be required, for example, for a line-to-line panel than would be needed for a center port panel. For room temperature injections, such as Derakane 441-400, a lower cost polypropylene tubing may be used, and thermocouple fittings are not necessary. Elevated temperature injections required the high-temperature PTFE tubing, as well as line thermocouples and heating tape. If

necessary, the pressure pot and lines were pressure-tested to check integrity. This became especially important with very low viscosity resins like the AroCy B10 cyanate ester.

The injection process begins by preheating the mold, lines, and pressure pot. A separate oil bath under a hood was also often used to heat the resin prior to being placed in the pot. Once mixed, the resin was warmed to a good flow temperature (usually near or below injection temperature), then placed in a vacuum oven for several minutes to degas. The resin and jar would then be placed into the pressure pot and allowed to heat to injection temperature. During this time, a vacuum pump was allowed to evacuate the mold. Once the resin reached injection temperature, the pot was pressurized and air bled from the lines. Injection pressure was set with the regulator on the pressure pot and the pressure transducer. When ready, the inlet valve was opened and the starting time recorded. Vacuum was usually turned off 1-2 minutes after the start of injection. When resin had filled the exit lines, the time of infiltration was recorded and the cure cycle allowed to begin. The inlet valve usually was not closed until the resin has reached a temperature at which the resin will gel.

Between panel injections, the mold and fittings were disassembled and cleaned. The panel was removed from the frame, measured, marked, and cut into mechanical specimens. Tubing was discarded, and most fittings washed in acetone, dried, and re-assembled for the next panel. Mold surfaces were cleaned of resin, o-rings replaced if necessary and the parts were re-assembled. Some fittings and resin ports on the mold

would have been filled with cured resin. These were drilled clear, cleaned with solvent, and re-used.

### 2.3.2 Injection Strategies

The simplest and most common injection strategy for flat plates is a line-source to line-sink scheme. In line-to-line injection, resin enters the mold on one side and fills a narrow channel which runs the width of the preform. Once filled, the resin flow front moves across the preform to the second channel located at the opposite side of the preform. Once this second channel is full, resin exits the mold. This injection scheme should, ideally, produce a one-dimensional flow front, with the flow front moving uniformly across the preform. In practice, however, there are considerable variations in flow through the preform. Resin near the walls flows more quickly than resin flowing through the center of the preform. Very large voids or dry regions can result. Infiltration times are also longer for line-to-line injection compared to other injection schemes, since the flow front must traverse the entire length of the preform. Several panels were attempted with line-to-line strategies in the course of this investigation. The results were so unsuccessful that the process was abandoned altogether in favor of center-port injection. However, this continues to be a common scheme for fabricating some Resin Transfer Molded composite laminates.

In a center-port injection scheme, resin enters the mold through a port in the top plate and flows radially through the preform to the edges. The preform was cut such that a 3.2 mm channel is left open beside the side exit ports. This, with the preferential selection of preform orientation, helps ensure that the entire preform is infiltrated before resin reaches the exit port. This process has the advantage of faster injection, as the resin travels only half the preform width (about 70 mm in this case). The radial flow pattern also minimizes edge effects on injection times. However, the flow will produce a non-uniform two-dimensional flow front, which requires finite elements or another more complicated solution to model. Also, the existence of the resin port at the center leaves the preform beneath less compacted, which results in a lower local fiber volume fraction. The area near the center stem is therefore unusable for mechanical testing.

## 2.4 Non-Destructive Evaluation of Completed Panels

The composite laminates were subjected to a series of tests to evaluate the quality of the panels. These tests include physical measurements such as resin, fiber and void content, and several mechanical tests. For most panels, both non-destructive and mechanical tests were carried out.

Non-destructive tests are an important part of assessing the quality of a composite laminate. Much information about the laminate must be obtained before mechanical

tests can be properly conducted. An accurate assessment of fiber volume fraction and void content is essential in evaluating mechanical test data. Ultrasound techniques can check both the quality of laminates, and evaluate damage after mechanical testing. Lastly, photo-micrograph techniques allow a "close look" inside the composite, to study the microstructure or verify void content.

### 2.4.1 Fiber Volume Fraction Measurements

Of paramount interest is an assessment of fiber volume fraction in the composite. Variations in fiber volume fraction affect the mechanical response and void content in a laminate made by resin transfer molding **(2).** Although the laminate is made in a closed mold, the preform compaction pressure on the plunger, and hence the fiber volume fraction, may change. Woven preforms will generally require far more compaction pressure to reach a required volume fraction than unidirectional tapes of the same materials. One cause of this is the woven nature of the fabrics. Since fiber tows cross one another in the weave, out-of plane undulations form "crimps" at the crossover. These irregularities also have the effect of making the ply thicker, and harder to compact. Plain weave fabrics, such as those used in this investigation, have a particularly large crimp density, and therefore require very high compaction pressures to achieve desired volume fractions. In this investigation, compaction pressures approaching 1400 kPa

were needed to achieve the target fiber volume fraction of 58% for carbon, or 55% for E-glass. It has been shown, however, that flow through plain woven preforms is generally easier than flow through satin-woven preforms with fewer crimps per unit area. It is believed that more macroscopic flow is present in the plain weaves, thus facilitating infiltration **(18)**.

A relatively simple method for obtaining volume fraction is based largely on knowing the amount of fiber in the preform. For many fiber systems, the entire preform can be weighed before it is loaded into the mold. Together with the known preform area, a preform areal weight can be calculated by dividing the preform weight by preform area. Some fabrics used in this investigation, however, are fragile and will fray easily if handled. The preform could easily come apart if the fabric is not loaded into the mold immediately after individual plies are cut. Preform areal weight, in units of mass per unit area, is more conveniently found by multiplying the areal weight of a single ply, denoted as $\xi$, by the number of plies, n. The fiber volume fraction of a laminate made from this preform can be found by

$$v_f = \frac{\xi \cdot n}{t \cdot \rho_f} \qquad \textbf{(2.4.1)}$$

where $t$ is the measured final panel thickness and $\rho_f$ is the fiber density. If the

distribution of fibers in the laminate can be considered to be uniform, then this calculation will return the true volume fraction of fibers in the laminate. However, this method does not distinguish remaining volume between resin and voids. Volume fractions were obtained by this measurement technique for each completed panel, and for each mechanical test specimen prior to testing. These values were later used to determine void content for each specimen.

Another common method of determining volume fraction is based on the composite density. The composite sample (usually a small portion of a panel) is weighed in air, and in a solvent of known density. In this investigation, composite samples were weighed on a Mettler AE 100 balance with an accuracy of 0.0001 g. Sample weights in the solvent were obtained by use of a wire basket suspended in a bath of Isopropyl alcohol. The wire basket is connected to the balance's load cell, and is isolated from contact with the pan containing the IPA bath. The composite density, $\rho_c$, can be computed by the following relation:

$$\rho_c = \frac{m_{air} \cdot \rho_{solvent}}{m_{air} - m_{Liq}} \qquad \textbf{(2.4.2)}$$

where $m_{air}$ is the weight of the composite in air, $m_{Liq}$ is the weight of the composite suspended in the liquid, and $\rho_{solvent}$ is the density of the liquid solvent used. In this investigation, isopropyl alcohol, with a density of 0.7854 g/cc, was used.

If the densities of the fiber and matrix are accurately known, the composite

volume fractions of fiber and matrix can be found using rule of mixtures relations:

$$\rho_c = v_f \cdot \rho_f + v_m \cdot \rho_m \qquad \textbf{(2.4.3)}$$

where $v_f$ and $v_m$ are volume fractions of fiber and matrix, respectively, and $\rho_f$ and $\rho_m$ are densities of the fiber and matrix, respectively. Recognizing that $v_m = (1 - v_f)$ and rearranging, we can solve directly for $v_f$ by:

$$v_f = \frac{\rho_c - \rho_m}{\rho_f - \rho_m} \qquad \textbf{(2.4.4)}$$

This method can estimate the volume fraction of a composite when the areal weight is not known exactly, and can easily be used on complex shapes. However, it does have several limitations. Since this method employs the rule of mixtures between only fiber and matrix, it cannot account for void content. This theory seeks to divide the composite volume between fiber and matrix only. Real composites, however, contain dry fibers, air pockets, and other voids, which tend to lower the composite density. The effect on the density method is to produce a lower number for fiber volume fraction than the areal weight method. Also, the density-based method is only valid if the densities and weights can be measured very accurately.

### 2.4.2 Void Determination

Generally speaking, values obtained for fiber volume fractions from the two methods above do not match exactly. In most cases, the areal weight method gives a higher value of volume fraction. One reason for this could be inaccuracy in measurement of resin density. A necessary assumption in using the density approach is that resin density in the composite is the same as that in bulk. This makes density values obtained from bulk samples usable for tests on composites. In actuality, resin densities within the composite tend to be slightly lower than bulk densities. This has the effect of indicating a slightly lower volume fraction in the composite. However, this effect is only slight, and would probably not account for variations of more than a few tenths of a percent. For large differences between areal weight method and density method fiber volume fractions, the best explanation is the existence of voids **(7)**.

Almost all composite materials contain voids to some degree. Measurement of void content in a composite material has been accomplished directly only by obtaining micrographic samples and graphically measuring void area. This technique is not only time consuming, but restricts void measurement to a cut (and polished) surface of the laminate. Observed voids would then be a function of local conditions on the surface in question, and would not represent the average void content of the specimen **(4)**. A method is needed to quantify the void content more quickly, without the need to polish and photograph a surface. Such a method was used in this investigation.

This method for measurement of voids is similar in technique to ASTM D2734-91(**7**). Determination of void content in a given sample is dependent upon knowing the measured composite density from the density-based fiber volume fraction method and the calculated fiber volume fractions from both density-based and areal weight methods. A necessary assumption is that the fiber volume fraction from the areal weight calculations is the true fiber volume fraction. Physically, this assumption makes sense. If the specimen is of a constant thickness, the number of plies and areal weight are known. This volume fraction is a true measure of specimen volume taken up by the preform. With the "true" fiber volume fraction and measured composite density, the fiber mass fraction, $m_f$, can be obtained as follows:

$$m_f = \frac{v_f \cdot \rho_f}{\rho_c} \qquad \textbf{(2.4.5)}$$

where $v_f$ is the volume fraction measured from areal weight, and $\rho_c$ is the measured composite density. Since voids contain no mass, then $m_f + m_m = 1$, where $m_m$ is the matrix mass fraction. The "true" matrix volume fraction now becomes:

$$(v_m)_{true} = \frac{(1 - m_f) \cdot \rho_m}{\rho_c} \qquad \textbf{(2.4.6)}$$

Finally, the volume fraction of voids, $v_v$, is found by subtracting the fiber and matrix volume fractions from unity:

$$v_v = 1 - (v_f)_{true} - (v_m)_{true} \quad \textbf{(2.4.7)}$$

This calculation also makes the assumption that the composite contains only closed voids, which means that voids in the composites are not open to the surface. Open voids would fill with solvent during immersion and measurement. The result could be a calculated void content slightly lower than the actual void content. Several samples specimens from the test matrix were checked for open porosity by reweighing the samples after being immersed in Isopropyl alcohol. The tests detected little or no open porosity in the samples.

This assessment of void volume can be tested by comparing photo-micrographs of composite specimens predicted to have high and low void contents. If the method is accurate, it could then be used to link void content with specific process conditions or material choices.

It should be noted here where the distinction is to be considered between low void content or high void content. Because of inaccuracies in measurements, experimental error, or variations in densities, some specimens with very low void content may have calculated void volumes near or even below zero. Specimens which have a calculated void volume below about 1% will be considered void-free. Certainly there will be some void content in the composite, but it would be below the reasonable capability to confirm with a micrograph measurement. Those specimens which indicate between about 1% and about 2% were considered to have a "low" void content. Those

specimens having greater than 2% void volume would be considered to have a "high" void content. These "low" and "high" void volumes can be confirmed, at least qualitatively, by micrograph study of a few panels.

### 2.4.3 Ultrasonic C-Scan

Ultrasonic C-scan is a common means of performing non-destructive evaluation on composites. The effective use of ultrasound in detecting voids and non-uniform areas in a composite is well documented. However, much of the work with ultrasound has been done on autoclave-cured prepreg tape laminates. These materials have a far more uniform microstructure as compared with woven fabric composites. Generally, tape composites contain many discrete layers of well-distributed fibers. Each fiber remains essentially straight and presents no obstacle to the ultrasound pulse. In a woven fabric composite, local variations in fiber direction, both in and out of plane, exist. Pockets of resin often exist between tows, and the woven nature of the fabric tends to create a surface which is wavy rather than completely flat. These factors have the effect of scattering the ultrasonic pulses, making it more difficult to obtain a good ultrasound picture of an RTM panel.

Despite the problems, ultrasound was an important tool in the evaluation of some panels in this investigation. Although ultrasonic C-scans were attempted on panels in

both the 6.3 mm and 3.2 mm thickness, signals were only able to penetrate the thinner panels. Many of the 3.2 mm inch panels were also unscannable. No suitable ultrasound scans were obtained for the fiberglass panels. Also, the presence of surface roughness or other superficial flaws could scatter enough sound to effectively obscure the interior. An otherwise good panel can appear to contain large pockets of voids in the presence of surface flaws. The RTM panels fabricated during this investigation have surface irregularities at the inlet/outlet port locations. It is therefore difficult to use ultrasound as a method of determining laminate quality.

Ultrasonic C-scans do not actually sense the presence of voids in a composite. The signal returning from a composite is a function of the acoustic uniformity of the composite. Voids and fiber misalignments can disrupt the sound pulses traveling through the composite, thus altering the return signal. In a woven laminate it is difficult to directly view irregularities within the material. However, it is possible to view internal damage in the composite after impact testing. Despite the existence of background clutter, the damage patch in the center of an impacted specimen can be noted with the C-scan and measured. Ultrasound evaluation was used to measure the impact damage of these panels, discussed in a later section.

### 2.4.4 Optical Microscopy

Photomicrogrpahs were collected and viewed to record the microstructure of the composite samples. Typically a small specimen is cut from the laminate and one edge is selected to be viewed. This edge will be sanded smooth, then wet sanded to 600 grit and polished on a polishing wheel at 150 rpm for about 20 minutes using a series of alumina suspensions with 1.0 micron, 0.3 micron, and 0.1 micron aggregate sizes. Several small samples are often "potted" together in epoxy resin and polished together to save polishing time. Under the optical microscope, views of up to 400x magnification are obtained. Photographs may be taken with either a Polaroid or 35mm camera mounted to the microscope. Typically one cross-section is obtained in the warp direction and one in the fill for each panel.

The primary use of the optical micrographs is to determine the void content in the laminates. Large concentrations of voids can be located in a cross-section. Their locations and sizes can be plotted and checked against other panels in the test group. Micrographs will show whether the voids are primarily macroscopic or microscopic. The micrographs are also used to check the validity of void measurement schemes discussed in section 2.4.2. Other uses for micrographs include checking resin/fiber distribution, tow deformation and spreading, and fiber volume fraction measurement. Micrographs may indicate areas of fiber wash, resin-rich regions, or other microstructural irregularities.

## 2.5 Mechanical Testing

Laminates manufactured in this investigation were cut into individual specimens and subjected to a variety of mechanical tests. The data from these tests were used to quantify differences in process conditions and material interactions. Often two or three panels of each material were manufactured to provide enough material for all tests to be conducted.

Compression tests were run on most systems using the short block compression (SBC) test. This test and geometry, developed by NASA, is considered to give higher values of compression strength than many other geometries, and has a low aspect ratio which is expected to reduce bending effects. Short block compression tests are commonly used on woven fabric composites. **(24)** The short block specimen is 1.50 in wide by 1.75 in long (38 mm by 44 mm) with ground edges. The specimen was outfitted with strain gages, placed in a fixture and end-loaded. A photograph of a short block specimen in the load fixture is shown in Figure 2.6. Care was taken when loading the specimen into the fixture that the specimen ends be set firmly against the fixture. The slider blocks must also be tight against the specimen faces, and flush with the edges. Loose or misaligned specimens can bear on corners, creating stress concentrations which reduce the compressive strength.

Strain gages were bonded to the short block specimen to measure the modulus of

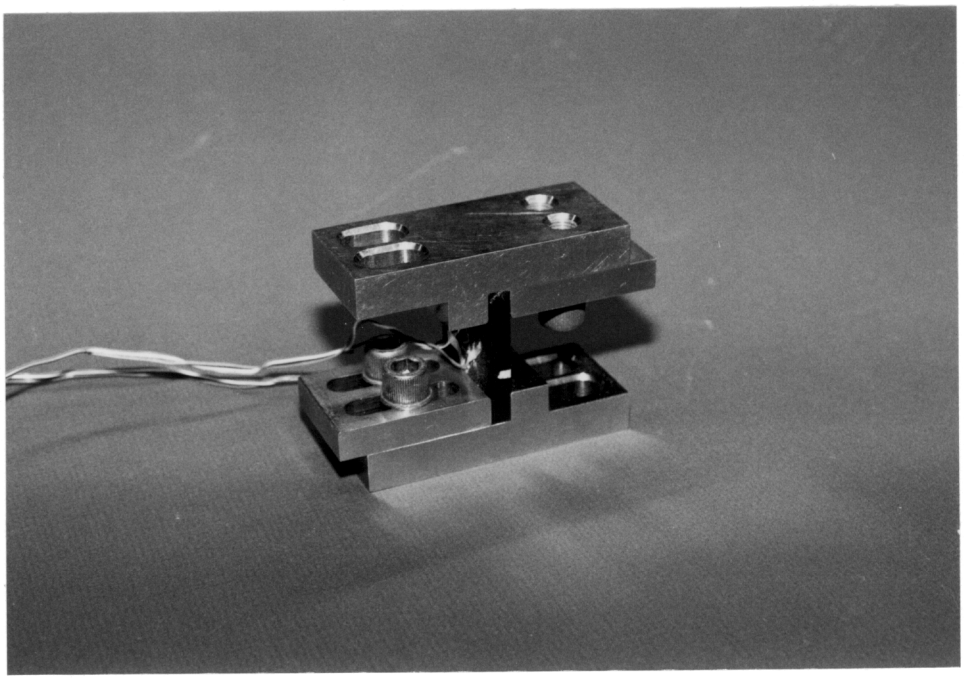

**Figure 2.6: Short block compression specimen and Test Fixture.**

the specimen. A Micro-Measurements CEA-13-250UW large-area strain gage was bonded to the center of each face. The use of strain gages on each face helps to assess any bending effects during the test. In practice, the short block compression fixture did not limit bending as much as predicted. Specimens are held in the fixture by means of a sliding block. This steel block is not tightened against the specimen, but rather against the base of the fixture. Any misalignment during loading may allow the specimen to move slightly in the grip. As a result, many specimens showed significant bending. An example is shown in Figure 2.7, which is the data acquired from a representative short block specimen experiencing bending. The three curves represent front face, back face, and average strain values. Strain data obtained from several specimens incurred too much bending to reliably use for modulus calculation. In addition, inadequate bonding of strain gages to the specimens caused a few gages to debond during testing. With only limited strain data for the systems considered, it was decided not to report modulus results, but to instead simply report problems associated with attempting to calculate modulus.

Compression testing was carried out at a crosshead speed of 1.2 mm/minute (0.05 in/minute) on a Tinius-Olsen Universal Testing Machine set to a 535 kN (120,000 lb) max load range. Stress in MPa is calculated by converting units from the testing machine, which reads pounds force. Short block tests are usually performed on 6.3 mm (0.25 inch) thick laminates. All 6.3 mm laminates made in this study were subjected to short block compression tests. These included AS-4 sized graphite, AU-4 unsized

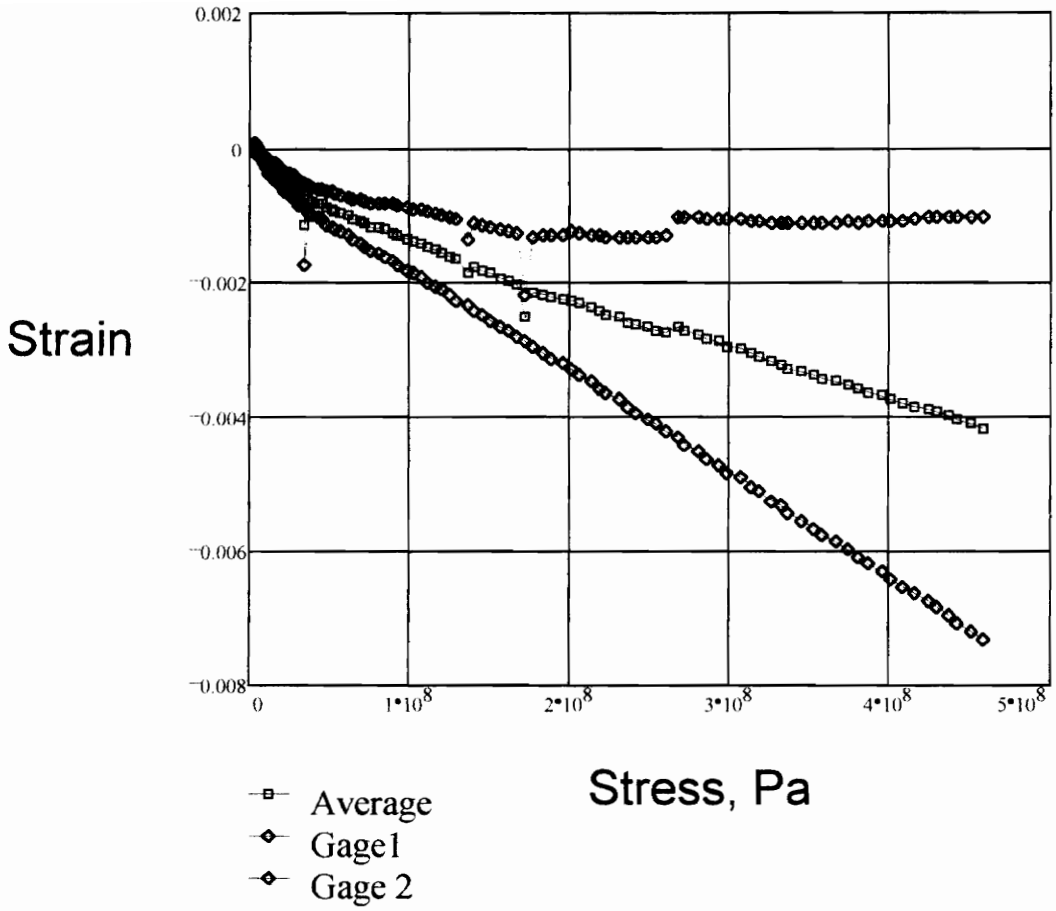


**Figure 2.7: Representative compression strain data, showing bending.**

graphite, and E-glass panels made with Derakane 441-400 and Shell RSL-1895. Short block compression tests were conducted in both warp and fill directions for these materials. Additional warp direction SBC tests were conducted for the temperature variation study. Compression tests of this type are considered to be highly dependent on matrix properties, fiber/matrix interaction, and void content.

The Iosipescu shear test was used to determine the in-plane shear strengths. The Iosipescu specimen is typically 3.00 inches (76 mm) in length and 0.750 inches (19 mm) wide. The Iosipescu test uses a notched geometry to induce shear failure in a specific region of the specimen. Two notches were ground into each specimen at the center, reaching a final radius of 1.3 mm. Strain gages (Micro-Measurement EA-13-061TV small element 0°/90° rosettes) were mounted in the gage section between the notches. This were mounted to each face of the specimen and used to generate shear strain data. The geometry for the Iosipescu specimen is shown in Figure 2.8. Several 3.2 mm laminates were subjected to Iosipescu testing in this study. The shear strengths of AS-4 fabrics with most resin systems and AU-4 fabric with Derakane 441-400 were measured. Iosipescui tests were conducted on specimens with the notches cut across the fill directions.

Bretz et al. **(16)** looked at the Iosipescu test in-depth and studied the stress patterns typical of the geometry. An isotropic photoelastic material underwent testing in the Iosipescu test geometry. They found that a constant shear stress will exist across the notches if the notch angle is great enough. They also studied effects of tabbing the

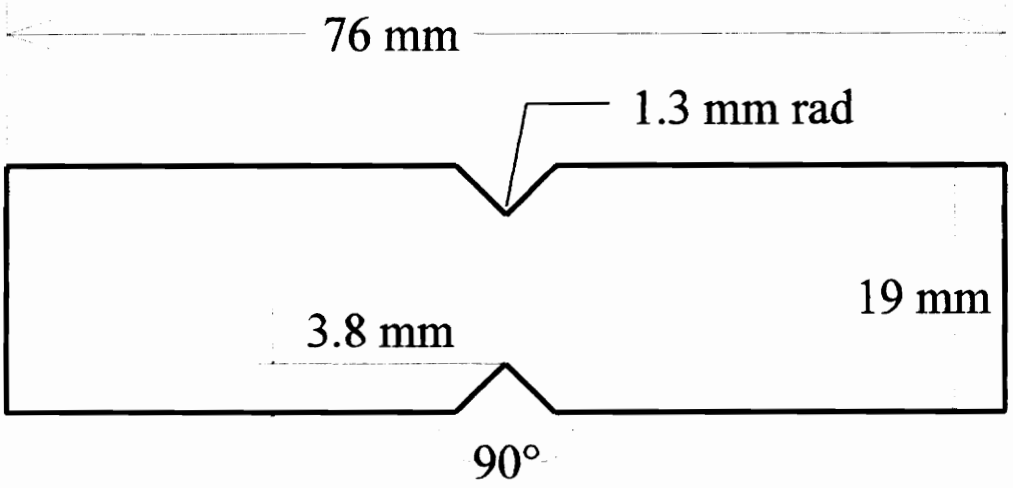


**Figure 2.8: Iosipescu test specimen geometry.**

samples and performed destructive experiments on fiberglass composites made with Derakane 411-C50. In their investigation, Iosipescu testing was conducted in the warp direction only.

Most systems in this study were subjected to impact testing. Impact tests were carried out on 3.2 mm thick panels. Four 65 mm by 65 mm specimens were cut from each panel. A horizontal gas gun, firing a round steel impacter, was used to perform the impact tests. Each specimen is impacted at a different velocity. Following the impact, ultrasonic C-scans are used to measure the size of the damaged area. Impact tests were conducted on AS-4 panels with all resin systems, on AU-4 panels with Derakane 441-400, and on E-glass panels with Derakane 441-400.

Following the impact testing, Compression After Impact (CAI) data is gathered from the panels. Compression specimens are cut from the center of the impact area. These specimens are cut and ground to dimensions of 52mm x 25.4mm. When combined with reference specimens prepared from undamaged 3.2 mm panels, residual strength after impact can be assessed. The residual strengths may be plotted against damage area or impact velocity. The compression after impact test measures the damage tolerance of the composites.

Work by Hackett and Griebling **(25)** attempted to relate impact and compression after impact properties of RTM-processed composites to fracture toughness. They performed such tests as drop-weight impact, CAI, Double Cantilevered Beam (DCB) for $G_{IC}$, and End-Notched Flexure (ENF), to find $G_{IIC}$. The tests were performed on IM-7

plain weave laminates made with three epoxy resins. The laminates were line-to-line injected at elevated temperature. They found that DCB numbers for $G_{IC}$ contained much scatter, and did not correlate very well with impact results. The ENF results for $G_{IIC}$ did correlate well to impact results. Damage due to impact increased between the three resins systems, following a similar decreasing trend in $G_{IIC}$. CAI, Flex, and Short Beam Shear tests also followed this trend.

Several specimens were subjected to interlaminar shear testing by the short beam shear (SBS) method. Samples were prepared from 6.3 mm thick panels according to ASTM D2344. SBS tests were conducted on AS-4 laminates with Derakane and RSL-1895, and unsized AS-4 laminates with Derakane. SBS specimens from the three AS-4/ RSL-1895 panels used in the injection temperature study were also prepared. In a short beam test, a 6 mm wide by 38mm long (0.25 in x 1.50 in) specimen is subjected to a three point bending test. With these dimensions, the internal shear forces are much larger than the bending stresses, and an interlaminar failure is induced. From this failure load, a comparison of bond strengths between plies can be made. However, this simple test has several limitations. As noted in the ASTM test standard, an apparent interlaminar shear strength can be calculated from the failure load. The short beam shear test is a mixed-mode test, where the specimen is subjected to both shear and bending loads. The mixed loading dictates that this test should not be used to generate useful design strengths, but instead can be used for comparison. For this reason, great care will be taken in the presentation of interlaminar shear results.

In addition to the tests described above, specimens from the injection temperature study were subjected to a four-point flexure test. This test, conducted in accordance with ASTM D790, uses a 12.5 mm (0.5 in) wide specimen with a total length of about 127 mm (5.0 inches). The outer support span used in these tests was 100 mm, and the inner support span was 34 mm. The four-point geometry is used to reduce shear stresses in the beam. The breaks should occur between the inner supports and should occur from compression or tension failure on the top or bottom surface. It has been shown by Ghiorse **(6)** that void content and matrix in a composite laminate can affect flexural properties.

# Chapter 3: Panel Manufacture

## 3.1 Injection Strategies

Early attempts to fabricate composite panels with various materials systems used line-to-line injection. 162 E-glass fabrics at a relatively low (~45%) fiber volume fraction were successfully injected with Derakane 441-400 resin. When the volume fraction was increased to 55%, however, less than half of the panel was resin infiltrated. Resin leakage around the edges of the fabric, next to the mold surface, caused a large dry region in the center of the panel. This, combined with similarly poor results obtained with carbon fabric, led to the decision to switch to center port injection.

Several fiberglass test panels were fabricated by the center injection technique . These panels, made with Shell RSL-1895 epoxy resin , showed the importance of proper selection of fabric orientation. This is shown graphically in Figure 3.1. In the top sketch, the fabric warp direction is placed between the exit vents. When the preform was placed in this orientation, resin filling the mold from the center port would reach the exit channels before reaching the mold's side walls. As a result, dry spots would form in the corners of the preform. In the lower sketch of Figure 3.1, the warp direction is placed perpendicular to the exit vents. When the preform is placed in the this orientation, the preform fully infiltrates. After panels were successfully injected with RSL-1895 and 162

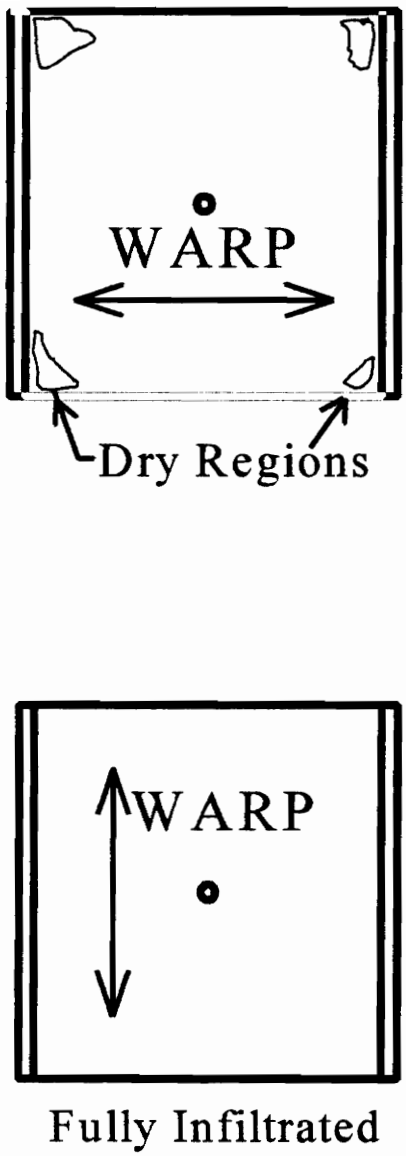


**Figure 3.1: Effect of preform orientation on resin infiltration.**

E-glass, a similar panel was produced with Derakane 441-400.

After several successes with fiberglass fabric, attempts were made to inject a carbon fiber preform with various resins. The available material was a Hercules AS-4 plain weave graphite fabric. Good panels were made with this fabric and all resin systems, including the Derakane vinyl ester. An unsized AS-4 plain weave fabric was also obtained for use with the vinyl ester system.

With a reasonable list of materials and a valid injection strategy in hand, a test matrix was assembled to examine several properties of various types of fiber/matrix systems. An assessment of the effects of injection temperature and injection pressure would be included in the test matrix. Also, direct comparisons of E-glass versus AS-4 fibers would be possible, as would comparison of sized and unsized graphite fibers for composites made with Derakane 441-400. Finally, three additional panels would be made to directly look at effects of injection temperature with RSL-1895. These panels would be subjected to interlaminar shear, four point flexure, and short block compression tests.

The main test matrix is shown in Table 3.1. Table 3.1 indicates the combinations of fiber and matrix to be considered and mechanical tests to be performed on each system. Generally, sized AS-4 plain weave fabric is used with all resin systems under consideration. The E-glass fiber is subjected to some tests with the RSL-1895 epoxy and with the vinyl ester. Derakane 441-400 vinyl ester is used on all fiber types considered.

**Table 3.1: Composite Panel Test Matrix - Tests Conducted by Material System**

| \ Fabric<br>\<br>Resin \ | Style 162 E-glass Plain Weave | Hercules AS-4 Graphite Plain Weave W Sizing | Hercules AU-4 Graphite Plain Weave Unsized |
|---|---|---|---|
| Derakane 441-400 Vinyl Ester | SBC, CAI | SBC, SBS, CAI, IOS | SBC, SBS, CAI, IOS |
| RSL - 1895 Epoxy | SBC | SBC, SBS, CAI, IOS, FLEX | |
| AroCy B10 Cyanate Ester | | CAI, IOS | |
| VTUFF 1520 Toughened Cyanate Ester | | CAI | |
| VTUFF 1525 Toughened Cyanate Ester | | CAI, IOS | |

SBC - Short Block Compression
SBS - Short Beam Shear
FLEX - Four Point Flexure
CAI - Compression After Impact
IOS - Iosipescu Shear

### 3.2 Injection Parameters

Most panels manufactured as a part of this test matrix were injected under similar conditions. All fabrics were center port injected. The inlet pressure transducer was not used for all injections, so pressure was read and set by the gauge affixed to the pressure pot's regulator. Vacuum assistance was used in all tests. However, in some cases the mold did not seal fully and a good vacuum was not achieved. Typically, the vacuum line was connected to one exit port 10-15 minutes before injection and continued for two to three minutes after the inlet port was opened and resin allowed to infiltrate the preform.

Several panels were initially injected at low pressures. When infiltration did not proceed as quickly as expected, the pressure was increased. Sometimes, to avoid resin gel before complete infiltration, pressure was increased as many as three times in a single injection. The initial pressure was set at 200-400 kPa (30 to 60 psi) for ten or fifteen minutes, then increased by 15 psi (~100 kPa) in ten minute intervals. A few panels were injected under constant pressure conditions.

Panels made with the Derakane system were all injected at room temperature. Resins systems which could be heated, however, often were injected at different temperatures to look at differences in speed of injection. Shell RSL-1895 epoxy was injected at 65°C or 85°. AroCy B10 was injected between 95°C and 105°C, with thermoplastic toughened variants injected at still higher temperatures. Reported

injection temperatures indicate the temperature of the mold and heated platens. The pressure pot was less easily controlled than the hot press, and would often be 5- 10°C cooler than the desired injection temperature, to prevent the resin reaction from accelerating. The resin was warmed to the desired injection temperature while passing through the heated lines and into the mold.

Table 3.2 contains the injection data for each panel used in this study. Several items on this table should be noted. First, each panel is numbered, and from here on will generally be referred to by its panel number. A few panels, made before the formal test matrix was devised, have been added to the list, with the prefix 0 (zero). These are early 6.3 mm panels made from Derakane 441-400 and RSL-1895. The injection temperature given represents the tool temperature for the injection. The injection pressures usually varied with injection, and often changed during injection. The initial and final pressure used in the manufacture of each panel is given in Table 3.2, as well as the total injection time. The pressure pot is equipped with a relief valve, which limits the maximum injection pressure to about 700 kPa (105 psi) at room temperature, and to about 650 kPa (95 psi) at elevated temperatures (~100° C).

The addition of the thermoplastic component to the toughened cyanate ester systems had the effect of dramatically increasing the resin viscosity. Only the least viscous of these modified resins, VTUFF 1520, was successfully pressure injected. VTUFF 1520 is a resin mixture containing 20% by weight of a 15K molecular weight

## Table 3.2: Injection Parameters for panels used in this study

| Panel Number | Fabric | Resin | Use for Panel | Date | Injection Temp | Initial Injection Pressure | Final Injection Pressure | Total Injection Time (min:sec) |
|---|---|---|---|---|---|---|---|---|
| 02 | 162 E-glass | DK441-400 | SBC | 8/10/94 | RT | 100 kPa | 200 kPa | 27:35 |
| 04 | 162 E-glass | RSL-1895 | SBC | 6/17/94 | 83° C | 140 kPa | 140 kPa | 5:05 |
| 1 | AS-4/PW/S | DK441-400 | SBC,SBS | 11/07/94 | RT | 200 kPa | 500 kPa | 56:00 |
| 2 | AS-4/PW/S | DK441-400 | CAI | 11/09/94 | RT | 200 kPa | 500 kPa | 54:02 |
| 4 | AU-4/PW/U | DK441-400 | CAI | 11/11/94 | RT | 200 kPa | 200 kPa | 12:00 |
| 5 | AS-4/PW/S | B10 | CAI | 11/14/94 | 95° C | 200 kPa | 400 kPa | 26:25 |
| 6 | AS-4/PW/S | VTUF1525 | CAI | 11/16/94 | 125° C | 470 kPa | 670 kPa | 71:00 |
| 8 | AS-4/PW/S | RSL-1895 | CAI | 11/21/94 | 63° C | 400 kPa | 600 kPa | 30:00 |
| 11 | AU-4/PW/U | DK441-400 | IOS, REF | 12/02/94 | RT | 400 kPa | 600 kPa | 35:10 |
| 12 | AS-4/PW/S | DK441-400 | IOS, REF | 12/05/94 | RT | 400 kPa | 600 kPa | 52:43 |
| 14 | AS-4/PW/S | VTUF1525 | CAI, IOS, R | 1/14/95 | RFI | | | |
| 15 | AS-4/PW/S | RSL-1895 | IOS, REF | 12/16/94 | 65° C | 400 kPa | 400 kPa | 22:57 |
| 16 | AS-4/PW/S | RSL-1895 | SBC, SBS | 12/19/94 | 80° C | 400 kPa | 630 kPa | 50:45 |
| 18 | AU-4/PW/U | DK441-400 | SBC, SBS | 12/14/94 | RT | 500 kPa | 600 kPa | 68:04 |
| 19 | AS-4/PW/S | B10 | IOS, REF | 3/09/95 | 110° C | 300 kPa | 400 kPa | N/A |
| 20 | AS-4/PW/S | VTUF1520 | CAI | 2/13/95 | 90° C | 540 kPa | 630 kPa | 52:40 |
| 21 | 162 E-glass | DK441-400 | CAI | 12/12/94 | RT | 400 kPa | 400 kPa | 6:15 |
| 24 | 162 E-glass | DK441-400 | REF | 6/04/95 | RT | 430 kPa | 430 kPa | 3:16 |
| 25 | AS-4/PW/S | VTUF1520 | REF | 6/19/95 | 100° C | 430 kPa | 500 kPa | 58:20 |
| 27 | AS-4/PW/S | VTUF1525 | CAI, REF | 6/22/95 | RFI | | | |
| 31 | AS-4/PW/S | RSL-1895 | SBC, SBS, FLEX | 8/10/95 | 65° C | 400 kPa | 400 kPa | 40:00 |
| 32 | AS-4/PW/S | RSL-1895 | SBC, SBS, FLEX | 8/17/95 | 85° C | 400 kPa | 400 kPa | 25:20 |
| 33 | AS-4/PW/S | RSL-1895 | SBC, SBS, FLEX | 8/19/95 | 75° C | 400 kPa | 400 kPa | 19:00 |

thermoplastic toughener. Unsuccessful attempts at pressure injecting VTUFF 1525 resulted in a pair of impact specimens with very high void content and poor performance. (Panel #6) Additional panels of VTUFF 1525 (panels #14 and #27) were manufactured instead by the resin film infusion (RFI) process. Similar to RTM, a predetermined amount of resin is cast into a film and placed at the bottom of the mold. The preform is placed above the resin film and the mold heated in a press. Once the mold has reached the melt temperature of the resin, pressure is applied, forcing the resin through the preform. When the preform reaches the desired thickness, the cure cycle can begin. This consolidation method is useful for high viscosity resins which would have difficulty fully infiltrating the preform before gel by liquid injection RTM methods. The needs of an RFI process are different from those of an RTM process, but the results for these RFI-processed material systems are reported here for completeness. A more detailed description of the RFI process can be obtained from Weideman et al. **(26)** or MacRae et al. **(27)**.

After completion of the main test matrix, it was decided to produce three more panels to look more closely at the effects of injection temperature. The RSL-1895 epoxy system had demonstrated the ability to be successfully injected at several temperatures. 6.3 mm thick AS-4 plain weave fabric preforms were injected with RSL-1895 at 65°, 75°, and 85°C. The panels were injected at a constant pressure of 400 kPa (60 psi). Differences in injection time, void fraction and mechanical performance were studied. A

viscosity model is available for RSL-1895 **(28)** which shows that viscosity does in fact drop with increasing temperature. However, the infiltration time for the preform injected with RSL-1895 at 75°C is significantly lower than the same preform injected with RSL-1895 at 85°C. Both panels appeared to be of similar quality and similar properties. The preforms used for each panel were arranged in the same orientation, and the resin was prepared similarly from the same batch of material. Panel #31, injected at 65°C, had considerable surface porosity which was absent in the other panels. Attempts were made to avoid these areas of high surface porosity when laying out the specimens to be cut.

### 3.3 Curing and Cutting of Panels

Once the panel is fully infiltrated, the resin's cure cycle is allowed to proceed. The cure cycle for each resin system was not varied between panels using the same system. All Derakane 441-400 panels, for example, were heated at 4°C/ minute from room temperature, where injection takes place, to a temperature of 120°C, where it is held for 30 minutes. At the completion of this hold, the panel is cooled at 4°C/ minute to room temperature. The cure cycle for the Derakane vinyl ester resin was provided by the resin supplier **(29)**. Cure cycles for the other resin systems can be more complicated. In

these cases, the mold and preform are first heated at 3°C/ min to the desired injection temperature. This temperature is held until infiltration is complete. The mold may then be heated to a final cure temperature, or may hold at another intermediate temperature. The cure cycles for the four types of resins are shown in Figures 3.2 and 3.3. Figure 3.2 shows the cure cycle for the Derakane system and for the RSL-1895 epoxy system. This cycle is recommended by the resin's manufacturer, and was studied by Hammond et al **(28)** to ensure proper cure. The cure cycles for AroCy B10 and for the toughened B10 systems are found in Figure 3.3. The cure cycles for B10 composites were developed by the manufacturer **(22)** and verified by Rau **(23)**. Typically the panel is removed from the mold, measured, and cut into mechanical specimens as soon as possible after cure.

The "Use for Panel" column in Table 3.2 indicates the mechanical test specimens cut from each panel. Generally three panels of each fiber/matrix combination are needed. The first will be a 6.3 mm (¼ inch) thick panel, which is used for short block compression or "SBC" in the "Use" column of Table 3.2. Interlaminar shear specimens were cut from graphite 6.3 mm panels, denoted in the table as "ILS". Most systems would also see impact and compression after impact testing. A second panel, in the 3.2 mm thickness, was manufactured for impact specimens. Finally, a third panel, also in the 3.2 mm thickness, was fabricated for undamaged compression test specimens, and for some materials, Iosipescu shear specimens. Systems subjected to impact and compression after impact testing will be given the notation "CAI" in Table 3.2. Iosipescu

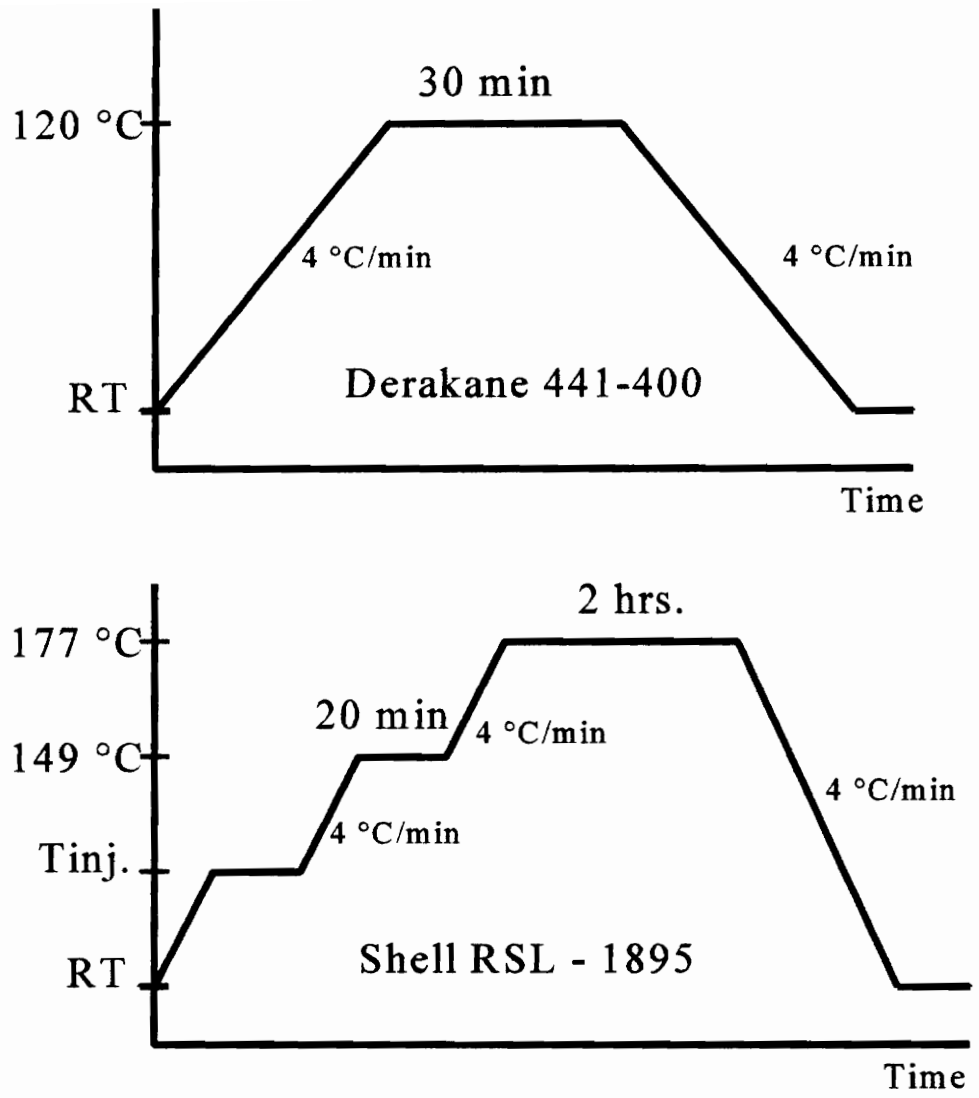


**Figure 3.2: Cure Cycles for Derakane 441-400 and RSL-1895 Systems**

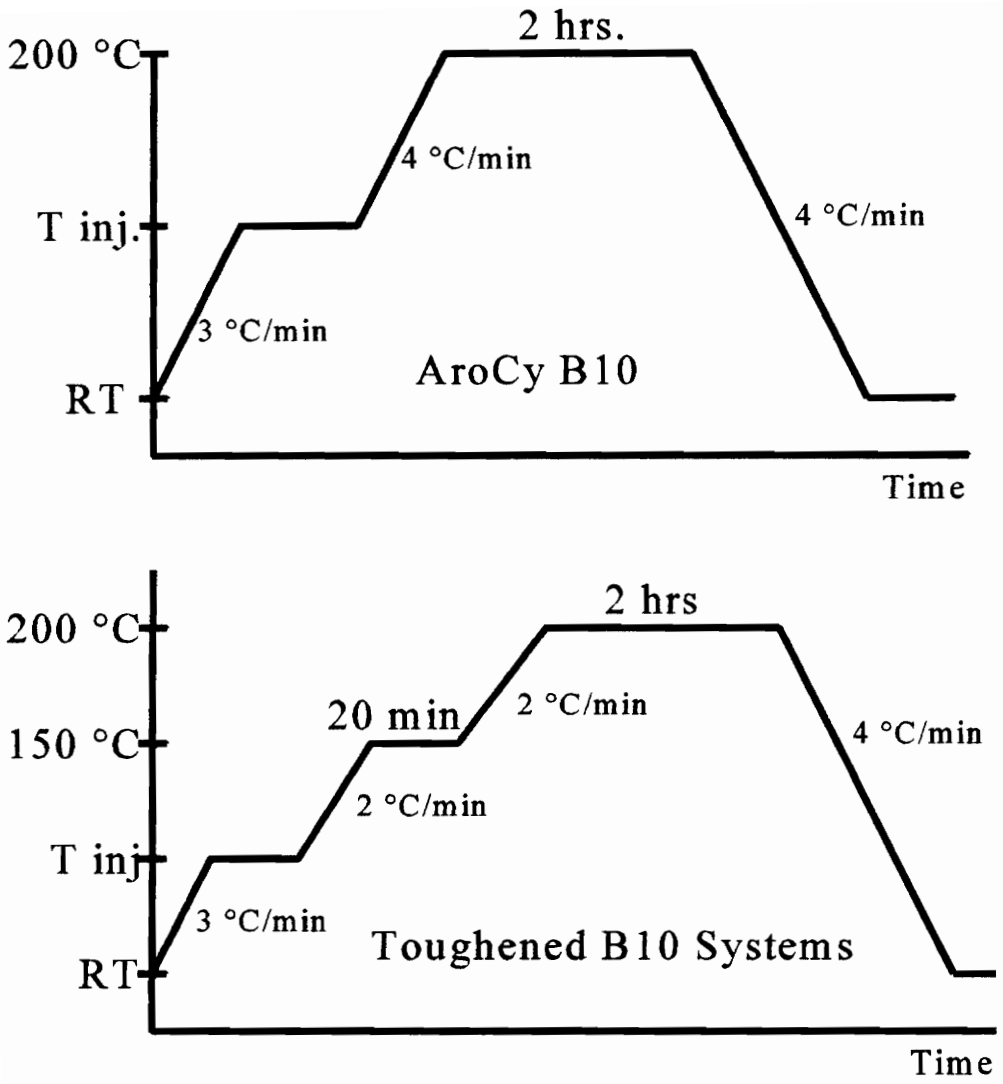


**Figure 3.3: Cure Cycles for AroCy B10 and Toughened B10 Systems.**

tests are denoted in Table 3.2 by "IOS".

All of the panels listed in Table 3.2 were cut for mechanical testing. The specimens from different panels were cut from the same locations in each panel. Although not intended to track properties as a function of position in the panel, it is useful to compare local void volumes or mechanical strengths of specimens taken from various locations in the panel. The panel edges and the region surrounding the inlet stem were avoided due to local variations in volume fraction or void content. A 3.2 mm (⅛ inch) separation from the edge is about standard. Shown in Figure 3.4 is the general layout for short block compression specimens. Interlaminar shear specimens were later cut from the remnants of these panels. Each specimen is given a designation indicative of the panel of origin and function. The suffixes A, B, and C were used to describe short block compression specimens to be tested in the warp direction of the fabric, while the suffixes X, Y, and Z denoted SBC specimens to be tested in the fill direction of the fabric.

Shown in Figure 3.5 is the layout of a typical 3.2 mm thick panel for impact testing. The four specimens for impact testing would use the suffixes IA, IB, IC, and ID. A similar layout diagram of 3.2 mm panels used for Iosipescu and reference compression is not available. The layout of these panels did not conform to a precise layout. Reference compression specimens were given the suffix R, or R1, R2, and R3 for those materials requiring multiple compression specimens. Three reference compression

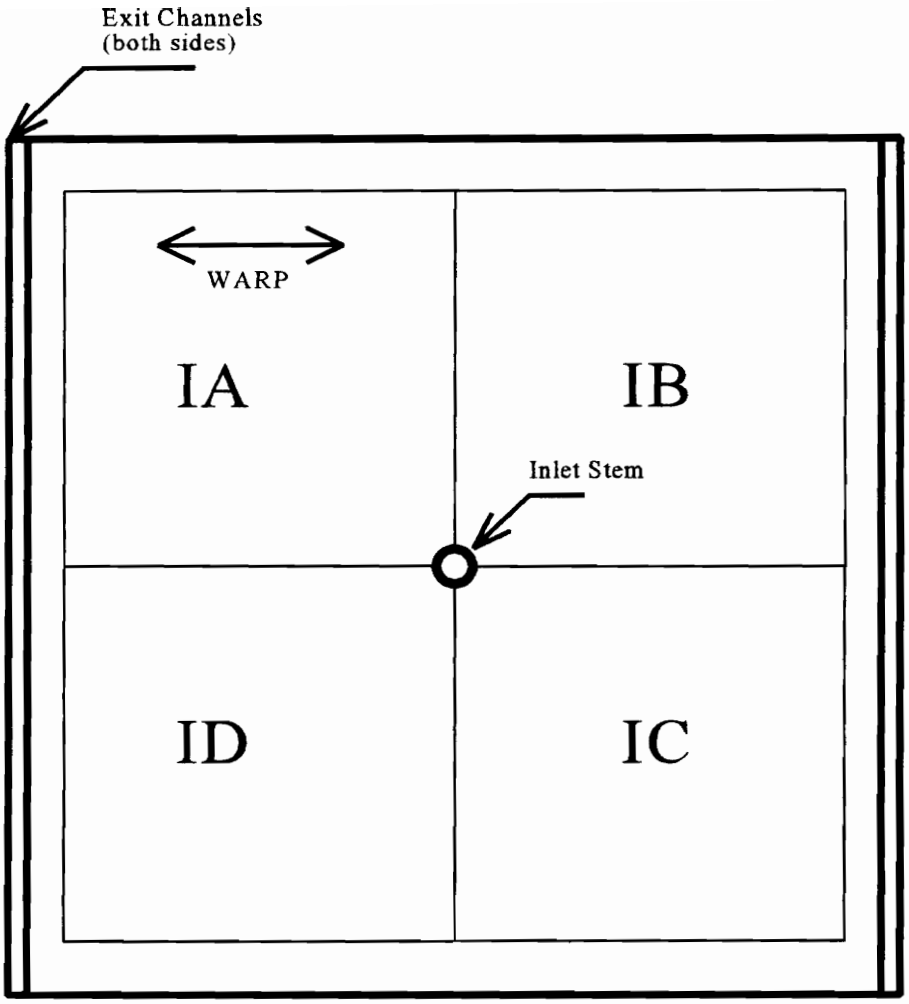


**Figure 3.5: Panel Layout for Impact Testing.**

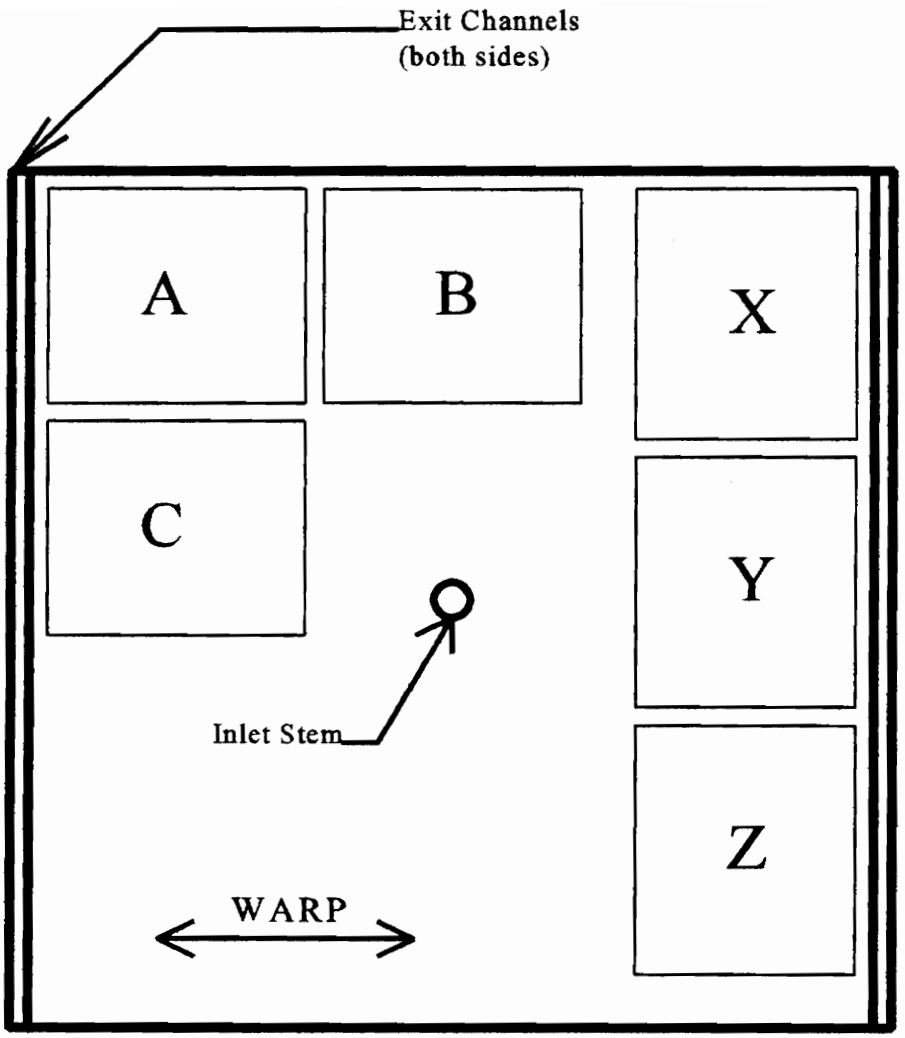


**Figure 3.4: Panel Layout for Short Block Compression Test Specimens.**

specimens were taken from panels containing the toughened cyanate esters, since no other compression tests of these materials were conducted. Iosipescu specimens were given the suffixes I, J, and K.

Figure 3.6 indicates the specimen layout of panels #31 - 33. Interlaminar shear specimens are denoted by the suffixes S1 through S6. Four point flex specimens, 12.5 mm wide by 127 mm in length, are denoted by F1 through F5. Three SBC specimens are taken (warp direction) from these panels, and are also denoted A, B, and C.

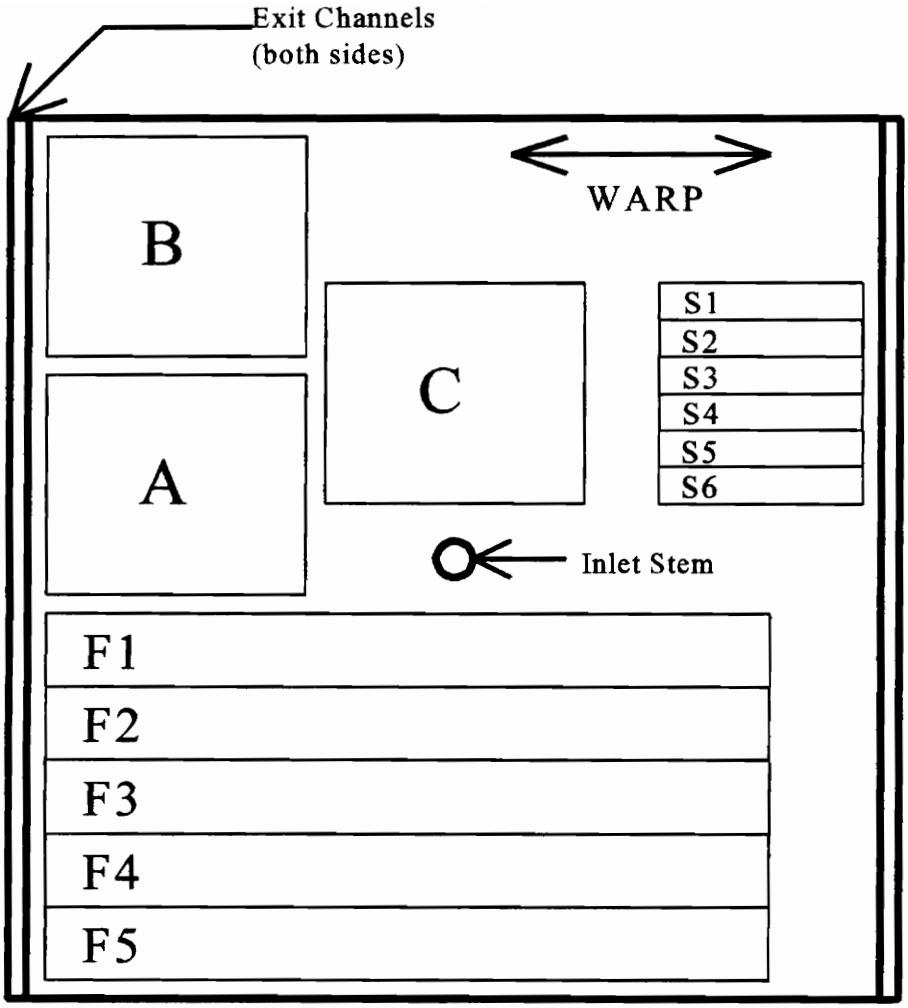


**Figure 3.6: Layout for Panels 31 - 33. Specimens were cut for SBC, SBS, and Flexure Tests.**

# Chapter 4: Physical Measurements

Weight, density, fiber volume fraction, and void content information were obtained for all specimens cut from the panels manufactured in this investigation. Calculations to find fiber volume fraction, based on preform areal weight, were performed as described in Chapter 2. Each specimen was also individually weighed in air and suspended in Isopropyl Alcohol to determine density and void content of the composite. The appendix contains the record of physical measurements for each specimen.

Several specimens were inspected by photomicrograph, to study void contents. A qualitative comparison of voids found in micrographs versus predicted void volumes is made. Some distinction is made between microvoids and macrovoids.

## 4.1 Volume Fraction and Void Fraction Measurements

In order to have accurate results for void calculations, accurate density and areal weight information must be obtained for the components. While areal weight calculations are fairly simple, obtaining good density numbers for fabrics and resins is more difficult. Densities for fabric samples are obtained in a similar manner to density measurements of the composite as a whole.

The density of the resin was obtained using the following procedure. Three

millimeter thick disks of resins were cast in a small mold containing a circular cavity. Once assembled the mold and resin will be placed in the computer-controlled hot press and subjected to the same cure cycle as a composite panel. Experience has shown considerable difficulty in removing bubbles from the resin disk prior to cure. The presence of bubbles in the disk will lead to error in density calculations. One technique used to reduce the void content of the neat resin is to degas the resin in a vacuum oven for several minutes before curing in the hot press. Remaining bubbles tend to form near the edges of the disk and can be trimmed off before measurement.

Table 4.1 contains the areal weight and density information for the resins and fabrics. Densities given by manufacturers were found to generally be accurate, and are given in the third column for comparison. The resin densities of the neat samples will be assumed to be the same for resin in the composite. In practice this is not always the case. Resin in the composites has been shown to have a slightly lower density than neat samples. This will result in an indication of slightly lower than true void content in all samples **(25)**. This may be in part a result of some unanticipated open void volume in the composites. A preliminary measurement of open and closed voids indicated a very low open void volume, but a few specimens may have surface voids or delaminations which extend well into the composite.

Table 4.2 presents the average fiber volume fractions and void contents for each panel. Fiber volume fractions as determined by the areal weight and density techniques are presented in Table 4.2 These calculations were carried out as described in Chapter 2.

**Table 4.1: Areal Weight / Density Data for Materials Used in This Study.**

| Material | Areal Weight As Measured ($g/m^2$) | Material Density As Measured ($g/cm^3$) | Manufacturer's Material Density ($g/cm^3$) |
|---|---|---|---|
| Style 162 e-glass Plain Weave | 391.8 | 2.565 | 2.4 |
| AS-4 Plain Weave, Sized | 193 | 1.78 | 1.8 |
| AS-4 Plain Weave, Unsized | 193 | 1.77 | 1.8 |
| Derakane 441-400 Vinyl Ester | N/A | 1.173 | 1.2 |
| Shell RSL-1895 Epoxy | N/A | 1.184 | 1.18 |
| AroCy B10 Cyanate Ester | N/A | N/A | 1.21 |
| VTUFF 1520 Toughened Cyanate Ester | N/A | 1.22 | N/A |
| VTUFF 1525 Toughened Cyanate Ester | N/A | 1.22 | N/A |

**Table 4.2: Fiber Volume Fractions and Void Contents of Each Panel.**

| Panel Number | Panel Materials | Avg. Fiber Volume Fraction | Highest Fiber Volume Fraction | Lowest Fiber Volume Fraction | Avg. Void Volume Fraction | Void Fraction Standard Deviation |
|---|---|---|---|---|---|---|
| 02 | 162 E-glass - DK 441-400 | 0.5459 | 0.5474 | 0.5452 | 0.02079 | 0.00375 |
| 04 | 162 E-glass - RSL-1895 | 0.5451 | 0.5478 | 0.5435 | -0.01247 | 0.0686 |
| 1 | AS-4/PW/S -DK 441-400 | 0.607 | 0.6166 | 6003 | 0.01848 | 0.0062 |
| 2 | AS-4/PW/S - DK 441-400 | 0.5722 | 0.5735 | 0.5696 | 0.00666 | 0.01478 |
| 4 | AS-4/PW/U - DK 441-400 | 0.5722 | 0.5774 | 0.5678 | 0.01027 | 0.00276 |
| 5 | AS-4/PW/S - AroCy B10 | 0.5804 | 0.5849 | 0.5748 | 0.01662 | 0.00837 |
| 6 | AS-4/PW/S -VTUFF 1525 | 0.592 | 0.5932 | 0.5909 | 0.02528 | 0.00337 |
| 8 | AS-4/PW/S - RSL-1895 | 0.6037 | 0.6064 | 0.6021 | 0.02066 | 0.00184 |
| 11 | AS-4/PW/U - DK 441-400 | 0.6142 | 0.6186 | 0.6108 | 0.0136 | 0.00206 |
| 12 | AS-4/PW/S - DK 441-400 | 0.6093 | 0.6108 | 0.6069 | 0.01658 | 0.00927 |
| 14 | AS-4/PW/S- VTUFF 1525 | 0.5562 | 0.5578 | 0.5499 | 0.0055 | 0.00176 |
| 15 | AS-4/PW/S - RSL-1895 | 0.5835 | 0.5866 | 0.5778 | 0.02019 | 0.00108 |
| 16 | AS-4/PW/S - RSL-1895 | 0.606 | 0.6127 | 0.604 | 0.015 | 0.00743 |
| 18 | AS-4/PW/U - DK 441-400 | 0.607 | 0.6146 | 0.5939 | 0.00741 | 0.00375 |
| 19 | AS-4/PW/S - AroCy B10 | 0.6064 | 0.6079 | 0.605 | 0.01031 | 0.00034 |
| 20 | AS-4/PW/S -VTUFF 1520 | 0.588 | 0.5936 | 0.5845 | 0.01565 | 0.00192 |
| 21 | 162 E-glass - DK 441-400 | 0.5332 | 0.5363 | 0.5319 | 0.00939 | 0.00195 |
| 24 | 162 E-glass - DK 441-400 | 0.5344 | 0.5388 | 0.5304 | -0.00029 | 0.00396 |
| 25 | AS-4/PW/S- VTUFF 1520 | 0.5824 | 0.5849 | 0.58 | -0.01304 | 0.01102 |
| 27 | AS-4/PW/S- VTUFF 1525 | 0.5792 | 0.5859 | 0.5739 | 0.0186 | 0.00616 |
| 31 | AS-4/PW/S - RSL-1895 | 0.6042 | 0.6013 | 0.606 | 0.01277 | 0.00588 |
| 32 | AS-4/PW/S - RSL-1895 | 0.605 | 0.607 | 0.6022 | 0.0104 | 0.0034 |
| 33 | AS-4/PW/S - RSL-1895 | 0.6021 | 0.6041 | 0.6003 | 0.01081 | 0.00801 |

The average fiber volume fraction (left bar, left axis) and void content (right bar, right axis) for several of the materials systems are shown graphically in Figures 4.1 - 4.5.

Figure 4.1 indicates the range of fiber volume fractions and void volumes for panels made with 162 E-glass. Note that, as calculated, several of the void volumes approach or are actually below zero. This could be an indication that resin density in the composite could be far less than bulk resin density. It would seem that panel 04, having an indicated void content of negative 1.25%, should be void-free. This will be verified with photomicrographs.

Figure 4.2 shows the fiber volume fractions and void volumes for Derakane 441-400 composites made with sized and unsized AS-4 fabrics. In the graph, the sized panels and unsized panels are denoted by a "S" or "U", respectively, beside the panels number. Although there appears to be no significant variation in fiber volume fraction, void volume fractions appear to be slightly lower, on average, for the panels made with unsized fibers. An exception to this is panel #2, which had quite a low average void content.

Figure 4.3 represents fiber volume fractions and void fractions for sized AS-4 composites made with Shell RSL - 1895 resin. Fiber volume fraction varies little within this group. The panels fabricated with different injection temperatures (panels # 31, 32 and 33) have very close fiber volume fractions. Void content in the injection temperature variance panels drops slightly with increasing temperature.

Figure 4.4 represents fiber volume fraction and void measurements for panels

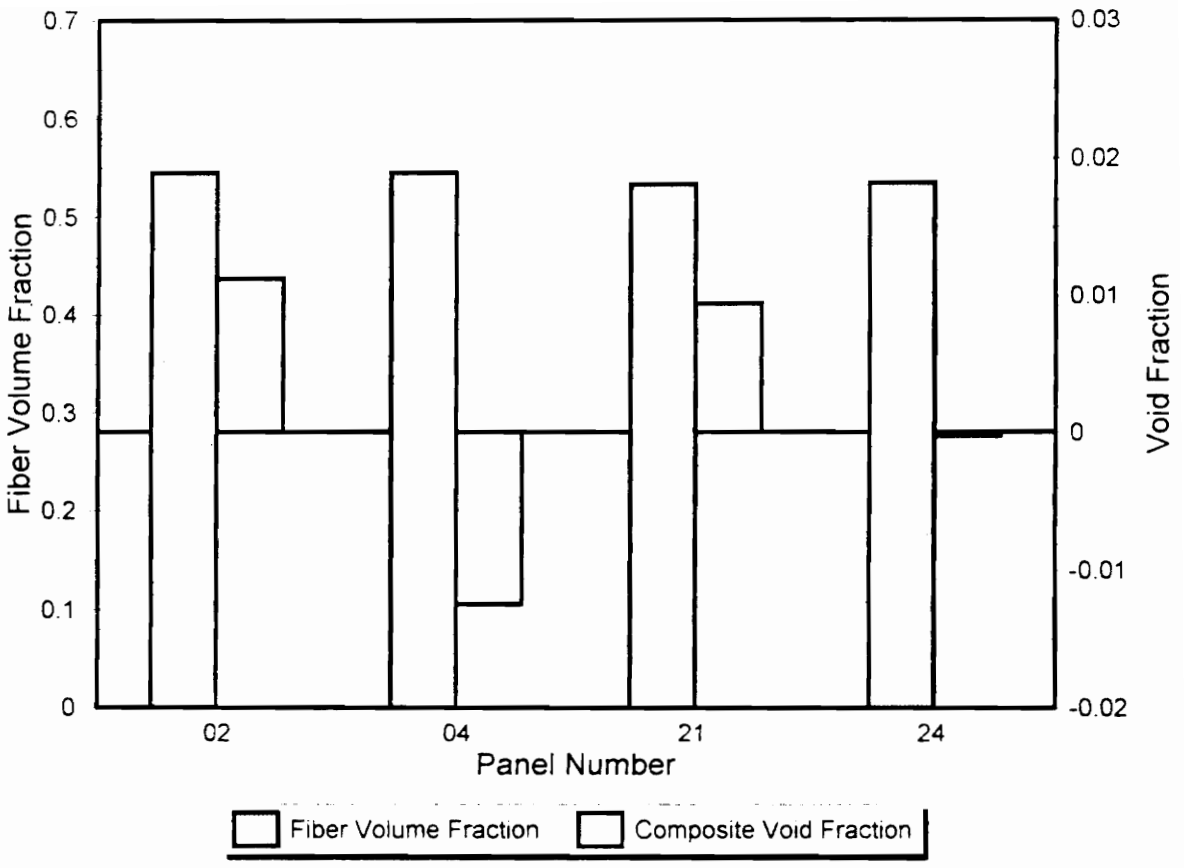


**Figure 4.1: Fiber Volume Fractions and Void Volume Fractions for 162 E-glass Composites.**

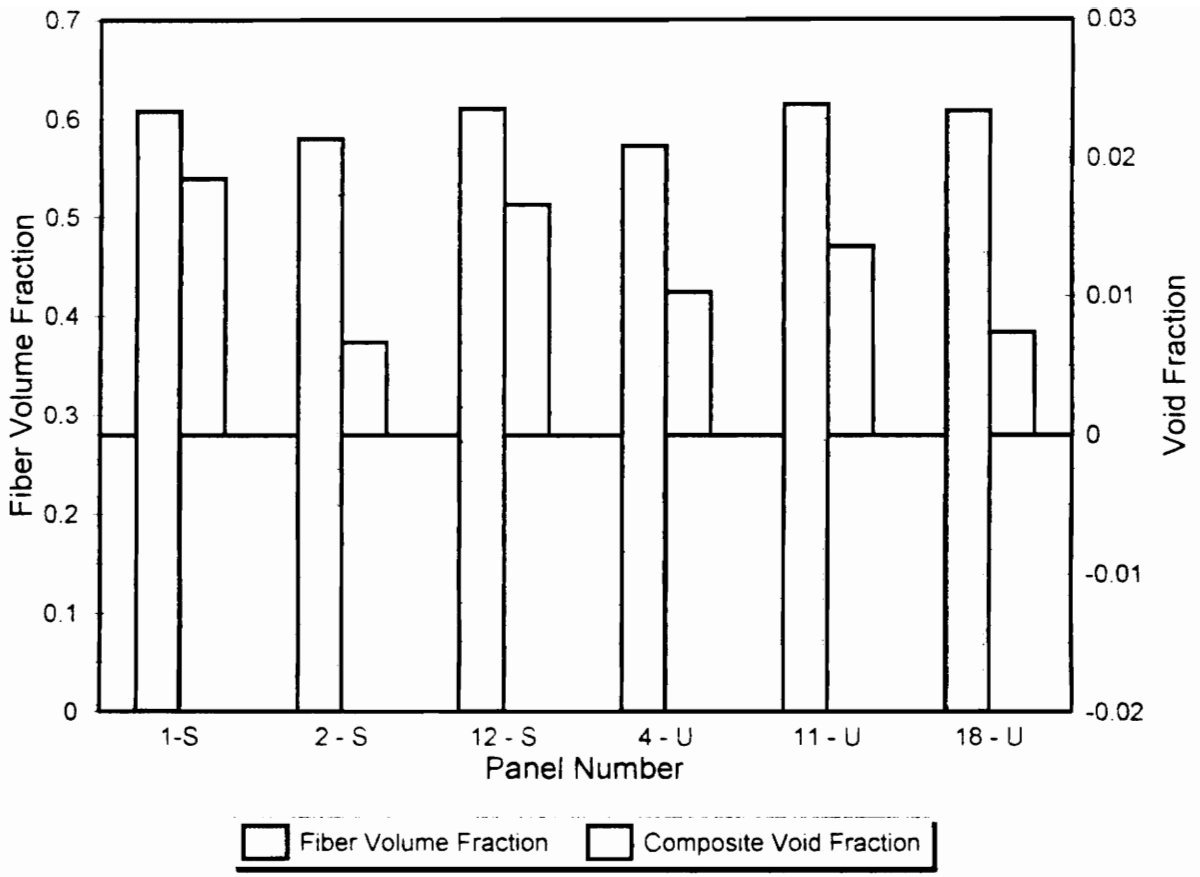


**Figure 4.2: Fiber Volume Fractions and Void Volume Fractions of Derakane Composites with Sized (-S) and Unsized (-U) AS-4 Fabrics.**

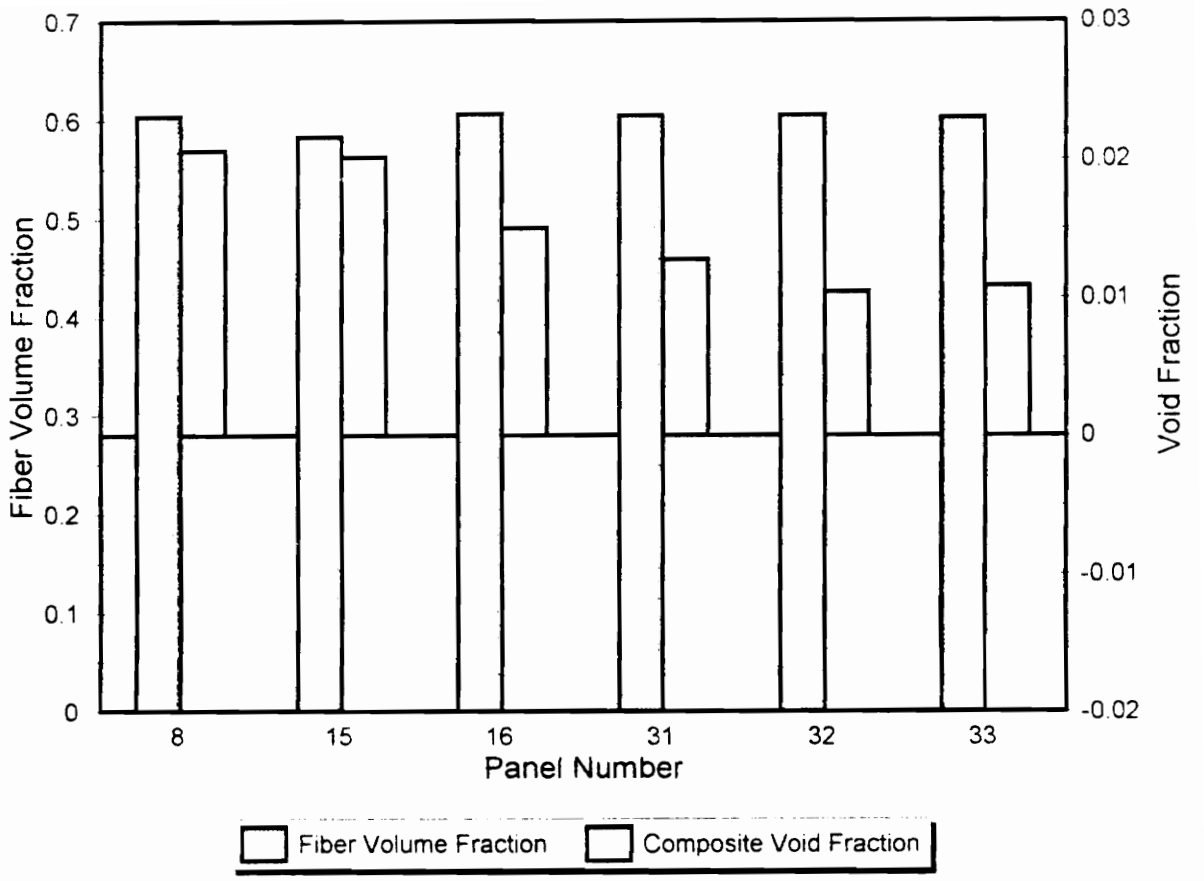


**Figure 4.3: Fiber Volume Fractions and Void Volume Fractions of RSL-1895 Composites.**

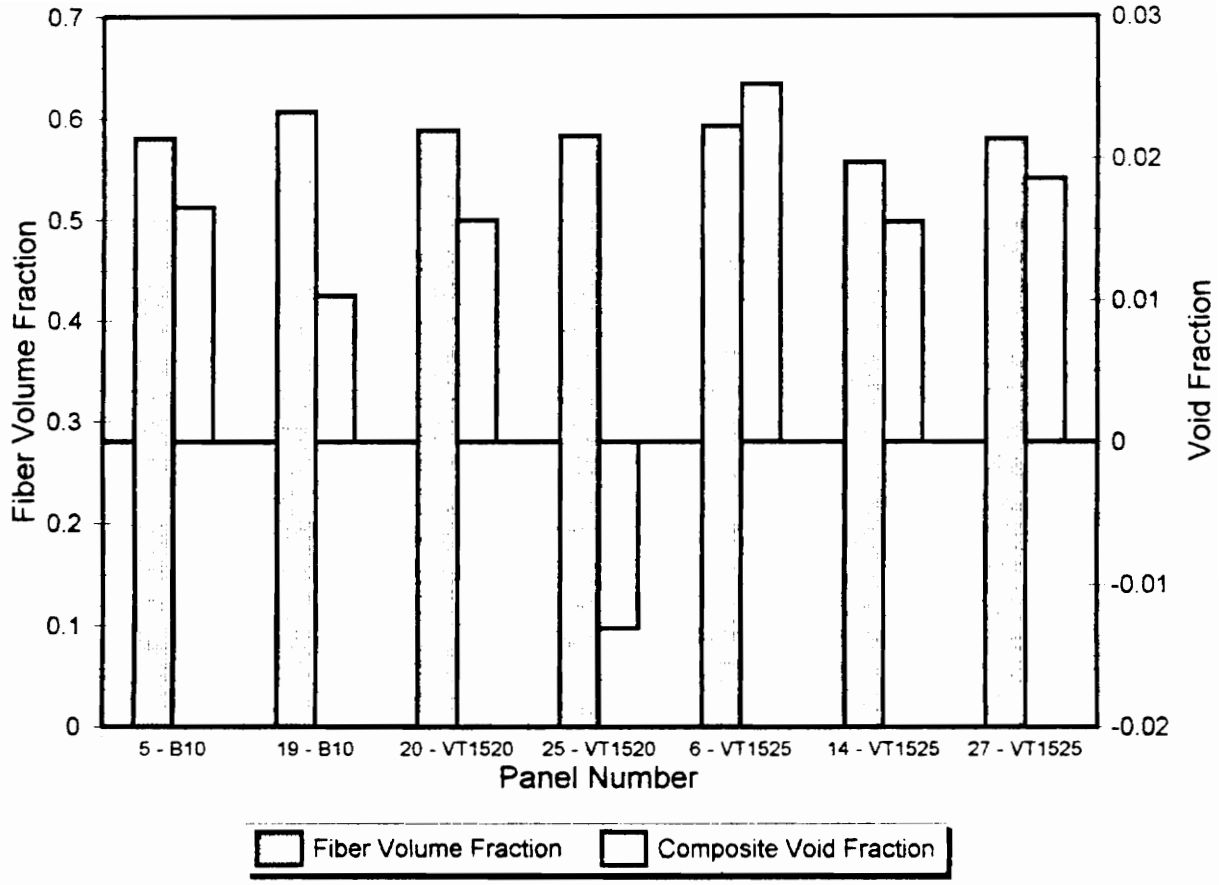


**Figure 4.4: Fiber Volume Fractions and Void Volume Fractions of B10 Cyanate Ester System Panels.**

made with the AroCy B10 and toughened VTUFF series resins. These appear to show a trend toward more voids as the toughener content increases. A representative VTUFF1525 resin panel processed by resin film infusion will be studied by optical micrograph in the following section.

The data given in Table 4.2 indicate that a relatively narrow range of void contents exist in the manufactured panels. Panel averages run from void-free, such as panel #04, to nearly 3% voids, as in panel #6. It should be noted again that slight inaccuracies in resin density, due to the difference between densities in the composite and in the bulk, will tend to lower the apparent void content. This may cause the calculated void content of Panel #04 to be negative. Obviously the panel cannot have a negative void volume. However, a good argument can be made concerning the relative void volumes of each composite sample. Certainly void content of specimens from Panel #6 would be considered far higher than those taken from Panel #04.

Since absolute void contents are not known, panels will be classified into one of three categories, based on calculated void contents. Those panels having an average calculated void content under about 0.7 - 1.0% will be considered "void free". This is not to say that the composite truly has no voids, but instead that the void content is very low and probably has little effect on the composite properties. The second classification involves panels with calculated void contents between about 1% and 2%. These will be considered "low" void content panels. Finally, panels containing about 2% calculated void volume or above will be considered to have a "high" void volume. These

classifications are necessary for micrograph confirmation of void contents. Photomicrographs will be taken of panels from each classification and compared. If a qualitative comparison of void content by micrograph matches the calculated values trends, then the calculation can be considered reasonably valid.

A close look at void fractions calculated for individual specimens shows considerable variation in some panels. Some of these variations appear to be related to locations in the panel, while others appear to be random. As an example, consider Panel #2, made from sized AS-4 plain weave and Derakane 441-400, and its four impact specimens. Void calculations indicate that three of the specimens contain almost no voids. However, the fourth impact specimen is calculated to have nearly a 3% void volume. Each of these specimens comprises about one quarter of the panel. There appears to be no obvious reason for a single quadrant to contain more voids than the others. Another example could be panel #16, made from sized AS-4 plain weave fabric and RSL-1895 epoxy. Short block compression specimens taken from this panel have a high void content, generally above 2%. The void calculations for interlaminar shear specimens taken from this panel, however, indicate voids of 1% or lower. In this case, short block specimens were cut from the periphery of the panel, while interlaminar shear specimens came from the interior.

## 4.2 Optical Micrographs

Optical photomicrographs were used to examine the microstructure of the composites generated in this study. Samples of panels calculated to have high and low void contents were polished and viewed at several magnifications. Representative photomicrographs of several of these panels are presented in the following series of figures. Included are photos of most materials systems, including AS-4 with RSL-1895, AroCy B10, VTUFF1525, and Derakane 441-400 resin systems. Derakane 441-400 panels reinforced with 162 E-glass, and sized and unsized AS-4 were also examined.

Inspection of micrographs can be used to determine the ability of density-based calculations to predict void content. Photos of several panels predicted to have significant amounts of voids were compared with those expected to have relatively few voids. Whenever possible, high and low void content panels of similar material systems are compared.

Some problems can exist when comparing void contents to calculated results. The void fractions given in Table 4.2 are averages, based on measurements taken from mechanical specimens. These calculations show that void content can vary significantly with location in the panel. Laminate sections for micrograph comparison are taken from scrap material, left after mechanical specimens have been cut. Void content can vary with position in the panel, which can lead to difficulties. An example of this is panel #2, which indicated very low voids for three of its four impact specimens, but indicated a

void content of more than 2% in the fourth.

Four panels, considered to have fairly high void contents (>1.5% voids) were selected for study. The first two examples, from panels #6 and #8, contain more than 2% voids and fit into the "high void content" category. The second pair, from panels #1 and #5, contain less than 2% voids, and therefore fit into the "low void content" category. Each of these panels are made with sized AS-4 fabric, and each contains a different matrix material.

Micrographs taken from panel # 6 are shown in Figure 4.5. Panel #6 was a panel of sized AS-4 fabric and VTUFF 1525 resin, which did not fully infiltrate. These two photographs clearly show large and, in some cases, extensive voids which exist between tows and between plies. The top photo is centered on the largest voids found in the samples. Many areas contained fewer and smaller voids, as shown in the lower photo. The calculation predicted a void content for this panel of over 2.5%. These photographs confirm a high void content. Scales on the photographs represent a distance of 0.05 mm.

Figure 4.6 shows a photomicrograph taken from panel #8, which was predicted to have about a 2.0% void content. Panel # 8 is made with sized AS-4 fabric and RSL-1895 epoxy resin. Despite the prediction, the sample used in the micrograph contained few readily apparent voids. Figure 4.6 represents the only macrovoid found in the cross-section. A similar result is found in Figure 4.7, which shows a photomicrograph of Panel #1. Panel # 1 was made from sized AS-4 and Derakane 441-400, and was expected to have 1.8% voids. Patches of microvoids can be seen in Figure 4.7, but it cannot be

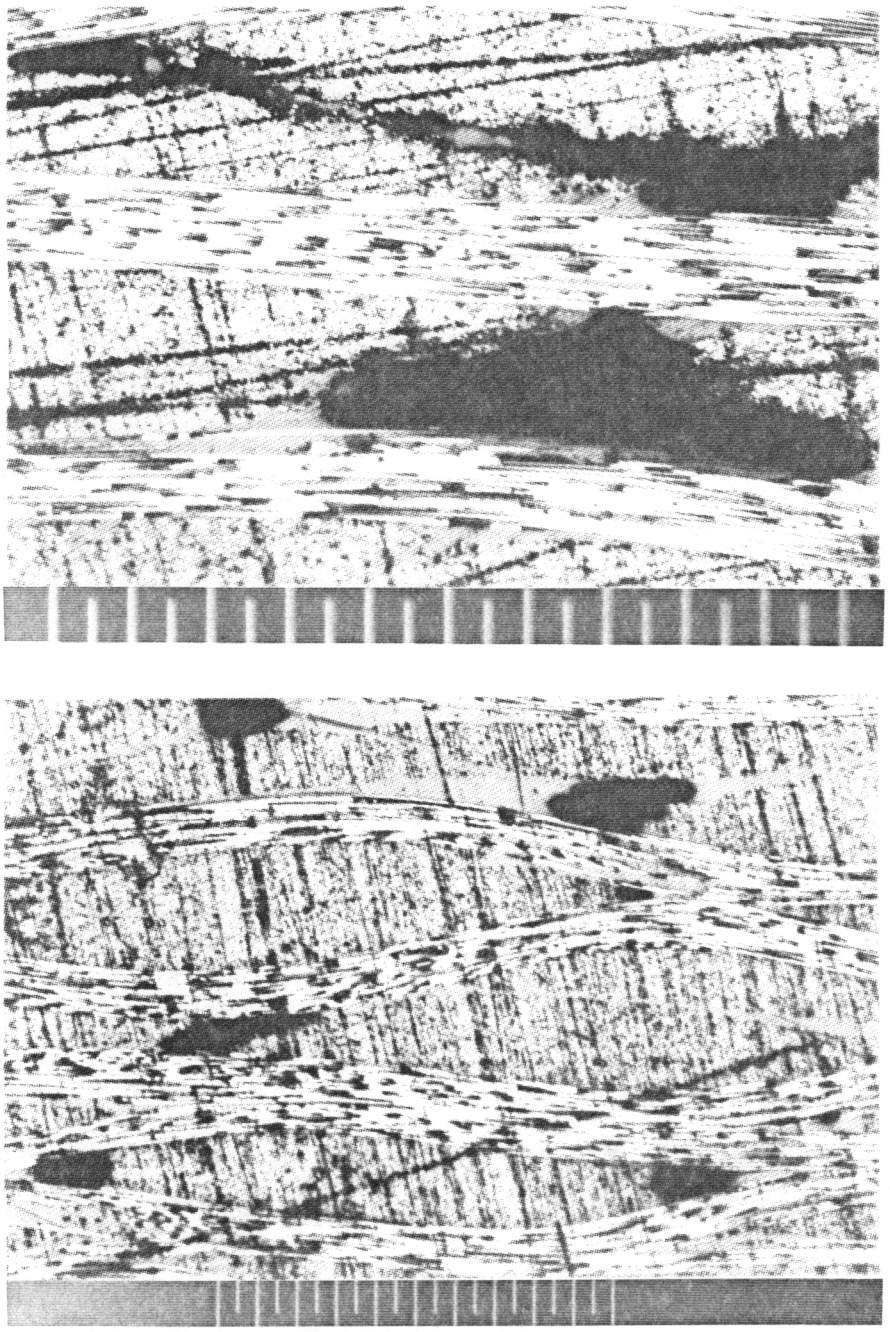

**Figure 4.5: Micrographs of Panel #6, AS4/PW/S and VTUFF 1525 (RTM Processed) Scale represents 0.05 mm.**

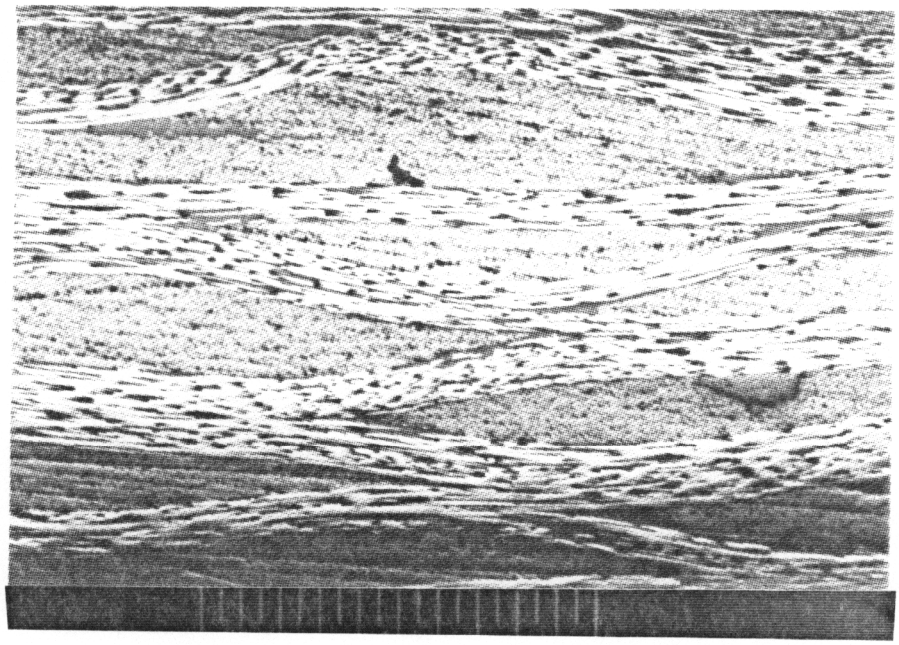

**Figure 4.6: Micrograph of Panel #8, AS4/PW/S and RSL-1895 Scale represents 0.05 mm.**

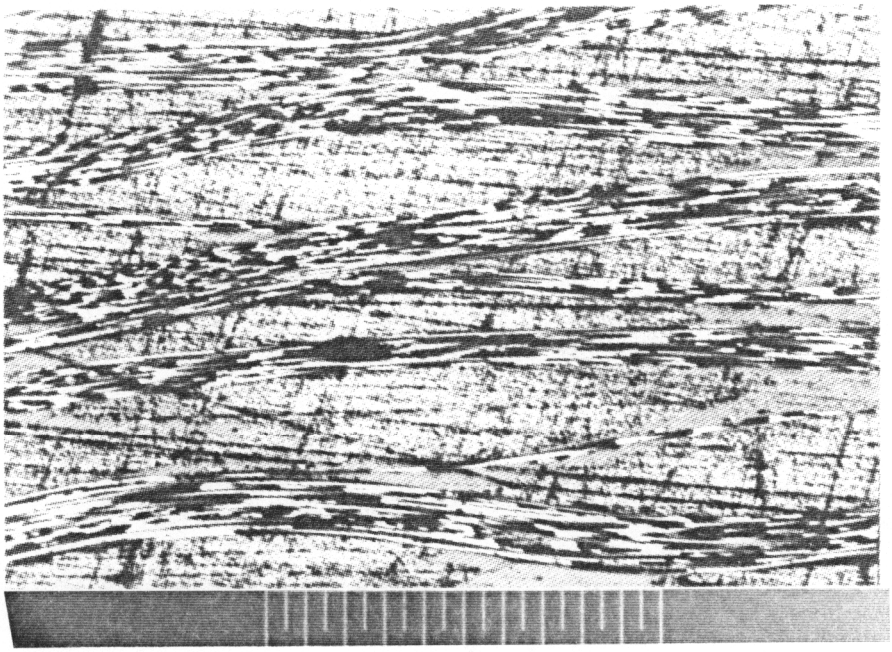

**Figure 4.7: Micrograph of Panel #1, AS4/PW/S and Derakane 441-400 Scale represents 0.05 mm.**

determined if a high void content exists in the panel. There was a significant variation in void contents in the specimens selected from panel #1 for SBC and SBS. It is possible that the micrograph specimen came from a region of relatively low void content.

Figure 4.8 shows micrograph results for panel #5, which was predicted to contain about 1.7% voids. Panel # 5 is made from sized AS-4 fabric and AroCy B10 resin. The two photos show a series of small macrovoids between tows, which seem to support the prediction of void content. The sized AS-4 fabric contains tracer threads of Kevlar. The top photo in Figure 4.8 shows a number of small voids formed near such a tracer tow. The second photo shows macrovoids formed between tows in several plies.

A second set of micrographs were prepared, taken from panels predicted to have very low void contents. These specimens have a void volume fraction of less than 1 %. Figure 4.9 contains two photos, taken of a section of panel #18. Panel #18 was made from Derakane 441-400 resin and unsized AS-4 fabric. Calculations predicted less than 1% voids for this panel. The top photo shows a section spanning several plies. No large voids are evident. The lower photograph shows a microvoid region within a tow. Here a smaller scale, with marks indicating 0.01 mm, is used.

Figures 4.10 and 4.11 contain micrographs taken from a panel made from Derakane 441-400 resin and style 162 E-glass fabric, panel #21. The density calculations predicted a low (0.9%) void content. The photographs in Figure 4.10 show a number of voids concentrated between plies. These photos were taken from a section fairly close to the center of the panel. These voids also appear to be concentrated in a region of

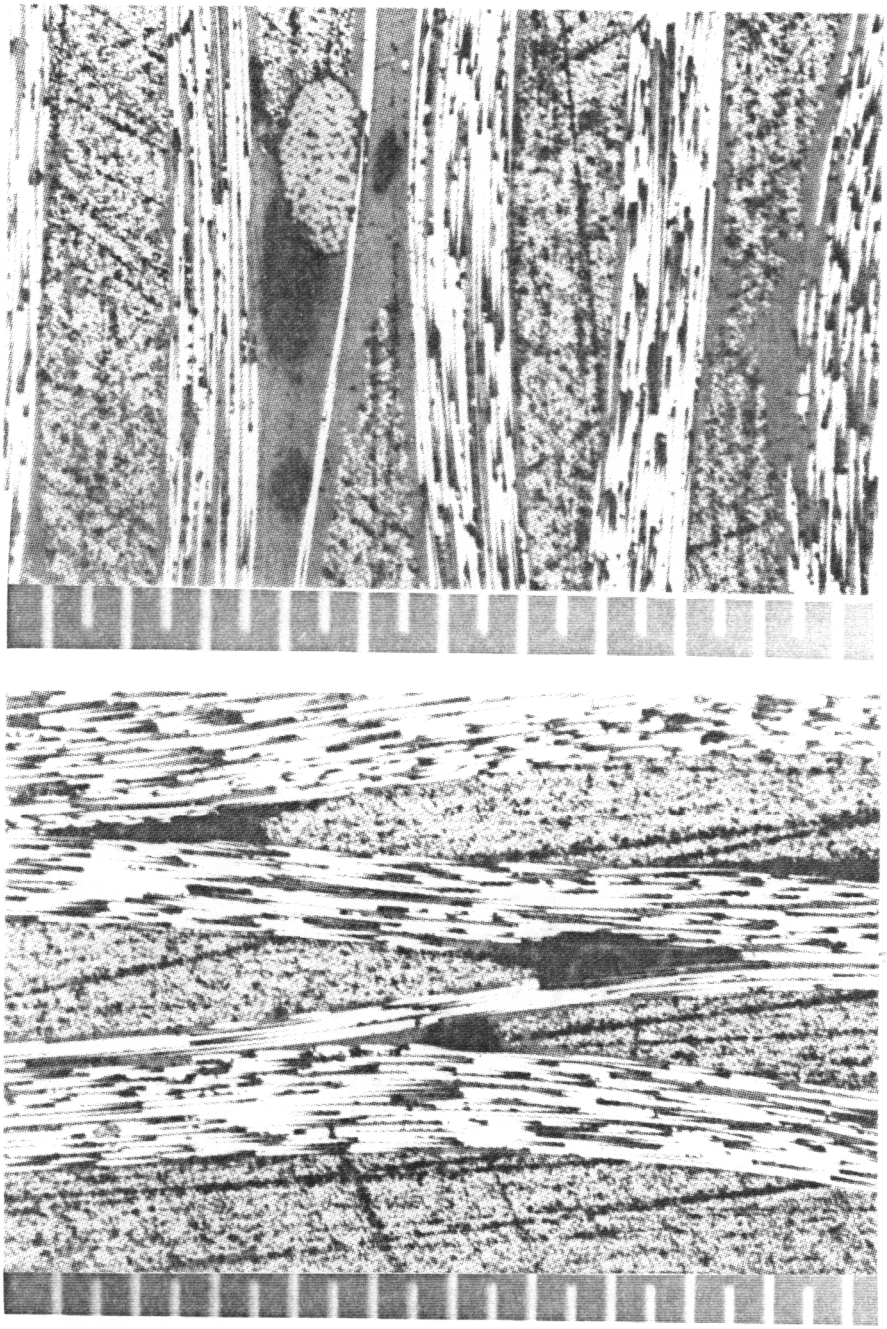

**Figure 4.8: Micrographs of Panel #5, AS4/PW/S and AroCy B10 Scale represents 0.05 mm.**

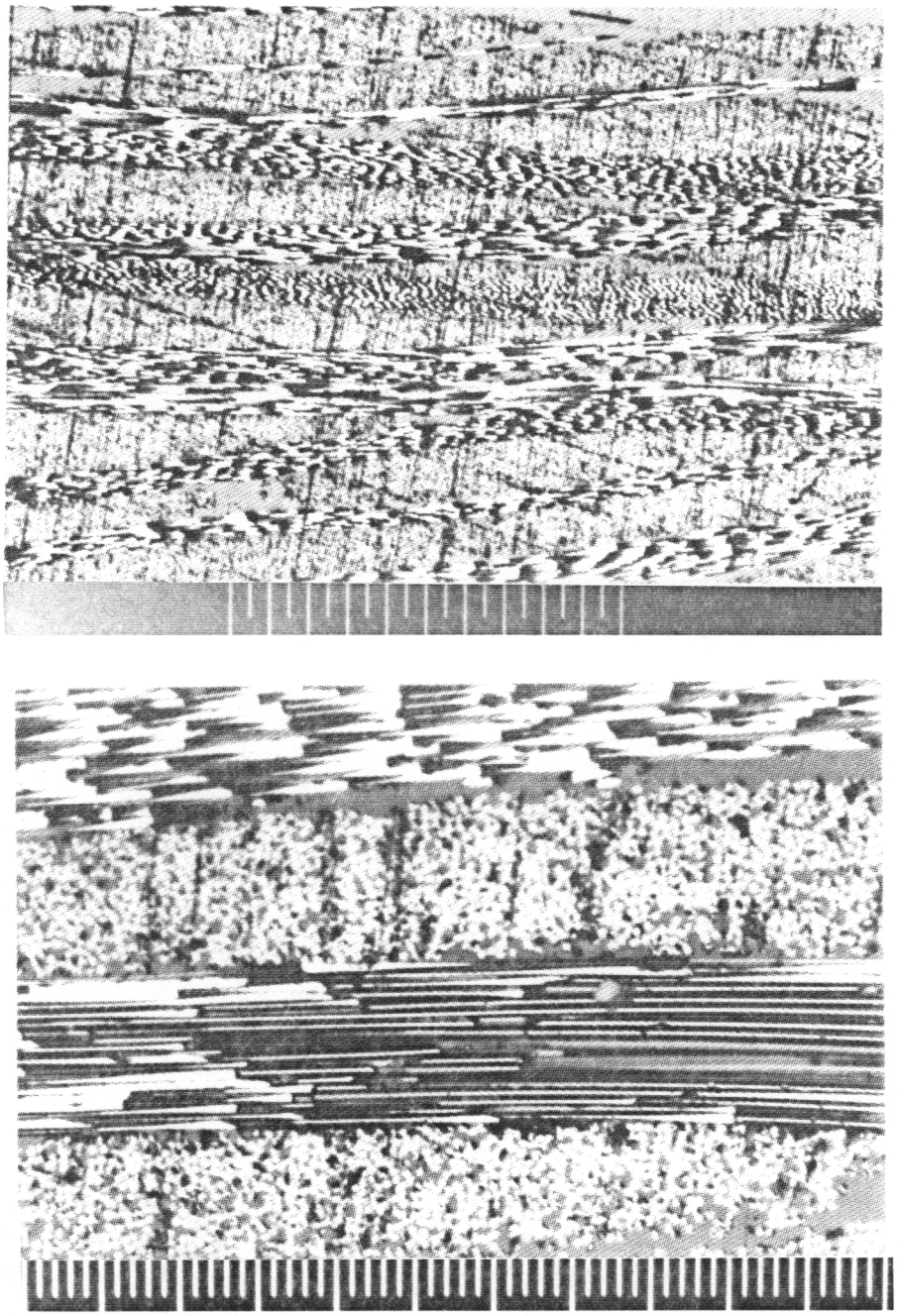

**Figure 4.9: Micrographs of Panel #18, AS4/PW/U and Derakane 441-400 Top and bottom scales represents 0.05 and 0.01 mm, respectively.**

**Figure 4.10: Micrographs from Center of Panel #21, Style 162 E-glass and Derakane 441-400. Scale represents 0.05 mm.**

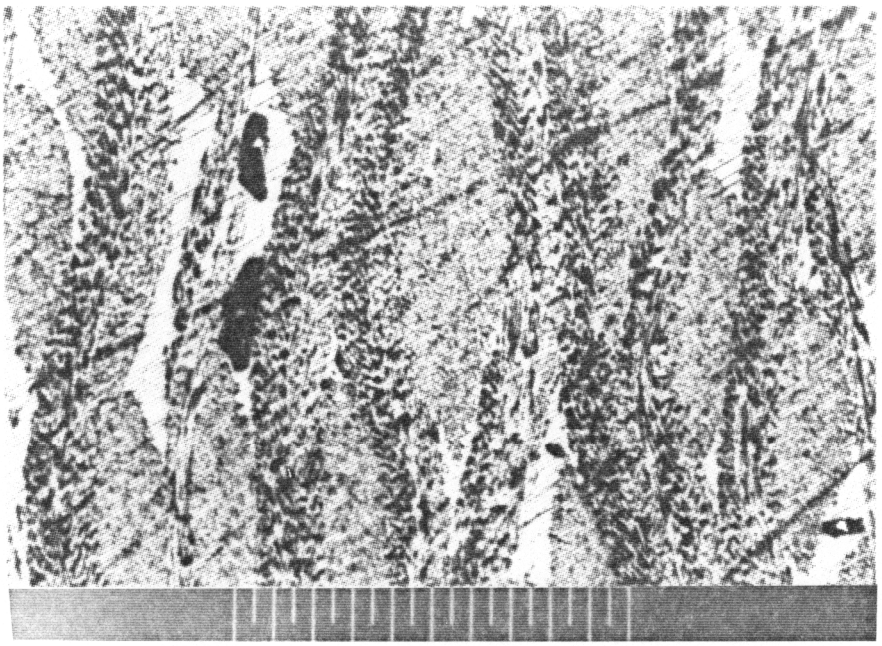

**Figure 4.11: Micrograph from Edge of Panel #21, Style 162 E-glass and Derakane 441-400. Scale represents 0.05 mm.**

relatively low fiber volume fraction. The photograph in Figure 4.11, however, was taken from a sample cut near the edge of the panel. This specimen contained far fewer voids than those from the panel center. Micrographs of specimens taken about halfway between the center and edge, not shown here, indicate an intermediate number of voids. On average, this panel appears to contain a higher void content than predicted. The panel appears to be in the 2% or greater (high void) category of void content.

Figure 4.12 contains two micrographs taken of panel # 04, made from Shell RSL-1895 resin and style 162 E-glass fabric. The density calculation actually predicted a negative void content of 1.25%. The two photographs were taken from different locations within the panel. No voids of any kind were found in either specimen. Despite the excessively low void prediction, the calculation has shown that the panel is truly "void-free".

Figure 4.13 contains micrographs taken from panel #14, made with sized AS-4 fabric and VTUFF 1525 resin, by the Resin Film Infusion process. There are no large voids evident in either of these photographs, although some microvoid regions can be seen in the lower photo. These results would appear to match the density calculation, which predicted about 0.5% voids.

A direct comparison was also conducted of void contents in Derakane panels with sized and unsized AS-4 fabric. Micrographs were made of panel #2, a sized AS-4 fabric panel, and #4, an unsized AS-4 fabric panel. Panel #2 was predicted to have voids of below 1%, while #4 was predicted to have about 1% voids. Figure 4.14 contains photos

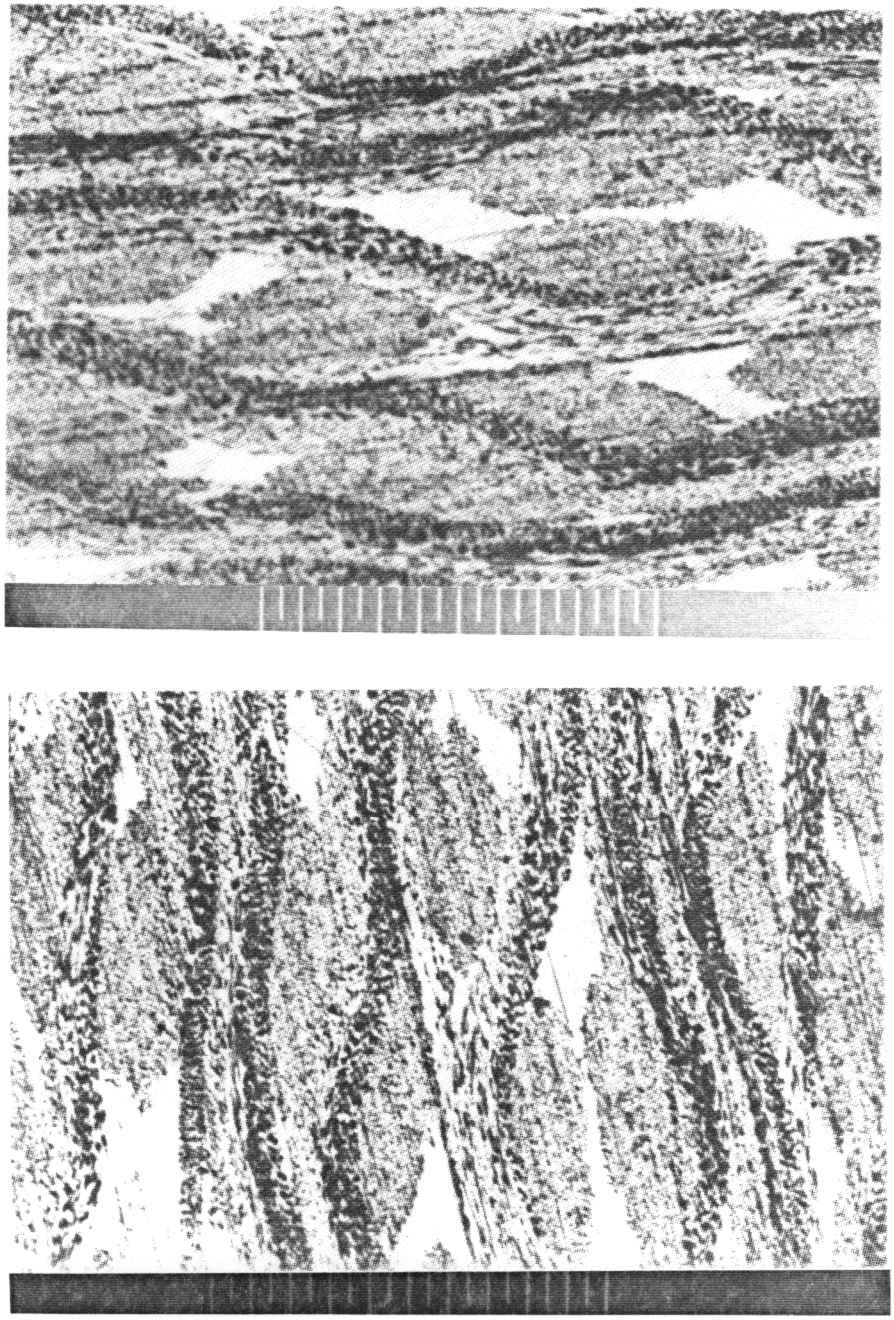

**Figure 4.12: Micrograph of Panel #04, Style 162 E-glass and RSL-1895 Scale represents 0.05 mm.**

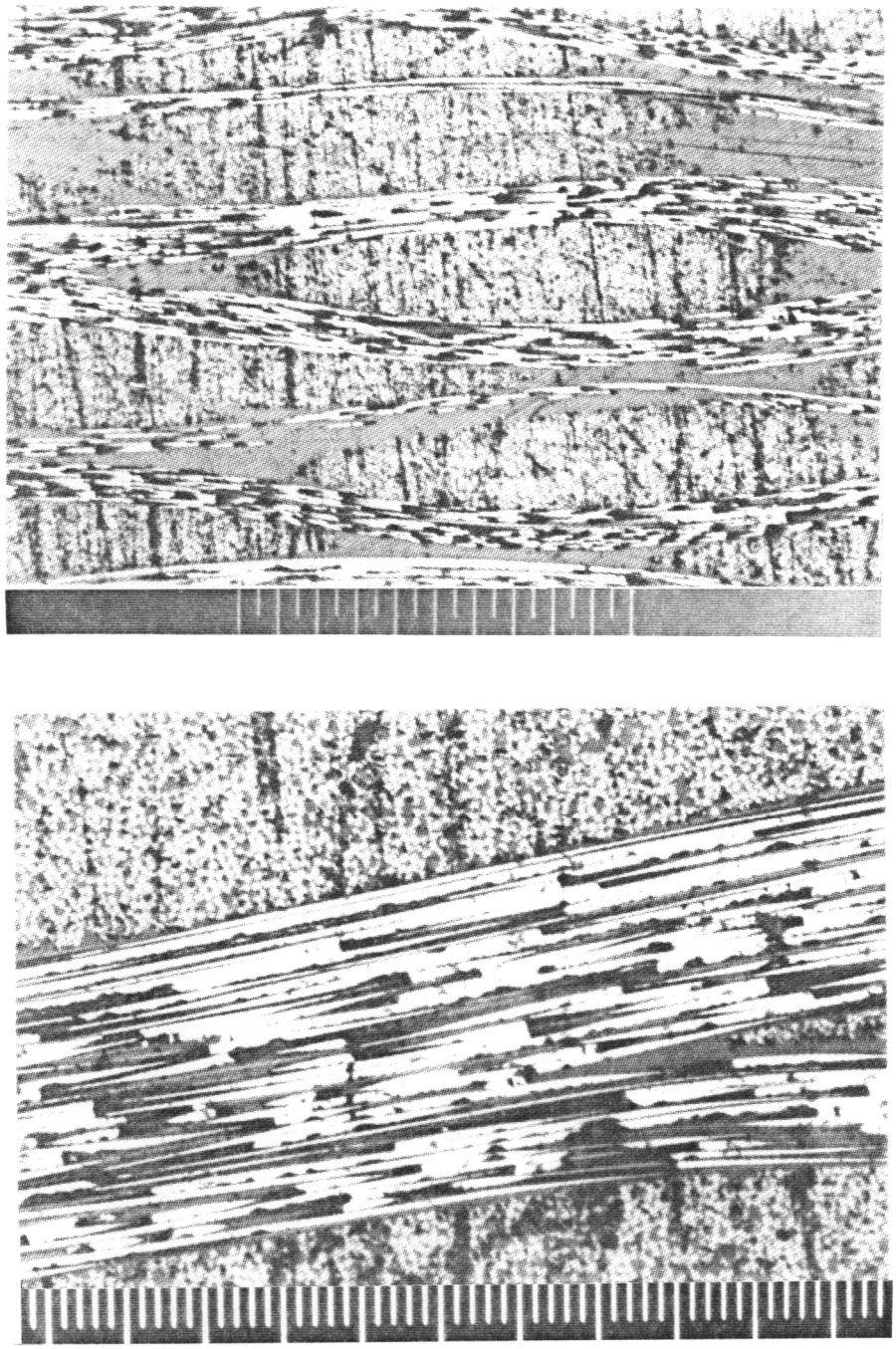

**Figure 4.13: Micrographs of Panel # 14, AS4/PW/S and VTUFF 1525 (RFI Processed) Scales represent 0.05 and 0.01 mm, respectively.**

of panel #2, and shows that the void content is indeed very low. The top photo shows a representative section, with only a few sparse voids. The lower photo shows a typical ply interface. Figure 4.15 shows photos for panel #4, with the unsized fiber. The panel has a few more voids than panel #2, but does not have a high void content. The lower photo of Figure 4.15 shows a pair of voids which formed between plies. Micrographs appear to support the calculated prediction that panel #4 has more voids than #2 but neither contains a large concentration of voids.

Micrograph specimens were polished and examined for each RSL-1895 panel used in the injection temperature study. Figure 4.16 shows photographs taken from panel #31, injected at 65°C. Portions of this panels contained several large macrovoids, as shown in the top photo. The panel contained very few microvoids, however, as shown in the lower photograph. Micrographs of panel #33, injected at 75°C, shows fewer voids (Figure 4.17). The top photograph in Figure 4.17 shows a small group of macrovoids between tows. The lower photo covers a larger area. Notice that, although a few microvoids exist, most of the panel is free of macrovoids. Figure 4.18 shows photographs taken from panel #32, which was injected at 85°C. This panel shows even fewer voids than the previous panels. A single macrovoid was found in this sample, as shown in the top photograph of Figure 4.18. The lower photo shows microvoids within two neighboring tows. The micrograph evidence for these panels supports the density calculations, which suggest a drop in void content with increasing temperature.

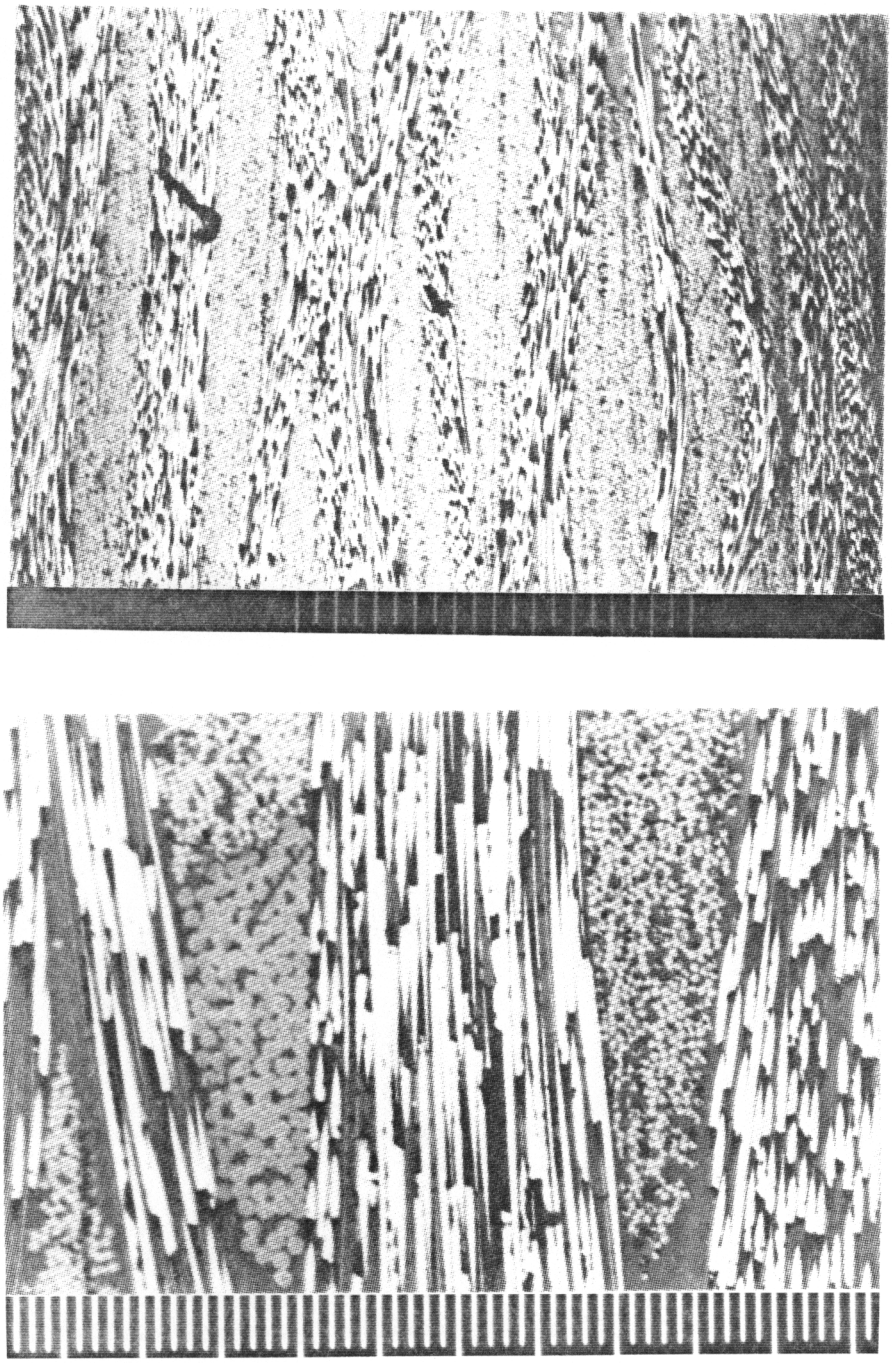

**Figure 4.14: Micrographs of Panel #2, AS4/PW/S and Derakane 441-400 Top and bottom scales represent 0.05 and 0.01 mm, respectively.**

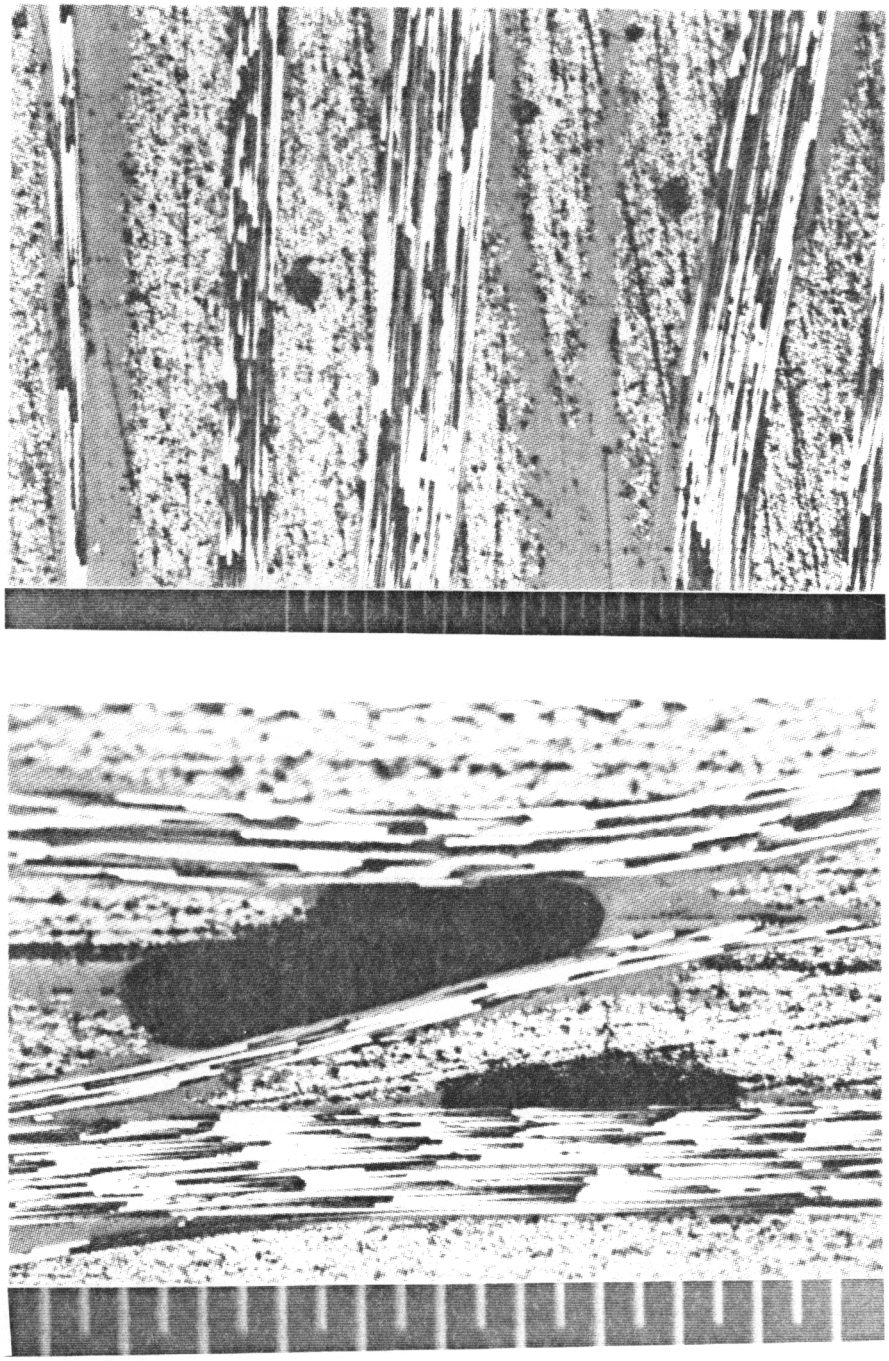

**Figure 4.15: Micrographs of Panel #4, AS4/PW/U and Derakane 441-400 Scale represents 0.05 mm.**

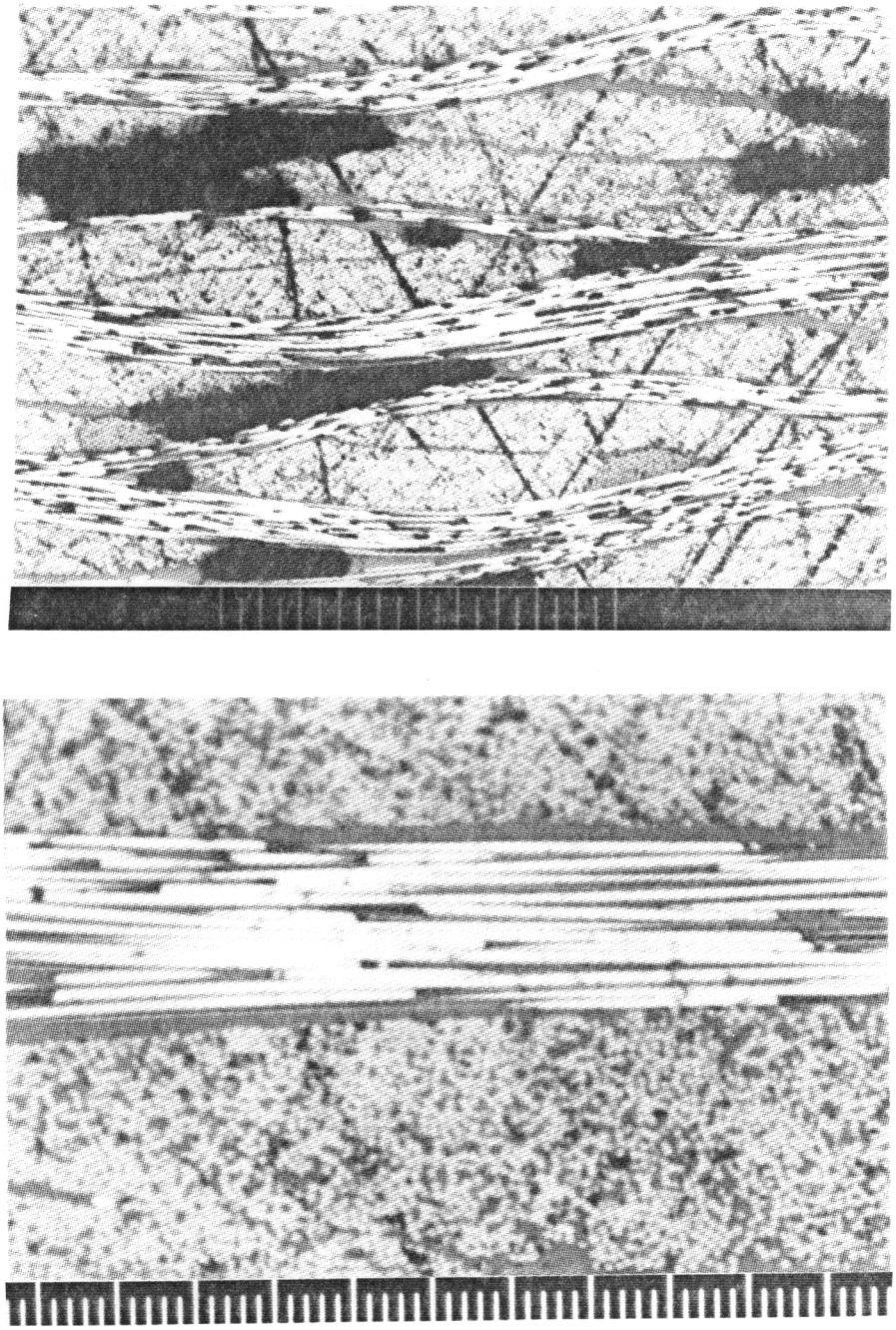

**Figure 4.16: Micrographs of Panel #31, AS4/PW/S and RSL-1895, Injected at 65°C. Top and bottom scales represent 0.05 and 0.01mm.**

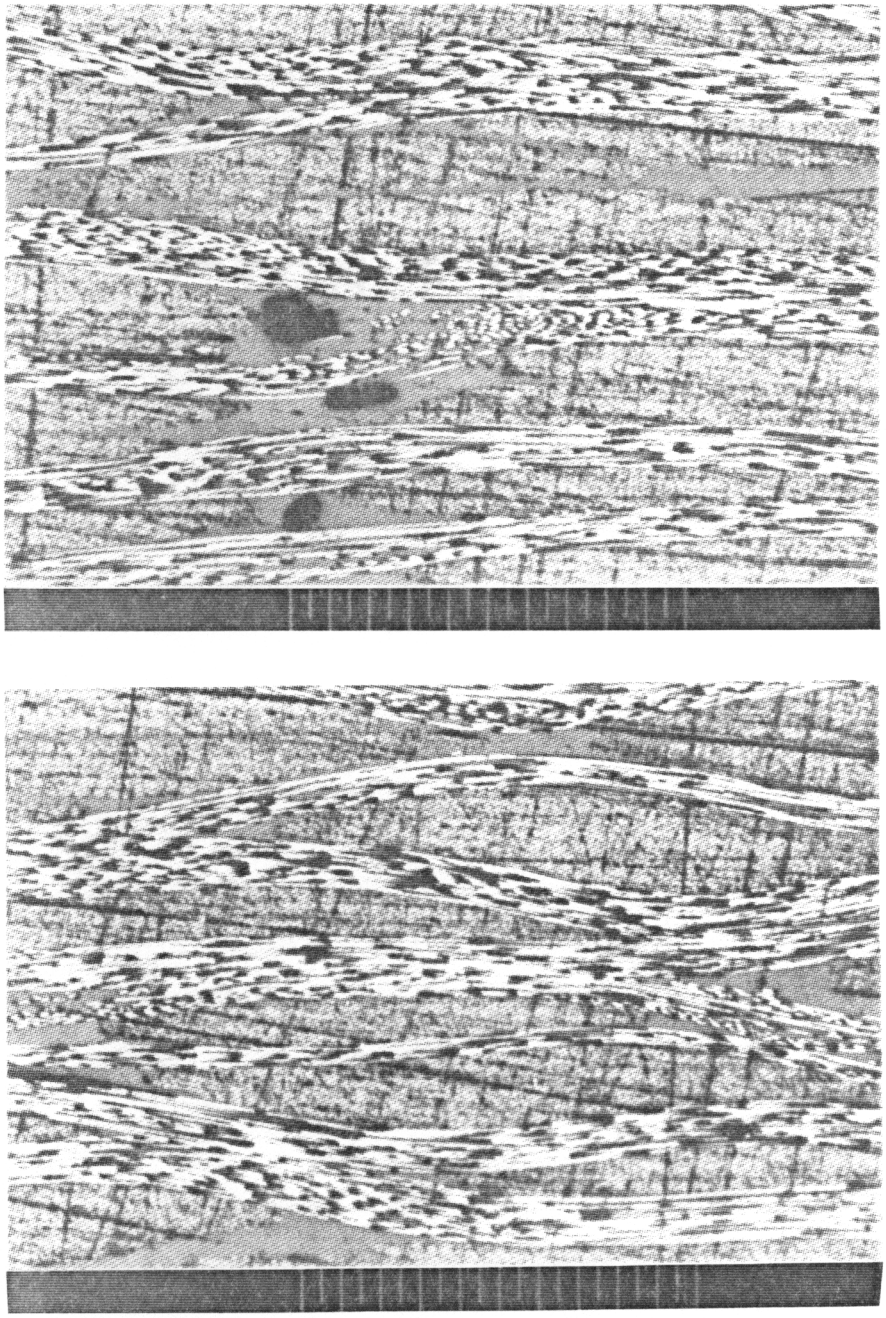

**Figure 4.17: Micrographs of Panel #33, AS4/PW/S and RSL-1895, Injected at 75°C. Scale represents 0.05 mm.**

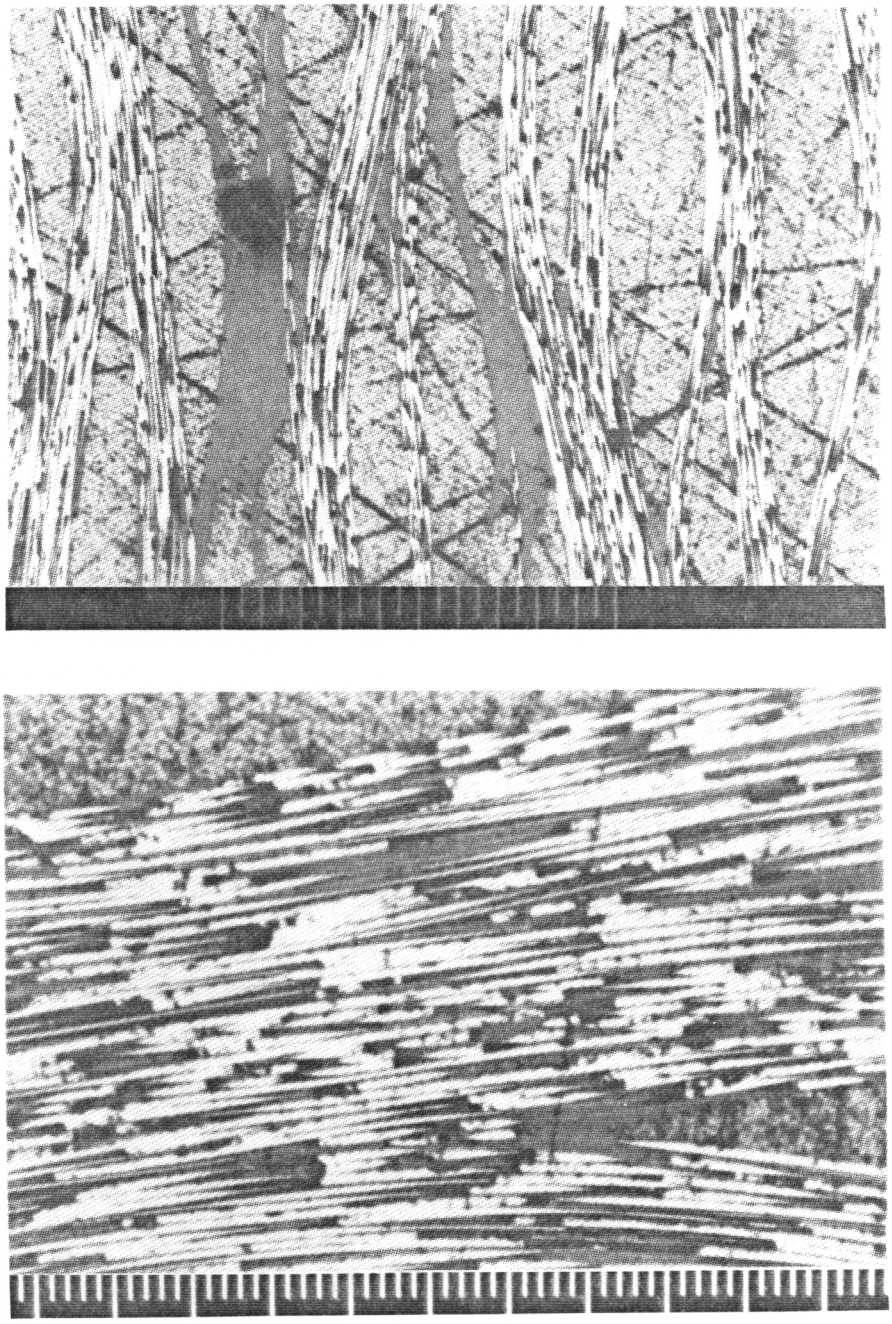

**Figure 4.18: Micrographs of Panel #32, AS4/PW/S and RSL-1895, Injected at 85°C. Top and bottom scales represent 0.05 and 0.01mm.**

# Chapter 5: Mechanical Test Results

All mechanical tests were performed in the manner described in Chapter 2. The test results are presented in the following pages, organized by type of test. Whenever possible, the load to failure, mode of failure, and peak stress will be provided for each specimen.

## 5.1 Short Block Compression

As mentioned before, short block compression tests were conducted on specimens machined from 6.3 mm (¼ inch) thick composite panels. These panels include RSL-1895 resin with 162 E-glass and AS-4 plain weave fabrics, and Derakane 441-400 resin with 162 E-glass and both sized and unsized AS-4 plain weave fabrics. Six specimens from each panel were tested, three in the warp and three in the fill directions. Additional short block compression tests were conducted on the three RSL-1895/ AS-4 composite panels used in the injection temperature study. These tests were conducted in the warp direction only.

Movement of the short block specimen in the grips during testing may have led to

some cases of premature failure. Inspection of specimens after failure has shown that a number of fractures actually initiated at the point at which the specimen met the fixture. This could indicate that, under load, the specimens are bearing on the corners of the sliding blocks. All short block specimens did not fail in this manner. A good failure will occur in the center of the specimen, and consists of interior buckling which buckles and breaks the outer layers, causing considerable fragmentation. This is considered a better failure since the fracture begins in the center of the specimen, and usually occurs at a higher load than fractures at the point of contact with the fixture. Graphite specimens commonly failed in this manner rather than by buckling near the corners of the fixture. However, due to the fact that such great care and a measure of luck are needed to properly load the specimen, the loading fixture should perhaps be changed. A fixture which could fix the specimen in place would probably produce more consistent results.

Table 5.1 contains the short block compression data. The load to failure and resulting compression strength are given for each specimen. Compression strength is calculated by dividing the failure load by the specimen's cross-sectional area. This cross sectional area is taken to be the thickness multiplied by the width of each specimen. The thickness and width measurements for each specimen can be found in the Appendix.

The results of short block compression tests, grouped by similar materials systems, are shown in Figures 5.1 - 5.3. Figure 5.1 contains results for composites made with the 162 E-glass fabric, and Derakane and Shell RSL-1895 resins. Results are

## Table 5.1: Short Block Compression Test Results

| Specimen | Max Load (Newtons) | Strength (MPa) | | Specimen | Max Load (Newtons) | Strength (MPa) |
|---|---|---|---|---|---|---|
| 02A | 55600 | 229.2 | | 16X | 117500 | 480.8 |
| 02B | 59200 | 242.9 | | 16Y | 117000 | 479.5 |
| 02C | 60100 | 244.1 | | 16Z | 126800 | 520.8 |
| 02X | 44500 | 183.7 | | 18A | 87200 | 359.2 |
| 02Y | 46300 | 191.5 | | 18B | 85400 | 354.5 |
| 02Z | 45400 | 187.0 | | 18C | 81000 | 336.8 |
| 04A | 80500 | 331.6 | | 18X | 83700 | 338.6 |
| 04B | 73000 | 300.5 | | 18Y | 94300 | 381.8 |
| 04X | 61400 | 251.7 | | 18Z | 87700 | 363.1 |
| 04Y | 61400 | 252.8 | | 31A | 114800 | 471.1 |
| 04Z | 63600 | 262.1 | | 31B | 95700 | 393.5 |
| 1A | 92600 | 384.6 | | 31C | 109500 | 451.0 |
| 1B | 100100 | 415.6 | | 32A | 116100 | 475.5 |
| 1C | 91200 | 377.8 | | 32B | 106800 | 438.8 |
| 1X | 85400 | 356.6 | | 32C | 107200 | 441.7 |
| 1Z | 92600 | 383.0 | | 33A | 115300 | 471.7 |
| 16A | 112100 | 460.6 | | 33B | 104600 | 428.1 |
| 16B | 122800 | 505.2 | | 33C | 110400 | 451.8 |
| 16C | 126800 | 522.3 | | | | |

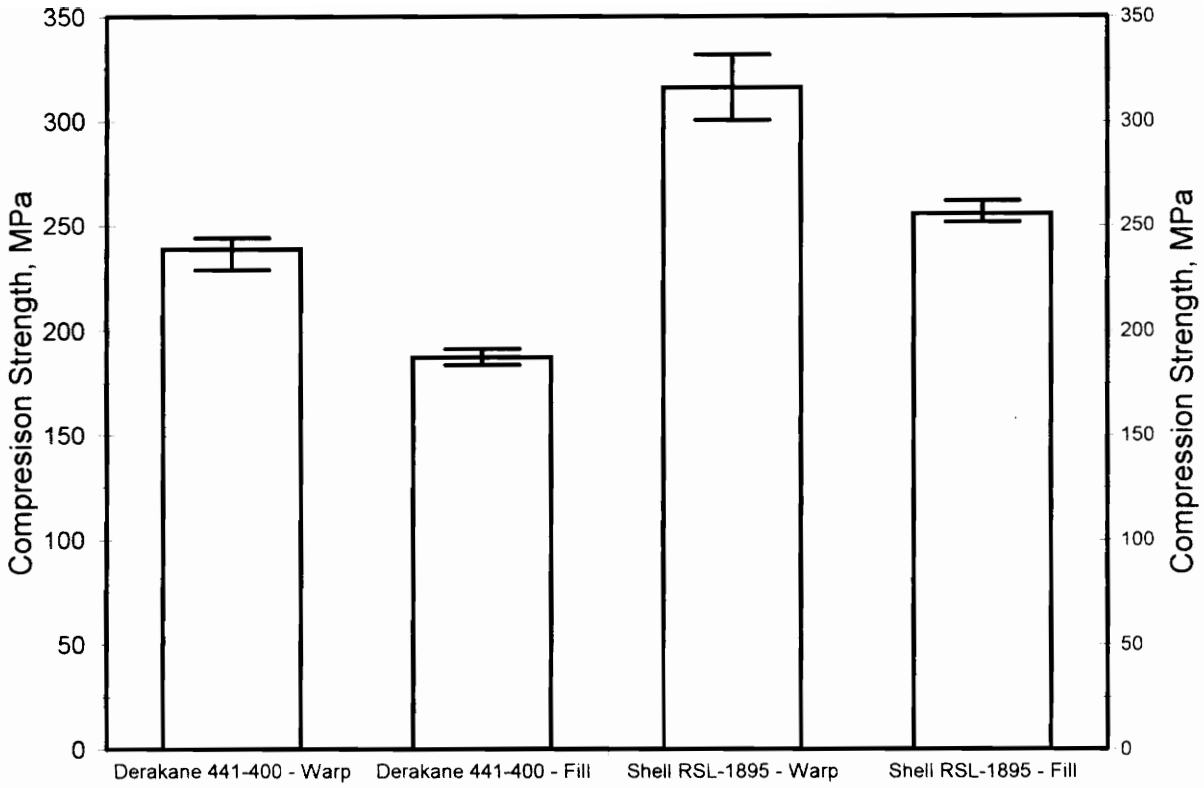


**Figure 5.1: Short Block Compression results for composites made with Style 162 E-glass.**

presented for both warp and fill directions, as denoted on the lower axis. The large open bars indicate the average strength for each panel. The error bars represent the highest and lowest recorded strengths for that material system. It can be seen that, for both materials, a significantly lower strength is recorded in the fill direction, as is usually expected with woven fabric composites.

Figure 5.2 contains results for the Derakane 441-400 and Shell RSL-1895 resin systems with carbon fabric reinforcements. The open bars represent average strength for each system, with error bars indicating the range of strengths recorded. The lower axis of the Figure indicates the material system and direction of test, with a "W" or "F" suffix to indicate warp or fill directions, respectively. The behavior of the carbon composites is similar to that of the E-glass composites in that warp direction compression strengths tend to be higher than fill direction strengths, with one notable exception. The composites made with unsized AS-4 plain weave fabric and Derakane 441-400 appeared to have a higher strength in the fill direction than in the warp. The data spread for warp and fill do overlap, but the average fill strength still appears to be somewhat higher than recorded strengths for the warp direction. Aside from the previously discussed problems associated with loading the specimen into the test fixture, no other explanation for this aberration can be found. In each case, however, the compression strengths for Derakane 441-400 and unsized graphite fabric were lower than the compression strength in the same direction for a Derakane 441-400 and sized graphite fabric.

Lastly, the warp direction compression strengths of the AS-4 fabric composites

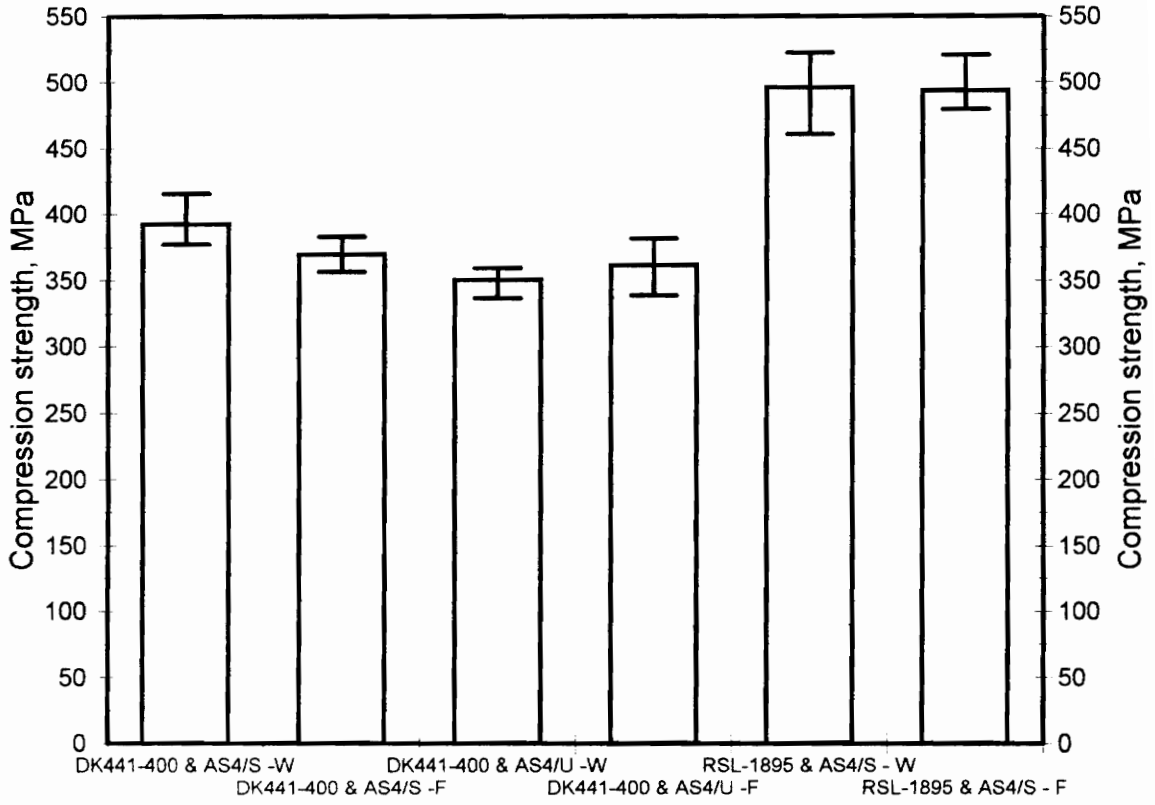


**Figure 5.2: Short Block Compression results for sized and unsized AS-4 composites made with Derakane 441-400 and RSL-1895 resins.**

injected with RSL-1895 resin at different temperatures are shown in Figure 5.3. The open bar represents the average of the panels. Superimposed error bars indicate the range of strengths measured for each panel. The results are plotted in order of increasing temperature, left to right. The "B" specimens from each of these panels (See diagram, Figure 3.6), which had been taken from the corner of the panel, registered a lower strength than the other specimens, which increased the strength range for each panel.

## 5.2 Iosipescu Shear Testing

The shear strengths and moduli of the composite panels were measured by the Iosipescu test method. Table 5.2 contains the results of the Iosipescu tests. Shear modulus does not vary significantly between materials systems. One exception to this is the evaluation of specimens from panel #14, which is an RFI-processed panel of sized AS-4 plain weave fabric and VTUFF1525. Panel #14 had a lower final fiber volume fraction than the other panels subjected to Iosipescu testing, only about 55%. This difference in volume fraction may also have reduced the shear strength for samples from panel #14. It can be seen that strength values for #14 (25% toughened cyanate ester) fall far short of those for panel #19 (Untoughened B10 cyanate ester).

For comparison, the data from Table 5.2 tests are displayed graphically in Figures 5.4 and 5.5. These plots present the average value for each material system, with error bars indicating a one-standard-deviation interval. Figure 5.4 shows the shear modulus,

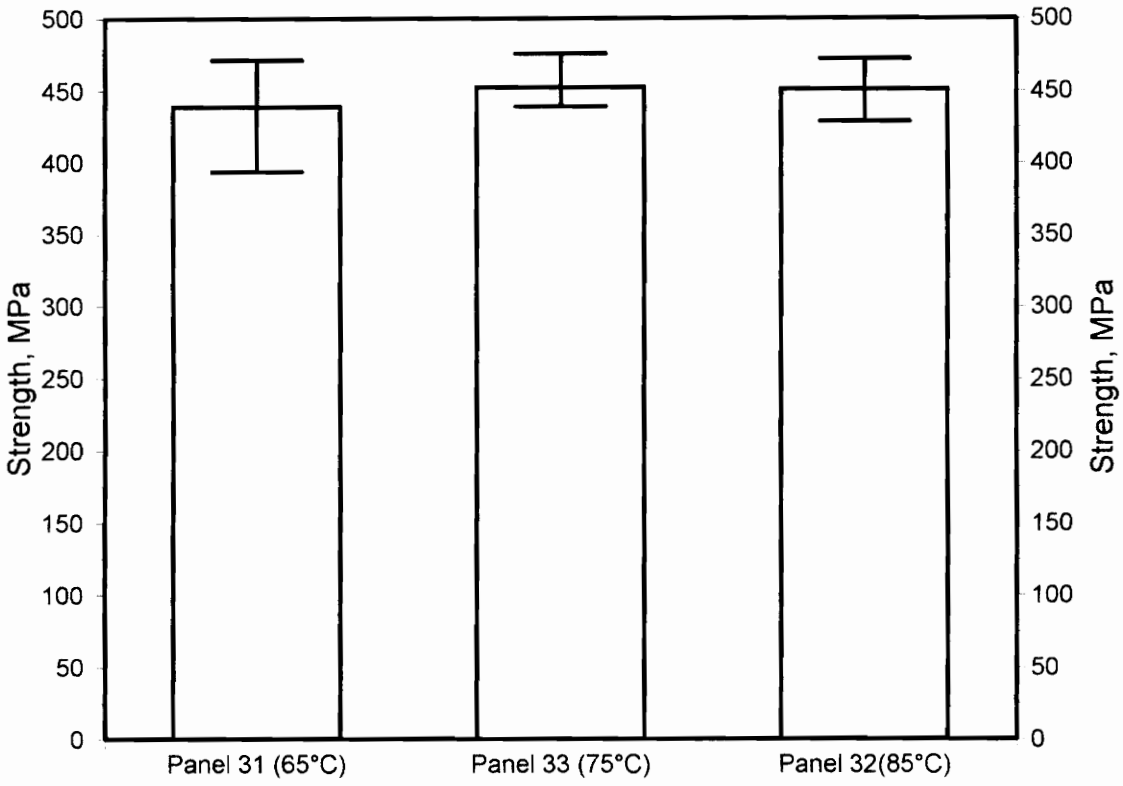


**Figure 5.3: Short Block Compression results for RSL-1895 composites using different injection temperatures.**

**Table 5.2: Iosipescu Shear Test Results**

| Specimen | Fabric | Matrix | Modulus, GPa | Strength, MPa |
|---|---|---|---|---|
| 11 I | AS-4 / PW / U | DK 441-400 | 5.26 | 89.0 |
| 11 J | AS-4 / PW / U | DK 441-400 | 5.85 | 83.3 |
| 11 K | AS-4 / PW / U | DK 441-400 | 5.96 | 92.1 |
| 11 Avg. | AS-4 / PW / U | DK 441-400 | 5.69 | 88.1 |
| 12 I | AS-4 / PW / S | DK 441-400 | 5.55 | 89.0 |
| 12 J | AS-4 / PW / S | DK 441-400 | 5.84 | 91.1 |
| 12 K | AS-4 / PW / S | DK 441-400 | 5.64 | 89.6 |
| 12 Avg | AS-4 / PW / S | DK 441-400 | 5.68 | 89.9 |
| 14 I | AS-4 / PW / S | VTUFF 1525 | 5.23 | 109.4 |
| 14 J | AS-4 / PW / S | VTUFF 1525 | 4.85 | 110.7 |
| 14 K | AS-4 / PW / S | VTUFF 1525 | 4.70 | 112.1 |
| 14 Avg | AS-4 / PW / S | VTUFF 1525 | 4.92 | 110.1 |
| 15 I | AS-4 / PW / S | RSL - 1895 | 5.36 | 108.3 |
| 15 J | AS-4 / PW / S | RSL - 1895 | 5.43 | 120.8 |
| 15 K | AS-4 / PW / S | RSL - 1895 | 5.24 | 121.1 |
| 15 Avg. | AS-4 / PW / S | RSL - 1895 | 5.34 | 116.7 |
| 19 I | AS-4 / PW / S | AroCy B10 | 5.73 | 126.5 |
| 19 J | AS-4 / PW / S | AroCy B10 | 5.27 | 132.9 |
| 19 K | AS-4 / PW / S | AroCy B10 | 4.95 | 130.4 |
| 19 Avg. | AS-4 / PW / S | AroCy B10 | 5.32 | 130.0 |

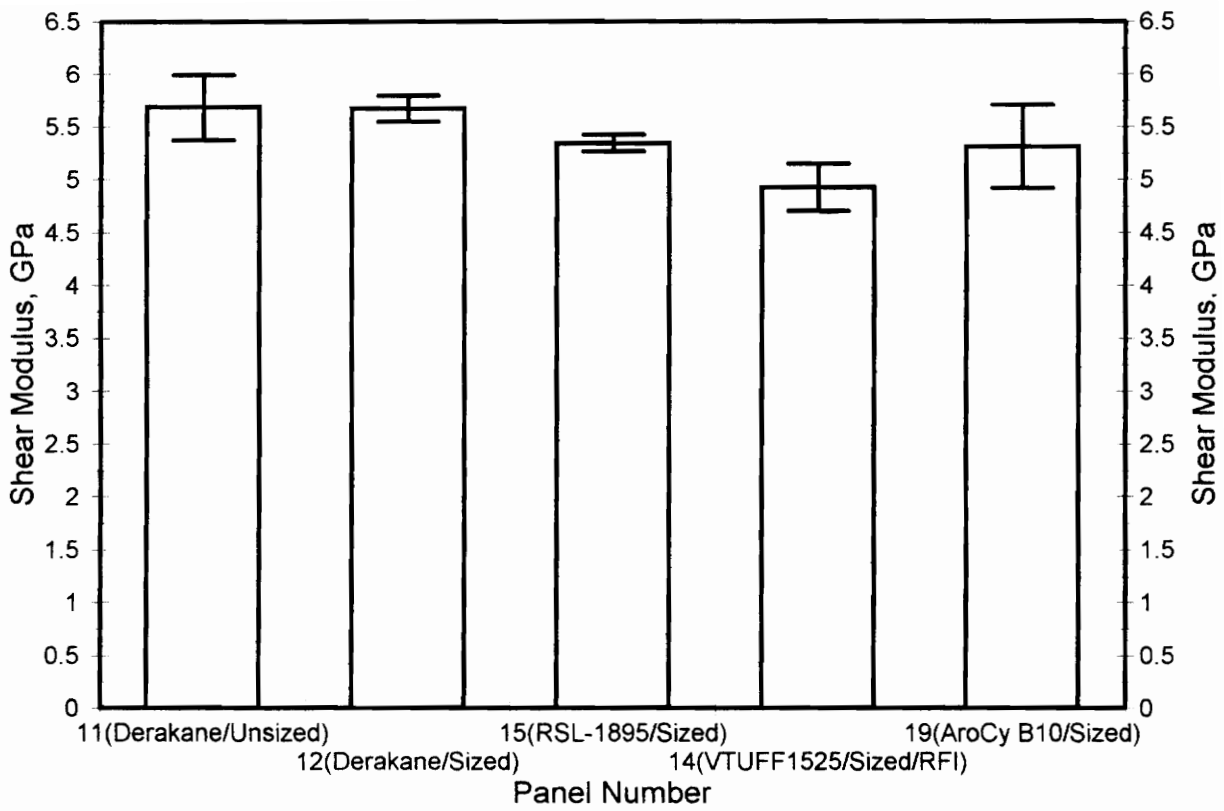


**Figure 5.4: Shear modulus results from Iosipescu testing.**

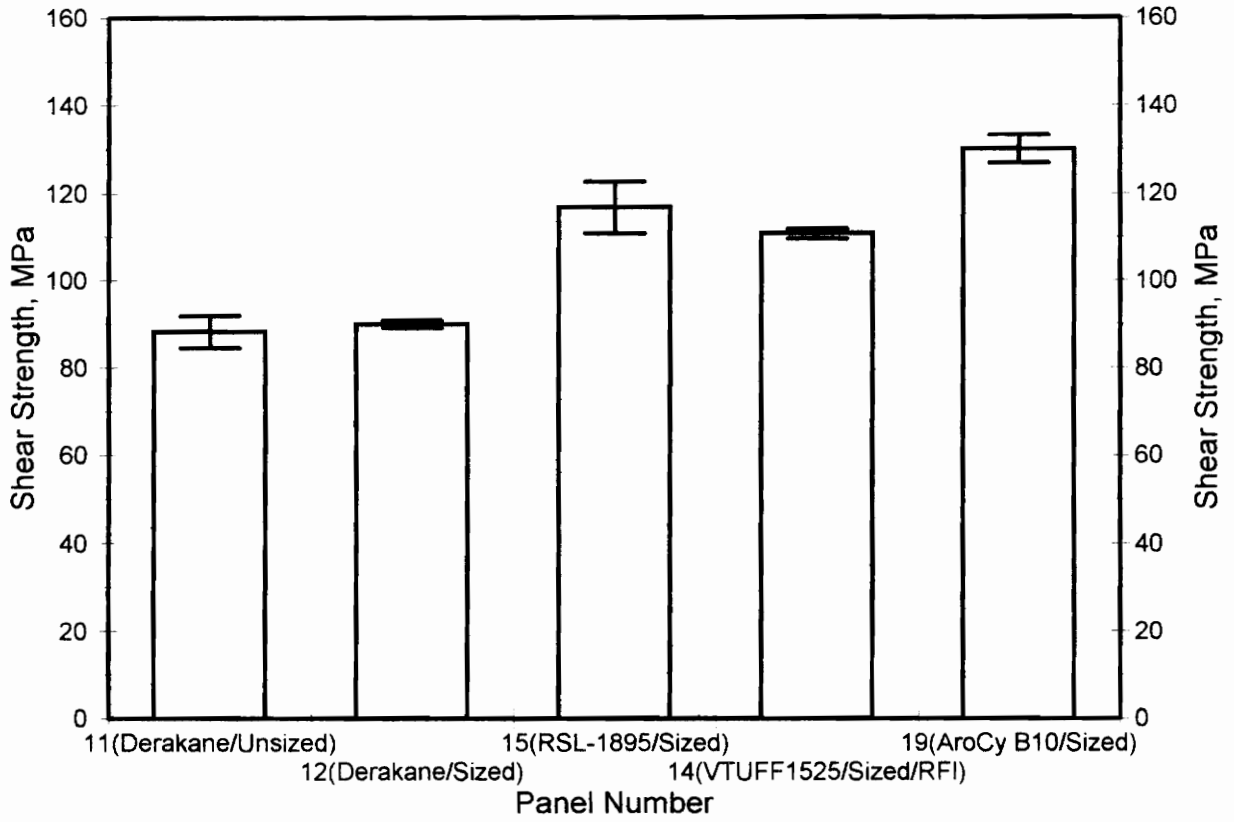


**Figure 5.5: Shear strength results from Iosipescu testing.**

while Figure 5.5 shows the shear strength.

The Iosipescu shear test was, as with most test methods for composites, originally developed for use with unidirectional prepreg tape composites. In unidirectional fiber materials, shear failure usually occurs as a definitive fracture near the specimen notches. Woven fabrics tend to distort under shear loading, and failure occurs in a more subtle way. At high loads, small cracks in the matrix will appear, allowing the fabric near the notch to distort. Although the specimen's ability to carry load will decrease, the specimen will not fracture, nor will a recognizable crack form at the notch. The failure load has therefore been taken to be the peak load seen by the specimen.

## 5.3 Impact Testing

Generally, four impact specimens were prepared and tested for each material system considered. The panel to be used was cut into quadrants for impact tests. An exception to this was the VTUFF 1525 resin with sized AS-4 plain weave fabric. An attempt at pressure-injected RTM resulted in a partially infiltrated panel (Panel #6) from which only two impact specimens were taken. Two additional impact specimens were cut from panel #14, which was an RFI panel of the same materials. The impact specimens taken from panel #6 contained such a high concentration of voids that it was later decided to repeat the impact tests with fresh specimens from a second RFI-processed panel (#27).

Table 5.3 contains the impact test data measured from all systems. Specimens

## Table 5.3: Impact and Compression After Impact Test Results

| Specimen | Material | Damage Area [mm²] | Impact Velocity [m/sec] | Impact Energy [Joule] | Comp Strength [MPa] | Residual Strength |
|---|---|---|---|---|---|---|
| | | | | | | |
| Reference | DK 441-400 | 0 | | | 410 | 1.000 |
| 2C | Sized AS-4 | 120 | 9.21 | 1.50 | 256 | 0.624 |
| 2A | | 211 | 12.49 | 2.75 | 215 | 0.524 |
| 2D | | 231 | 14.55 | 3.73 | 211 | 0.514 |
| 2B | | 448 | 18.1 | 5.77 | 164 | 0.399 |
| Reference | DK 441-400 | 0 | | | 341 | 1.000 |
| 4C | Unsized AS4 | 103 | 8.73 | 1.34 | 263 | 0.771 |
| 4A | | 166 | 13.02 | 2.99 | 211 | 0.620 |
| 4D | | -- | 16.2 | 4.63 | 166 | 0.487 |
| 4B | | 282 | 16.8 | 4.97 | 164 | 0.482 |
| Reference | DK 441-400 | 0 | | | 232 | 1.000 |
| 21C | 162 e-glass | 82 | 9.16 | 1.48 | 197 | 0.849 |
| 21D | | 86 | 10.76 | 2.04 | 190 | 0.819 |
| 21A | | 161 | 12.81 | 2.89 | 172 | 0.742 |
| 21B | | 321 | 17.48 | 5.39 | 135 | 0.583 |
| Reference | RSL-1895 | 0 | | | 511 | 1.000 |
| 8C | Sized AS-4 | 173 | 9.33 | 1.53 | 255 | 0.500 |
| 8A | | 229 | 12.62 | 2.81 | 231 | 0.451 |
| 8B | | 308 | 18.93 | 6.32 | 173 | 0.339 |
| 8D | | 560 | 22.84 | 9.19 | 127 | 0.249 |
| Reference | AroCy B10 | 0 | | | 542 | 1.000 |
| 5C | Sized AS-4 | 116 | 9.52 | 1.60 | 364 | 0.671 |
| 5A | | 162 | 12.94 | 2.95 | 291 | 0.537 |
| 5B | | 264 | 18.62 | 6.11 | 227 | 0.419 |
| 5D | | 371 | 23.03 | 9.35 | 182 | 0.335 |
| Reference | VTUFF 1520 | 0 | | | 535 | 1.000 |
| 20B | Sized AS-4 | 120 | 11.91 | 2.50 | 317 | 0.592 |
| 20A | | 180 | 14.97 | 3.95 | 283 | 0.530 |
| 20C | | 253 | 21.01 | 7.78 | 225 | 0.421 |
| 20D | | 316 | 24.38 | 10.48 | 183 | 0.342 |
| Reference | VTUFF 1525 | 0 | | | 507 | 1.000 |
| 6A | Sized AS-4 | 46 | 9.04 | 1.44 | 375 | 0.740 |
| 6B | | 163 | 13.32 | 3.13 | 320 | 0.631 |
| 27B | | 183 | 15.48 | 4.22 | 301 | 0.593 |
| 14C | | 328 | 18.88 | 6.28 | 203 | 0.400 |
| 27A | | 299 | 24.2 | 10.32 | 166 | 0.327 |
| 14D | | 567 | 25.09 | 11.10 | 154 | 0.304 |

from each system are arranged in order of increasing impact velocity. Table 5.3 indicates the impact velocity and the damage area measured by ultrasonic C-scan after the impact. Plots of impact energy vs. damage area for several materials systems are shown in Figures 5.6 - 5.8. . Impact energy is taken to be the kinetic energy associated with the impact bullet, which is half its mass multiplied by the square of its velocity. The impact bullet mass is 35.25 g.

Figure 5.6 displays impact information for the three Derakane panels. It can be seen that, as expected, the 162 E-glass fabric is less susceptible to damage than the carbon composites. One material's impact damage resistance is said to be higher than another's when it suffers less damage as a result of the same impact energy. It is clear that Derakane composites of unsized AS-4 are more damage resistant than those with sized AS-4 fabric. At higher impact energies, unsized graphite approaches the performance of the E-glass. Figure 5.7 shows damage area versus impact energy for sized AS-4 plain weave fabric with the Derakane vinyl ester, RSL-1895 epoxy, and AroCy B10 cyanate ester resin systems. The B10 system appears to have better impact damage resistance than the other two systems. The B10 composite also has a plot which seems nearly linear. Figure 5.8 presents impact damage resistance plots for B10 composites and VTUFF 1520 toughened resin. The impact damage data for the VTUFF 1525 composites is not shown, as these data were taken from three panels made by both RTM and RFI and contains more scatter. The 20% toughened system, however, appears to improve impact damage resistance over the stock B10.

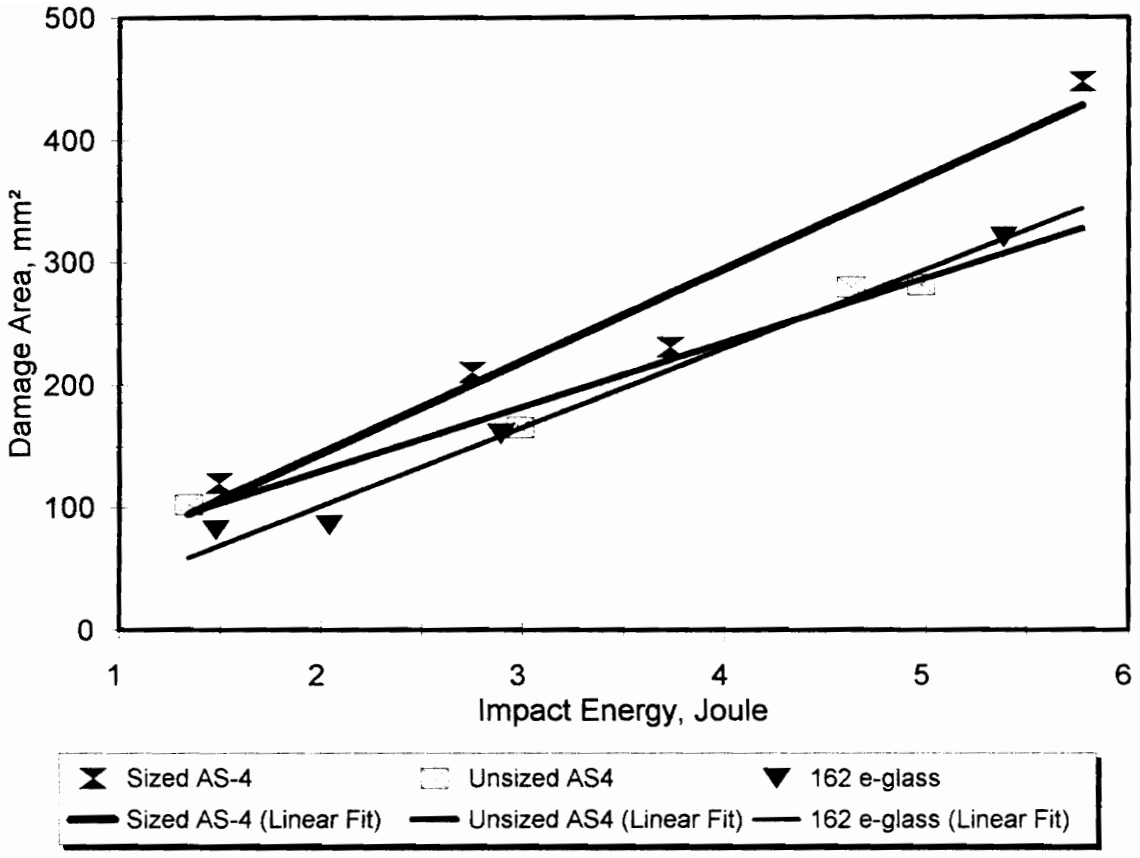


**Figure 5.6: Plot of impact damage area versus impact energy for Derakane 441-400 composites.**

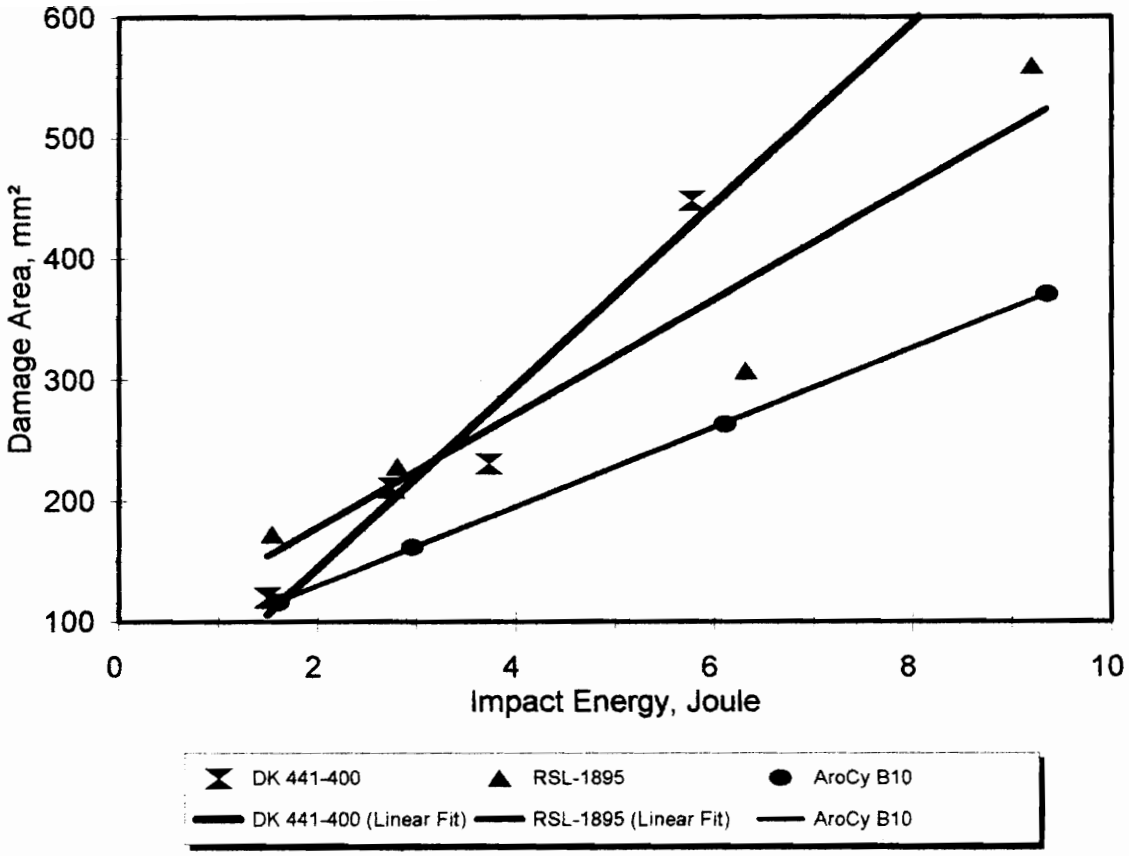


**Figure 5.7: Plot of impact damage area versus impact energy for sized AS-4 fabric composites with Derakane 441-400, RSL-1895, and B10 resin systems.**

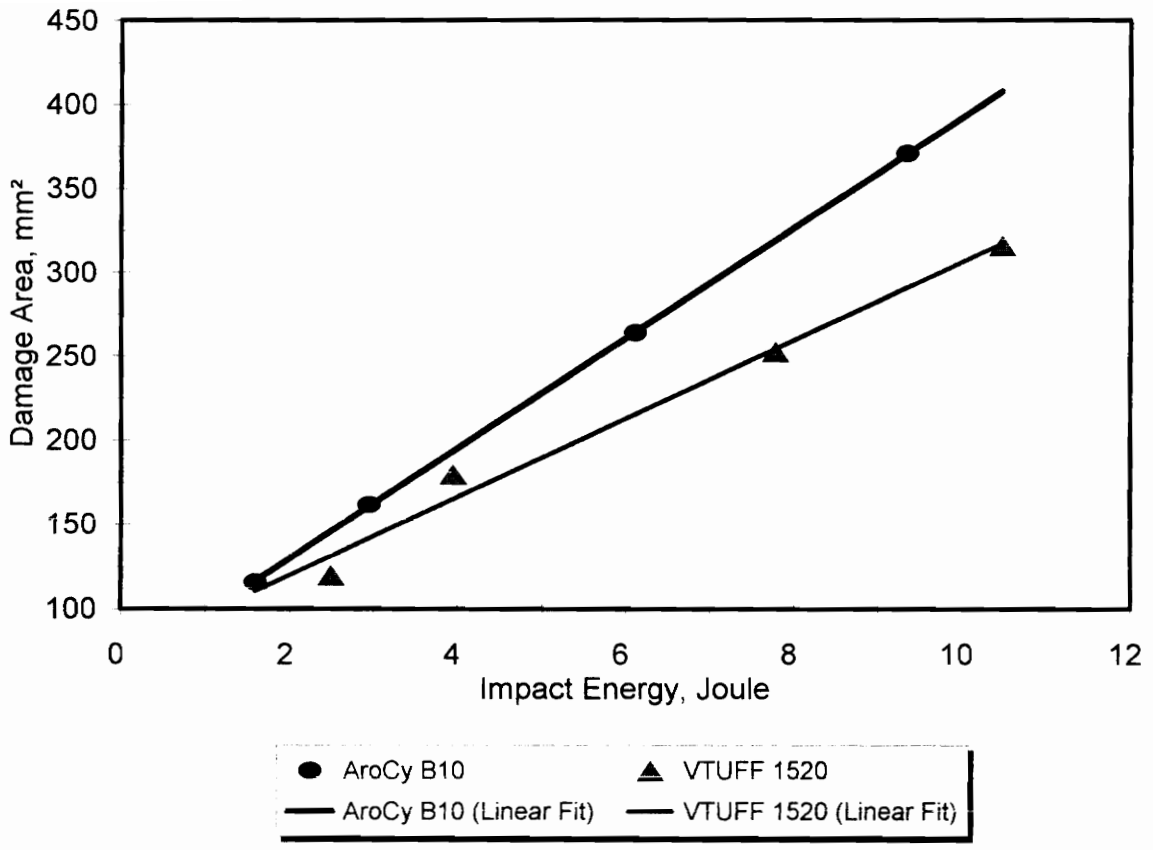


**Figure 5.8: Plot of impact damage area versus impact energy for B10 cyanate ester resin systems.**

## 5.4 Compression after Impact

One to three reference compression specimens were cut from separate panels to measure each material's undamaged compression strength. The vinyl ester and epoxy systems were subjected to short block testing, so a single compression specimen in the CAI geometry was used to verify undamaged compression strength. These strengths agreed with compression strengths found in the short block compression tests. The cyanate ester systems, however, did not undergo short block compression tests. To get a reliable compression strength for these systems, the strengths of three undamaged specimens were averaged. Strain gages were affixed to these samples to generate strain data for modulus calculation and to check against bending in the specimens. Undamaged compression strengths are listed for each material system in Table 5.3, on the row marked "Reference".

Damaged compression-test specimens were cut from the center of each impact specimen, including, whenever possible, the entire damage area. The dimensions of these specimens matched the undamaged reference specimens. CAI compression tests were conducted by the same technique as the undamaged specimens, with the exception that impacted specimens could not be equipped with strain gages.

The compression after impact data for all systems are also given in Table 5.3. Again, for simplicity, the data for each system are given in order of increasing impact velocity. The damaged compression strength and normalized residual strength for each

specimen is given. Normalized residual strength is defined as the ratio of damaged to undamaged compression strengths. The first row for each material system indicates the undamaged compression strength, and has a normalized residual strength value of 1.000. The CAI strength of impacted specimens is seen to decrease with increasing damage area, or impact velocity. Impact velocity and impact energy for each specimen are also given in this table, and will be used for plotting normalized residual strength. Impact energy is taken to be the incident kinetic energy of the impact bullet, which is half its mass multiplied by the square of its velocity. Results of compression after impact tests often use the term "impact damage tolerance". This term is used to relate the normalized residual strength with either damage area or impact energy. Materials systems will be compared by their respective impact tolerances.

Normalized residual strengths are plotted against impact energy and specimen damage area in Figures 5.9 - 5.16. Figure 5.9 shows the normalized residual compression strength versus impact energy of Derakane composites. Impact tests were conducted with sized and unsized AS-4 fabrics, and with 162 E-glass fabrics. Although strengths were lower for the E-glass composites, their improved impact damage tolerance can clearly be seen. The normalized residual strengths versus damage area for the Derakane resin composites are shown in Figure 5.10. Similar plots for AS-4 composites with Derakane, RSL-1895 and AroCy B10 resin systems are presented in Figures 5.11 and 5.12. The composites made with Shell RSL-1895 have poor impact damage tolerance versus impact energy, compared with the other systems. The RSL-1895 and B10 systems

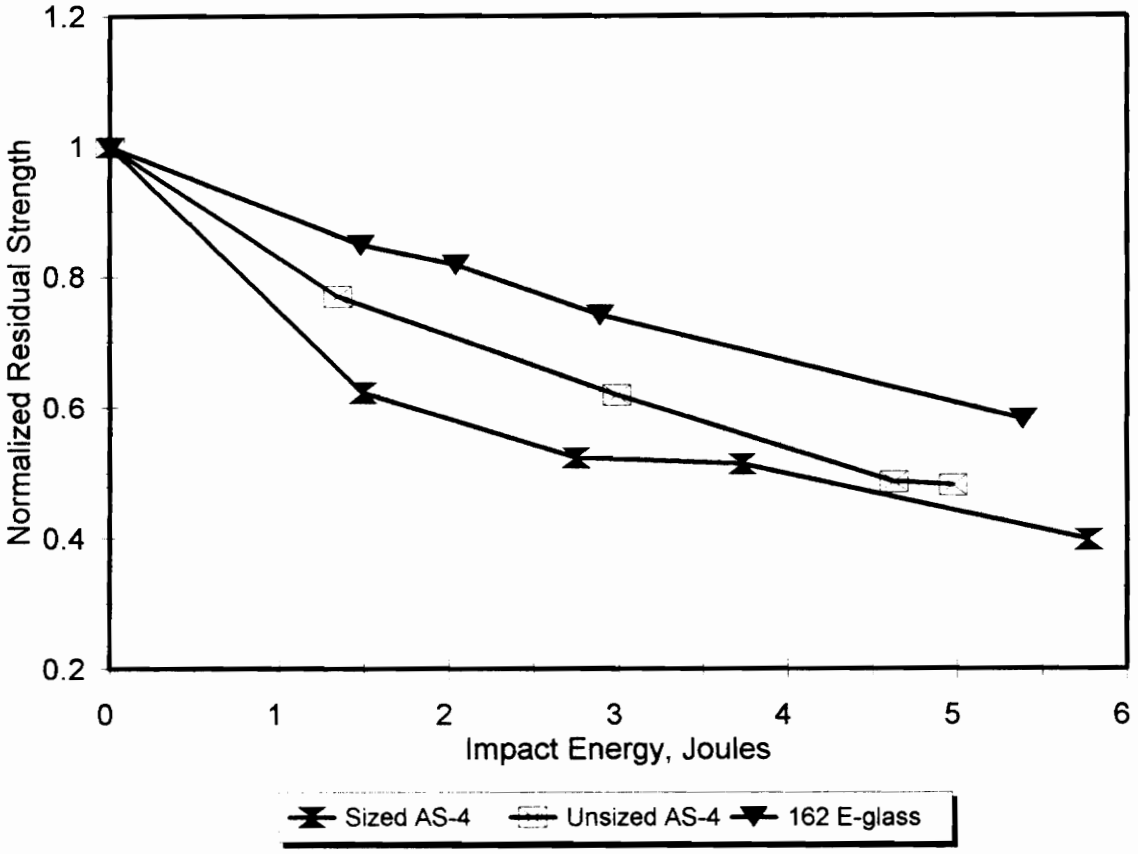


**Figure 5.9: Plot of normalized residual compression strength versus impact energy for Derakane 441-400 composites.**

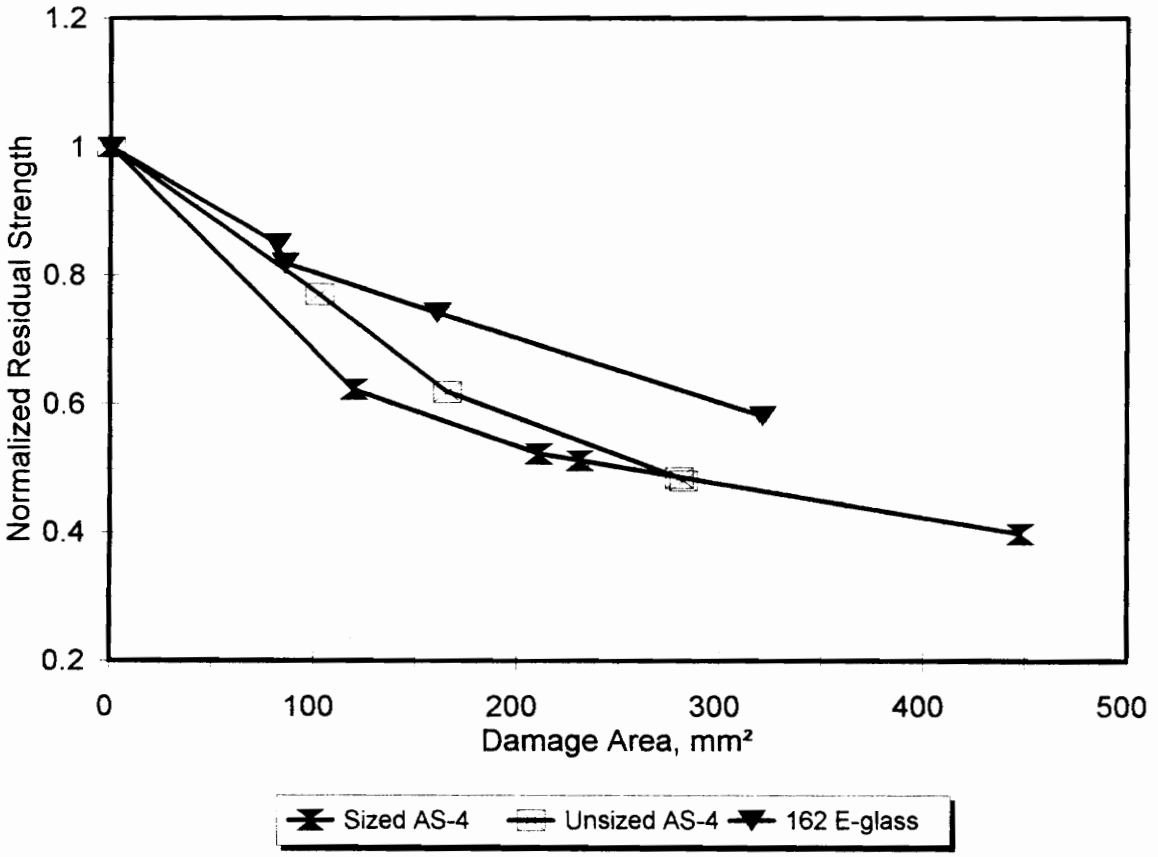


**Figure 5.10: Plot of normalized residual compression strength versus damage area for Derakane 441-400 composites.**

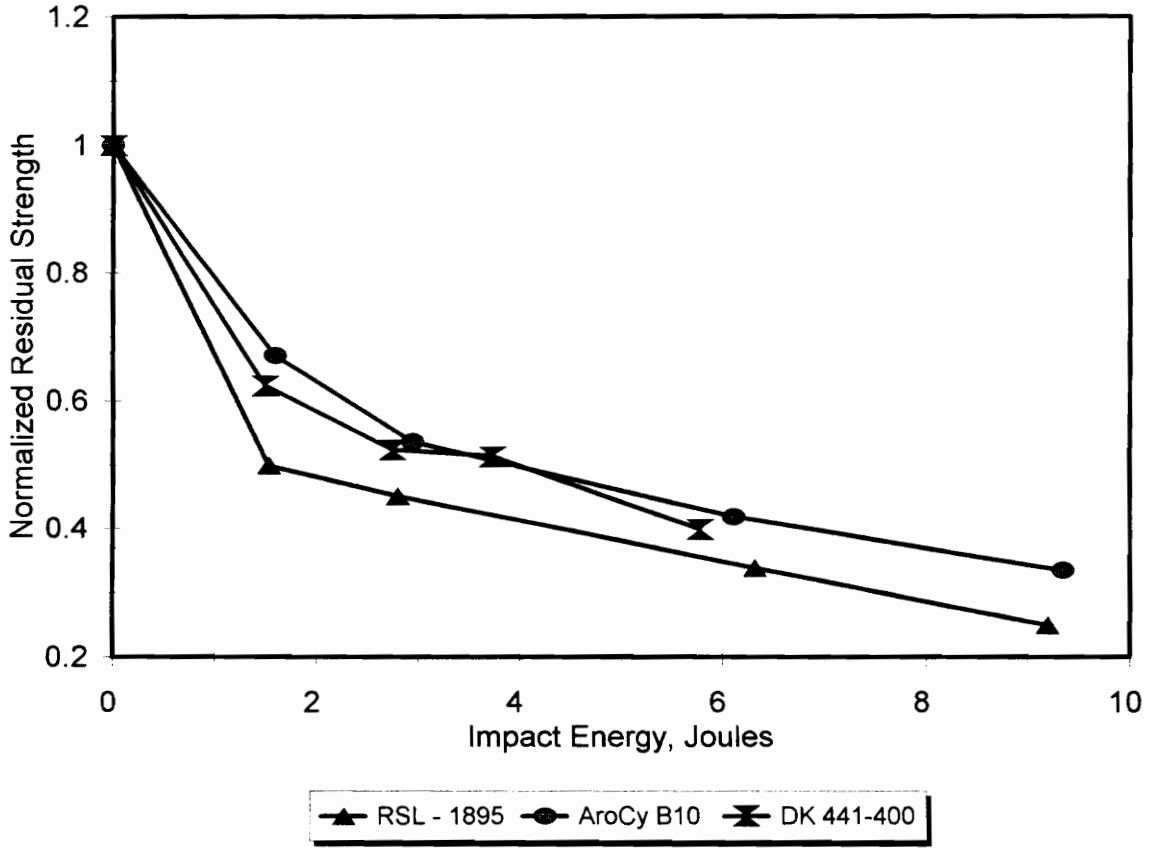


**Figure 5.11: Plot of normalized residual compression strength versus impact energy for sized AS-4 fabric composites with Derakane 441-400, RSL-1895 and B10 resin systems.**

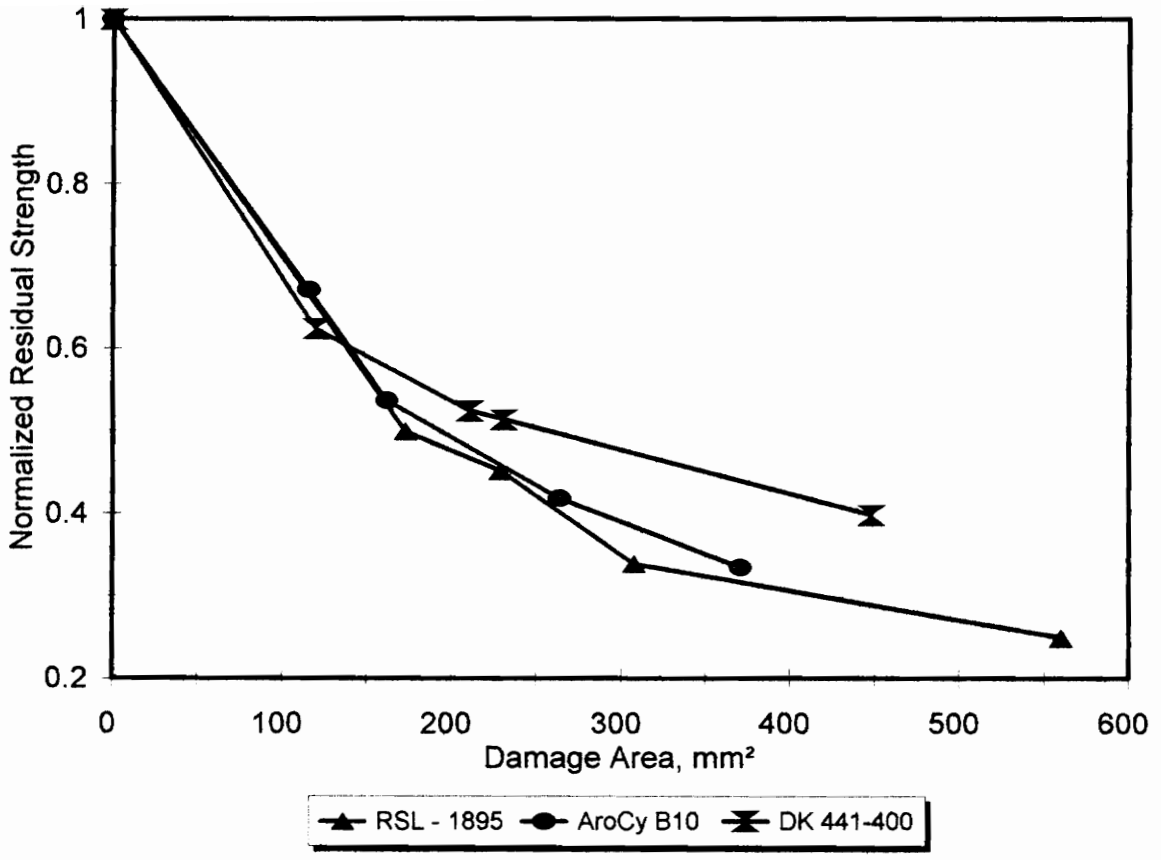


**Figure 5.12: Plot of normalized residual compression strength versus damage area for sized AS-4 fabric composites with Derakane 441-400, RSL-1895, and B10 resin systems.**

appear to follow a very similar curve for residual strength vs. damage area, while Derakane appears able to retains a higher normalized residual strength for similar damage area.

Figures 5.13 and 5.14 present the CAI results for the toughened cyanate ester systems. Figure 5.13 shows the residual strength versus damage area for B10, VTUFF 1520, and VTUFF 1525. The VTUFF 1525 tests were conducted with both RTM-processed and RFI-processed specimens. Only the two leftmost data points (corresponding to lowest damage area or impact energy) were conducted on RTM-processed panels. The combination of impact specimens from different process techniques is probably a major cause of the scatter in VTUFF 1525 results. A plot of normalized residual strength versus impact energy for these systems is given in Figure 5.14. This figure more clearly shows an improvement in damage tolerance with the addition of the thermoplastic component. The curves appear to have similar shape, but are offset from one another. The curve for VTUFF 1525 appears to follow this trend at the lower impact energies, but shifts at higher energies. The dropoff of performance could be explained by the fact that two impact specimens, made from the first RFI panel, were manufactured to a lower volume fraction than the other specimens considered. This could reduce their indicated residual strength.

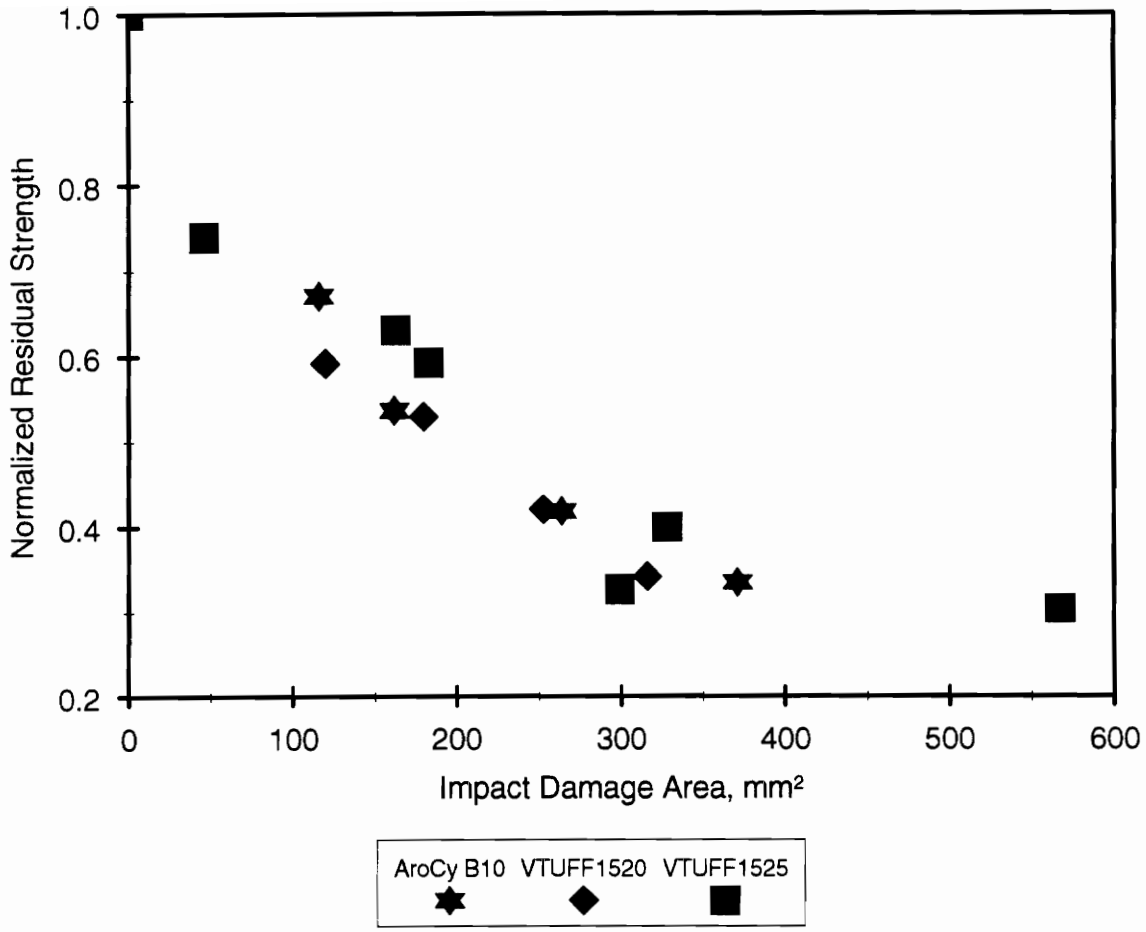


**Figure 5.13: Plot of normalized residual compression strength versus damage area for B10 cyanate ester resin systems.**

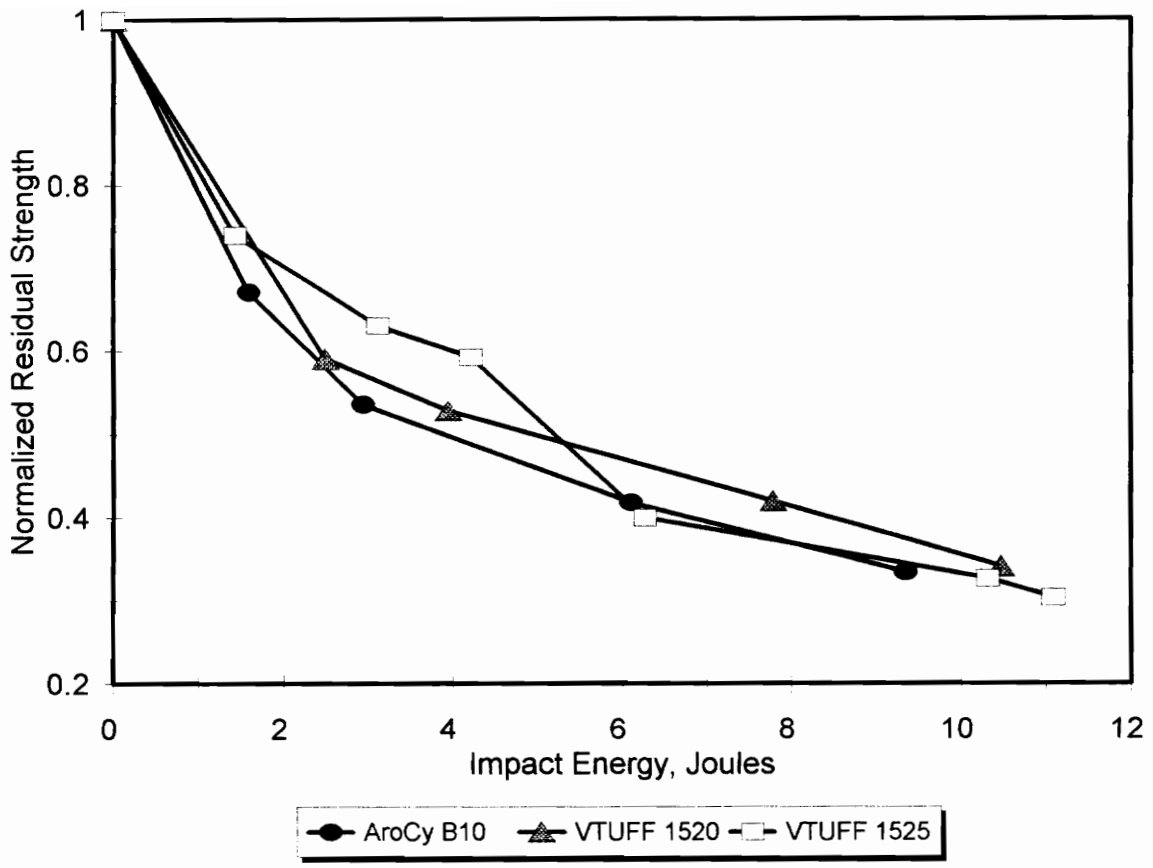


**Figure 5.14: Plot of normalized residual compression strength versus impact energy for B10 cyanate ester resin systems.**

## 5.5 Interlaminar Shear Testing

Interlaminar (or Short Beam) shear tests were conducted on specimens cut from the Derakane panels with sized and unsized graphite, and on panels made from Shell RSL-1895 with sized AS-4 plain weave fabric. These include a 6.3mm panel made as a part of the original test matrix, and the three panels manufactured with different injection temperatures. Six specimens from each of the panels were tested according to ASTM D2344. All specimens failed properly in shear between the load points.

Table 5.4 contains the results of all of the interlaminar shear tests. Due to the large number of specimens, the average strength and standard deviations for each system are presented. Figure 5.15 presents SBS results for the Derakane systems. As with previous graphs, average values for "apparent" interlaminar shear strength are represented by the main bar, while error bars represent the standard deviation for each panel. Standard deviations are fairly large, due to the small sample size from each panel. However, a slightly higher interlaminar strength is noted for the unsized graphite fabric than for sized graphite fabric panels. The interlaminar shear strength of Shell RSL-1895 and AS-4 sized plain weave fabric is presented in Figure 5.16. This figure includes panel #16, from the original test matrix, and panels #31-33, from the injection temperature variance group.

## Table 5.4: Interlaminar Shear Test Results

| Specimen | Failure Load (newtons) | Apparent Shear Strength (MPa) | | Specimen | Failure Load (newtons) | Apparent Shear Strength (MPa) |
|---|---|---|---|---|---|---|
| 1 S1 | 2764 | 50.84 | | 31 S1 | 3584 | 66.45 |
| 1 S2 | 2623 | 48.18 | | 31 S2 | 3505 | 64.89 |
| 1 S3 | 2497 | 46.45 | | 31 S3 | 3554 | 65.90 |
| 1 S4 | 260 | 47.77 | | 31 S4 | 3407 | 63.27 |
| 1 S5 | 2541 | 46.89 | | 31 S5 | 3258 | 60.50 |
| 1 S6 | 2617 | 48.37 | | 31 S6 | 3125 | 58.22 |
| 1 Avg. | | 48.09 | | 31 Avg. | | 63.21 |
| 16 S1 | 3553 | 65.87 | | 32 S1 | 3413 | 63.38 |
| 16 S2 | 3223 | 59.67 | | 32 S2 | 3450 | 64.27 |
| 16 S3 | 3411 | 64.05 | | 32 S3 | 3376 | 62.99 |
| 16 S4 | 3345 | 61.93 | | 32 S4 | 3557 | 66.27 |
| 16 S5 | 3322 | 61.50 | | 32 S5 | 3264 | 60.90 |
| 16 S6 | 3435 | 63.49 | | 32 S6 | 3062 | 57.13 |
| 16 Avg. | | 62.75 | | 32 Avg. | | 62.49 |
| 18 S1 | 2583 | 48.20 | | 33 S1 | 3528 | 64.80 |
| 18 S2 | 2652 | 49.33 | | 33 S2 | 3346 | 61.56 |
| 18 S3 | 2784 | 51.95 | | 33 S3 | 3564 | 65.57 |
| 18 S4 | 2777 | 51.73 | | 33 S4 | 3575 | 65.67 |
| 18 S5 | 2701 | 50.32 | | 33 S5 | 3554 | 65.49 |
| 18 S6 | 2510 | 46.76 | | 33 S6 | 3369 | 62.08 |
| 18 Avg. | | 49.72 | | 33 Avg. | | 64.19 |

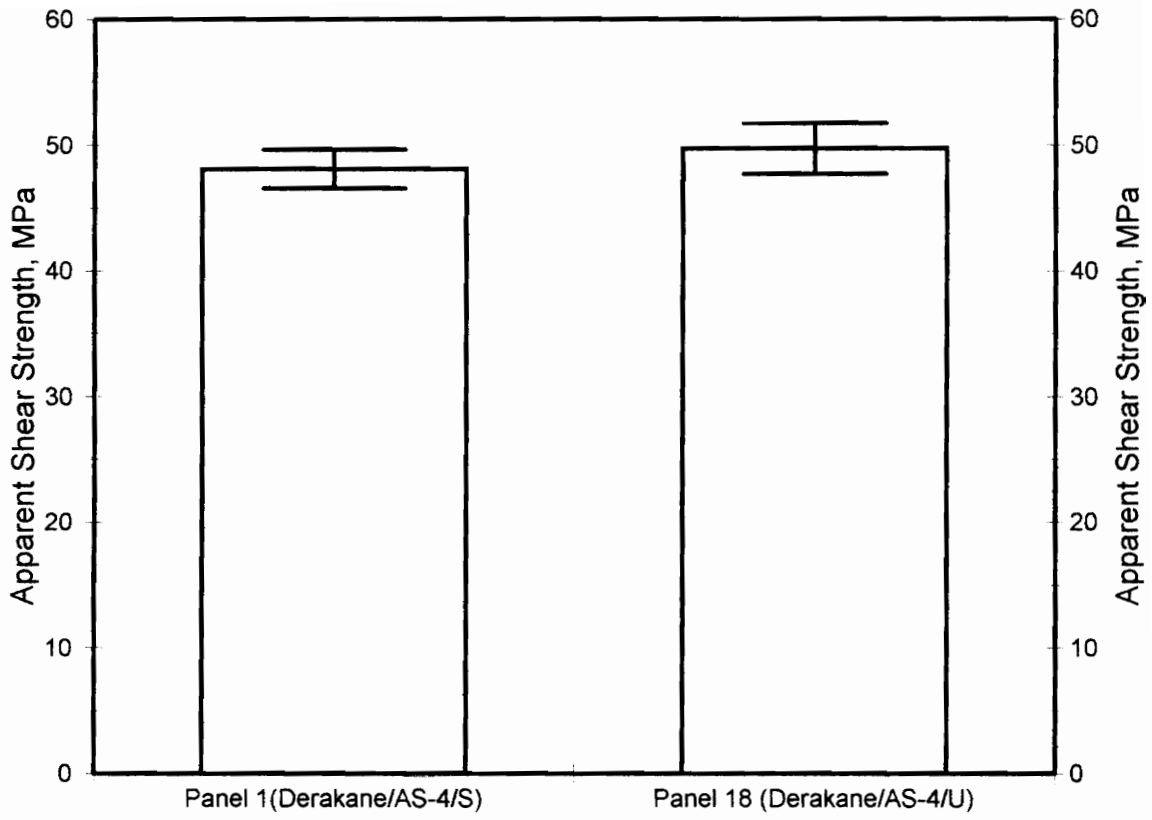


**Figure 5.15: Short Beam Shear results for carbon fiber composites with Derakane 441-400 resin.**

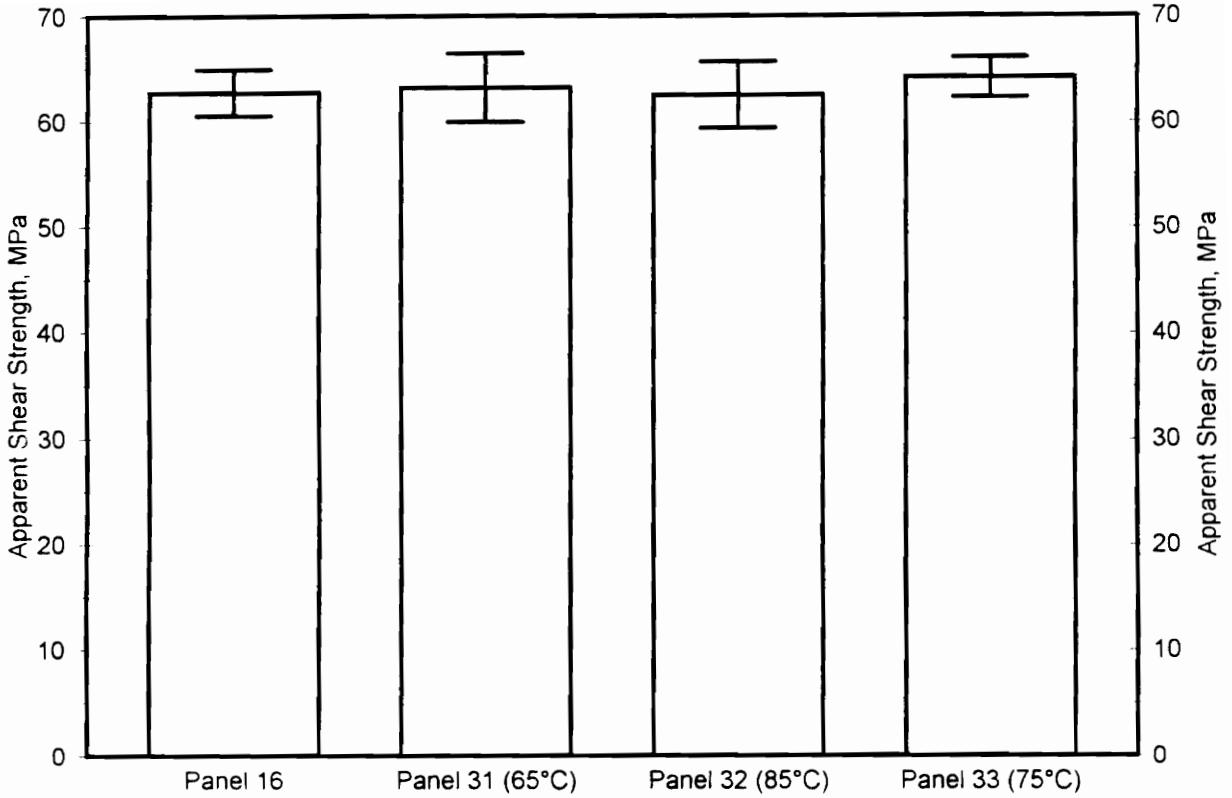


**Figure 5.16: Short Beam Shear results for carbon fiber composites with RSL-1895 resin at different injection temperatures.**

## 5.6 Four Point Flexure

Four point flexure tests were conducted on panels of RSL-1895 with sized AS-4 plain weave fabric, processed with different injection temperatures. Five flexure specimens were cut from each panel. These specimens were cut parallel to one another, using about one-half of the panel as a whole (See Figure 3.6). The fifth of these specimens, taken from the very edge of each panel, contained significantly higher void contents than the other flex specimens. This local increase in void content in one case was over 3%. These specimens also failed at a load which was significantly lower than the average for each panel.

The results of four point flexure testing are presented in Table 5.5. The table contains information on failure load, specimen strength, and failure mode for each specimen. Strength was calculated as specified in ASTM D790, and is presented in MPa. Failure mode was recorded by observation of the specimen during testing. In each case, specimen failure occurred by compression or tension failure in the outmost plies. Compression failure would occur between the inner load points, often near one contact point. Tension failure likewise occurred between the inner load points. It should also be noted that no particular panel was more susceptible to a single mode of failure than others. Specimens taken from each panel experienced both tension and compression failures, though compression failure was generally more common.

Plots of the four point flex results can be found in Figure 5.17. Results are

**Table 5.5: Four Point Flexure Test Results**

| Specimen | Injection Temp (°C) | Failure Load (Newton) | Max Stress (MPa) | Mode of Failure |
|---|---|---|---|---|
| 31F1 | 65 | 3662 | 715.2 | Compression |
| 31F2 | 65 | 3239 | 634.6 | Compression |
| 31F3 | 65 | 3968 | 777.4 | Compression |
| 31F4 | 65 | 4340 | 847.7 | Tension |
| 31F5 | 65 | 3350 | 650.2 | Compression |
| 31 Avg. | 65 | | 725.0 | |
| 32F1 | 85 | 4016 | 786.8 | Tension |
| 32F2 | 85 | 3374 | 659.5 | Compression |
| 32F3 | 85 | 3957 | 772.9 | Compression |
| 32F4 | 85 | 3744 | 733.0 | Compression |
| 32F5 | 85 | 3932 | 570.4 | Compression |
| 32 Avg. | 85 | | 704.5 | |
| 33F1 | 75 | 3640 | 715.5 | Compression |
| 33F2 | 75 | 3950 | 769.1 | Compression |
| 33F3 | 75 | 4111 | 852.4 | Tension/Compression |
| 33F4 | 75 | 4313 | 845.0 | Tension |
| 33F5 | 75 | 3016 | 589.5 | Compression |
| 33 Avg. | 75 | | 754.3 | |

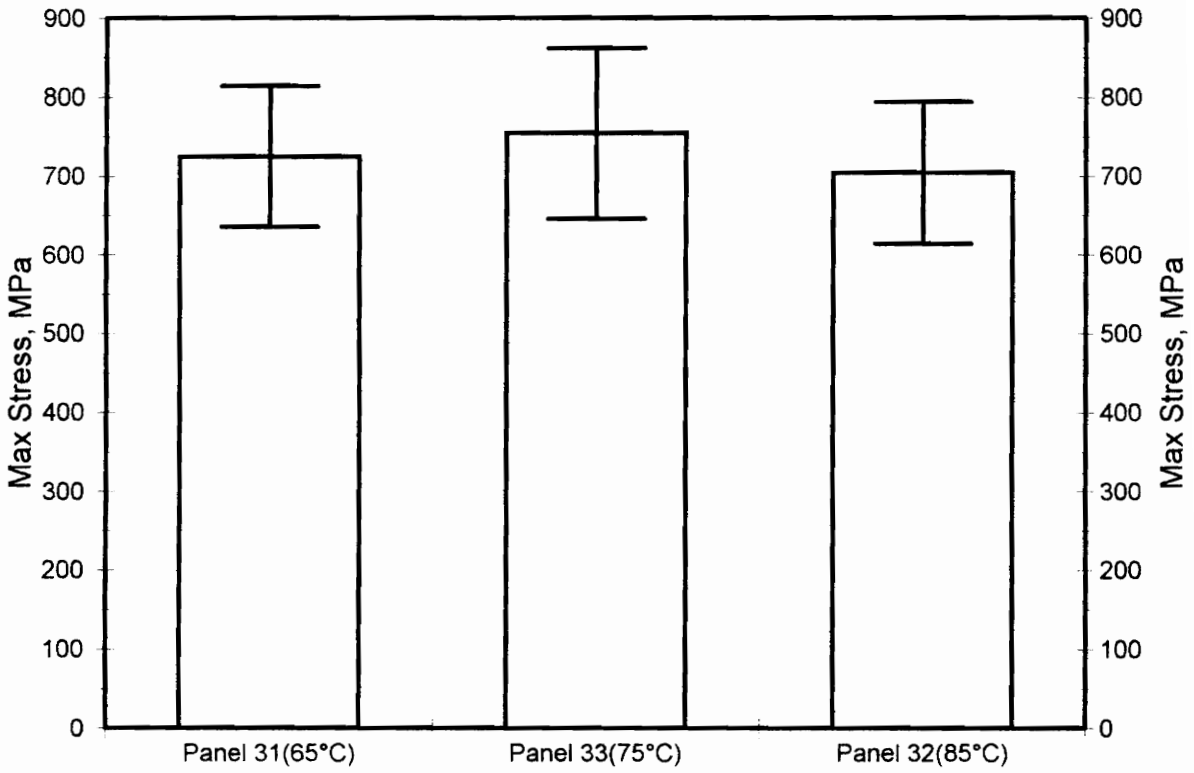


**Figure 5.17: Results of Four Point Flexure Tests for RSL-1895 composites using different injection temperatures**

presented in order of increasing injection temperature. The main bar again represents the average strength of specimens from each panel, with error bars representing an interval of one standard deviation from the mean. The existence in each group of the fifth specimen, containing an exceptionally high void content, has increased the standard deviation of each panel. Each of these high void specimens failed at a much lower load than other specimens in each set.

# Chapter 6: Discussion of Results

This chapter compares the results presented in the preceding three chapters. The accuracy of the density-based void calculation are assessed, by referring to mechanical results and evidence from the optical micrographs. Direct comparisons of materials systems are made, with respect to void content and mechanical performance. Particular attention is placed on the various B10 cyanate ester systems, and on Derakane 441-400 with the three fiber types. The effects of injection temperature and pressure will then be analyzed, based in part on the three RSL-1895 panels injected at different temperatures.

## 6.1 Assessment of Void Calculation

If nothing more, the void calculations give a reasonable estimate of the void contents in RTM fabricated composites. Many of the void estimates for panels made in this study were checked in Chapter 4 by optical photo-micrographs. The micrographs, in most cases, detect voids in the laminate and add to the validity of the calculation. A good example of this is the comparison between AS-4 sized fabric and VTUFF 1525 panels #6 and #14. Panels #6 and #14 were predicted to have very high and very low

void contents, respectively. Micrographs taken from each panel indicate that this prediction was correct. Panel #6 contained a number of sizable macrovoids, while panel #14 contained relatively fewer small microvoids. Micrograph evidence also supported the prediction of voids in panels #8 and #5.

Large void contents, such as those described above, can result in a sizable change in the density of a composite. These large density changes would be relatively easy to detect. Perhaps of more importance is the ability to detect smaller changes in void content. The void calculation appeared to be able to do this as well, and a few examples were also shown in Chapter 4. One good example would be the comparison of Panels #2 and #4, which are Derakane 441-400 with sized and unsized AS-4, respectively. A relatively small difference in void content was calculated for the two panels, less than 0.4%. Optical micrograph images show that in fact there were slightly more voids in panel #4 than in panel #2, including a few sizable macrovoids. Another example of the accuracy of the void calculations is in the comparison of the three panels injected with RSL-1895 epoxy resin at different temperatures. Calculations for Panel #31 predicted about a 1.3% void content, while the void contents for panels #32 and #33 were 1.0% and 1.1%, respectively. Micrographs show that panel #31 does indeed contain more voids than the other two. There is also evidence suggesting that perhaps fewer voids exist in panel #32 than in #33. This suggests that the void calculation may be able to detect void changes as low as 0.1%, but certainly would detect changes of 0.3% or more.

There was considerably more error in the assessment of voids in the fiberglass

composites. Optical micrographs of panel # 04 showed that the composite was almost void free. The calculated void content was -1.25%. Panel #21, an E-glass fabric/Derakane composite had a high void content. The calculated void content, however, was less than 1%. Calculations for panel #24, an E-glass fabric and Derakane vinyl ester resin composite, indicated a slightly negative void content. While the calculations appear to be in error, they do predict the relative differences in void contents between these panels. Why this should happen only to fiberglass composites is not clear. Both the areal weight and the density of the E-glass fabric has been checked many times, and all results were in agreement. A possible explanation might be added open-pore voids in the fiberglass samples. The solvent used in density calculations might be more easily absorbed by the fiberglass composites than by similar carbon composites. The result of such absorption of alcohol would be a lower calculated void content than is actually present in the composite.

### 6.2 General Comparison of Materials Systems

The material systems used in this study were W-sized, AS-4 plain weave fabric injected with three resin systems. The resin systems included Derakane 441-400 vinyl ester resin, RSL-1895 epoxy resin, and AroCy B10 cyanate ester resin. A series of mechanical tests was conducted to compare the performance of the systems. This

section examines the results of the tests. Several modifications to the base systems, such as the use of thermoplastic-toughened cyanate ester resins or the use of unsized fibers, will be discussed in the following sections.

Comparison of the materials should begin with ease of processing. The Derakane 441-400 resin system is fairly easy to use. The resin can be mixed and used at room temperature, relieving the operator of the need to set up and control heating tape and pressure pot temperatures during infiltration. However, the Derakane resin often takes the better part of an hour to fully infiltrate the carbon preforms. The Shell RSL-1895 epoxy resin is far too viscous at room temperature for RTM use, and must be heated to obtain a good injection viscosity. When heated, the resin flows easily and will infiltrate the preform fairly quickly; but additional effort is required to set up and maintain the heated lines. AroCy B10 must also be heated, as the monomer is a solid at room temperature. Upon melting, the resin becomes a liquid with an extremely low viscosity. This is good for injection, as infiltration can occur very quickly under moderate pressure, but the low viscosity can cause some problems in the equipment. Great care must be taken to prevent leakage of the B10 liquid resin during injection, and any material that does leak from a line will crystallize onto whatever it touches.

Volume fraction and void content data for the three systems do not vary significantly. Panels made for impact testing all appear to be near 58% fiber volume fraction, while panels used for compression testing are all slightly below 61% fiber volume fraction. Panels made from Derakane and AroCy B10 average slightly above 1%

void volume fraction. Most panels in this series made from sized AS-4 fabric and RSL-1895 resin, however, have greater than a 2% calculated void volume. The final three RSL-1895 panels, injected at different temperatures, had lower void volume fractions, slightly above 1%. Despite the increased void volumes, all of the RSL-1895 panels performed adequately in mechanical tests.

AS-4 fabrics injected with each of three resin systems were tested in compression. Short block compression tests indicate that RSL-1895 resin composites are far superior to Derakane resin composites in compression. The difference in strength is so pronounced that RSL-1895 laminates were stronger in the fill direction than Derakane specimens in the warp direction. Despite the higher void content, the AS-4 fabric composite with RSL-1895 resin had a warp direction strength of about 510 MPa, compared to about 410 MPa for AS-4 fabric with Derakaneresin . The B10 resin composites were not subjected to short block compression testing. However, three B10 resin composite specimens with AS-4 fabric were tested for undamaged compression strength in the CAI geometry. The average compression strength for B10 was about 540 MPa, higher even than the RSL-1895 strength in the same geometry. It is interesting to note that the compression strengths recorded on these reference specimens were at least as high as the short block compression strengths obtained for the Derakane vinyl ester and Shell epoxy systems. These compression data are given in Tables 5.1 and 5.3.

Three specimens of each material were subjected to in-plane shear testing by the Iosipescu test. The Derakane composites with sized AS-4 fabric have a relatively low

shear strength, only about 90 MPa. Similar specimens with RSL-1895 resin showed a shear strength of about 117 MPa. The measured shear strength for the AroCy B10 composite was higher still, averaging about 130 MPa.

Interlaminar shear tests were conducted only on specimens made with Derakane 441-400 and RSL-1895. The specimens made from RSL-1895 indicated a much higher apparent shear strength than those made with Derakane. The apparent shear strength for RSL-1895 was about 63 MPa, compared to about 48 MPa for Derakane. These strengths were fairly consistent between specimens taken from four panels.

Although the RSL-1895 seemed to outperform Derakane in other tests, the epoxy matrix did not perform well under impact and CAI testing. Measurements of damage area versus impact energy indicate that composites made with RSL-1895 and Derakane resins were about the same, while those made from B10 resin showed greater resistance to impact damage. Among the three major systems, RSL-1895 had the lowest impact damage tolerance. When plotting normalized residual strength against impact energy, RSL-1895 falls well short of Derakane and B10, whose curves follow one another closely. When plotting the normalized residual strength against damage area, the performance of RSL-1895 is a bit lower than that of B10, but both carry less normalized residual strength than the Derakane. A close look at the data, however, shows that absolute strength for the damaged Shell and Derakane specimens is very close for similar impact energies, while absolute strength for B10 is often somewhat higher.

A few panels were manufactured using the style 162 E-glass with the Derakane

and Shell systems. In this case, the RSL-1895 panel with 162 E-glass was void-free, while a similar panel made with Derakane contained a fairly large void content. Short block compression specimens were cut from these panels and compared to previous results. As with the AS-4 fabric, fiberglass compression specimens made with RSL-1895 epoxy proved to be much stronger than specimens made with Derakane vinyl ester resin. This was true of both warp and fill directions.

### 6.3 Comparison of Vinyl ester composites with sized and unsized carbon

From a processing standpoint, there was little difference in the sized or unsized fiber preforms. When injected with Derakane under similar pressure profiles, complete infiltration would take about the same time with either fiber. Generally, for the same fiber volume fraction, the void contents for composites made with unsized fibers were a bit lower than composites made with sized AS-4. Comparisons between panels #2 and #4, however, indicated that the sized fiber panel contained marginally fewer voids. Panels #2 and #4 were used for impact testing of sized and unsized carbon fabric composites, respectively.

The two materials did perform differently under mechanical testing. In compression tests, the AS-4 sized fiber composites returned higher strengths. This is true both of the short block geometry and the undamaged compression specimens in the CAI

geometry. Warp direction strengths in the short block geometry averaged about 390 MPa for Derakane with sized fabric and 350 MPa for unsized. In the CAI geometry, the difference was even larger, 410 MPa as compared with 340 MPa. This difference in strength is probably a result of the less robust unsized fabric. The unsized fiber tows were frail and easily broken. The fabric was easily damaged by simply unrolling it for cutting. It is quite possible that local snags or other fiber flaws could have led to lower compression strengths.

Specimens of Derakane with sized and unsized fibers were subjected to interlaminar and in-plane shear testing. In Iosipescu in-plane shear tests, the two materials returned nearly identical results. Interlaminar shear strengths, however, were slightly higher for unsized fabric, about 50 MPa, than for sized fabric, about 48 MPa. Standard deviations for these data sets do overlap, and the separation is small, but the difference in strengths may be significant.

Impact properties of Derakane with sized and unsized carbon fibers were compared with E-glass. With about the same impact energy, the unsized carbon and E-glass materials sustained about the same amount of damage, while sized carbon composites suffered more damage. When plotted against impact energy or damage area, the E-glass composites have a far higher normalized residual strength than the graphite composites. The sized AS-4 fiber composites have lower normalized residual strengths compared with the unsized AS-4 fiber composites. The absolute compression after impact strengths for the two carbon fabric systems, however, are very close for similar

impact energies.

## 6.4 Thermoplastic-modified B10

The addition of a thermoplastic phase in the cyanate ester resin system reduced the static properties of composites, but increased the impact performance of cyanate ester composites. Iosipescu tests were conducted on specimens of sized AS-4 composites with untoughened B10 and VTUFF 1525. The untoughened B10 composite had an average shear strength of about 130 MPa. Average shear strength for the VTUFF 1525 material was lower, about 111 MPa. Shear modulus suffered a similar drop. When comparing undamaged compression strength, the strengths decreased with increasing toughener content. For example, while the AS-4 composites made with untoughened B10 had a strength of 542 MPa, the VTUFF 1520 composites' strength was only 534 MPa, and the VTUFF 1525 was only 503 MPa. These effects are probably due to the relatively soft thermoplastic phase in the matrix.

Damage due to impact changes significantly with the existence of the thermoplastic phase. Increasing toughener content was seen to decrease the damage caused by a given impact energy. Normalized residual compression strengths were seen to increase in a similar fashion, when compared against damage area and impact energy.

Normalized residual strengths for the family of B10 matrix composites fall on parallel curves when plotted against impact energy. Absolute strengths for each material were seen to be similar, however, when comparing similar impact energies.

## 6.5 Effect of injection temperature and pressure

Although attempts were originally made to directly compare the effects of injection pressure, many panels were made with different injection profiles. This made it difficult to make direct comparisons. However, a few empirical comparisons can be made, referring to the Shell RSL-1895 resin system. Several panels with this resin system were made, with both stepped and single-pressure injection profiles. The E-glass and RSL-1895 panel containing the lowest void content was injected at 83°C and 140 kPa (20 psi). This panel contained no visible voids. The sized AS-4 and RSL-1895 panel injected at 85°C and 400 kPa (60 psi) contained about 1% voids. Other RSL-1895 panels with sized AS-4 began injection at 85°C and 140 kPa (60psi) and ended at about 600 kPa (90 psi). More than half of the injection time was at the higher pressure. These panels had calculated void contents above 2%. RSL-1895 therefore appears to show the trend of increasing void content with increasing injection pressure.

Three RSL-1895 panels were injected at temperatures with 10°C increments Although the viscosity of the resin drops as temperature increases, the injection times did

not decrease as expected. Although the time decreased between the 65° and 85°C injections, the 75°C injection time was shorter than the 85°C time. The RSL-1895 viscosity model **(28)** indicates that resin viscosity would not increase significantly during an infiltration period of this length. Analysis of the specimens cut from the panel revealed that fiber volume fractions of the three panels were about the same. Void content decreased significantly between the 65° C and 75° C injections. However, the void contents of the panels infiltrated at 75°C and 85°C were about the same.

Test specimens from the three panels were subjected to flexure, interlaminar shear, and short block compression tests. The short block compression test results suggest that the compression strength increases with increasing temperature. The large scatter in the compression strength data is largely the result of the very high void content one of the compression specimens from each panel. These specimens subsequently had a much lower compression strength. However, each of the short block specimens from these panels exhibited a good failure in the center of the specimen.

Short beam shear and four-point flexure test results for the temperature variance panels were more complicated. The highest recorded strengths for each of these tests occurred in the 75°C panel. In the four-point flexure test, standard deviations for each of the panels are fairly large and overlap, but clearly there is a temperature effect. The relatively large standard deviations for these three panels are a result of the end specimen from each panel. This specimen, taken from the very edge of the panel, contained a very high void content, and failed at a lower load in all cases. No specific failure mode was

seen in any one panel, although failure on the compression side of the specimens, near one load point, was generally more common.

Interlaminar, or short beam, shear tests also indicated highest strengths in the 75°C panel. Short beam results for the 75°C panel also have a smaller standard deviation than the other two panels. Still, the standard deviations of the three data sets do overlap. Perhaps interlaminar shear specimens were taken from areas of each panel containing relatively low void volume fractions. Calculated void contents for these specimens are lower than the average for the panel. The effect is that the panel average void contents appear to have little effect on short beam shear strength.

# Chapter 7: Summary and Conclusions

Several resin transfer molded panels were made in this investigation under varying process conditions. Using a constant-pressure injection system and a 152mm x 152 mm (6" x 6") mold, three types of matrices were center-port injected into carbon and glass preforms with varying pressures and temperatures. The comparisons that were made between materials systems and process conditions included void prediction and measurement, photomicrograph study and a series of mechanical tests. Resins used included a vinyl ester system, an epoxy, and a cyanate ester resin. Fabrics used included a plain weave E-glass fabric, and sized and unsized carbon plain weave fabrics. Vinyl ester composites were made with unsized carbon fabric, and thermoplastic-toughened cyanate ester composites were manufactured with sized fabric. Generally two or three panels were made from each material system to fulfill the test matrix.

The test matrix, as originally conceived, appears to be deficient in a few areas. Although good comparisons of RSL-1895, Derakane, and AroCy B10 were made in the impact and CAI testing, some areas of the test matrix are incomplete. When the original test matrix was laid out, the B10 cyanate ester and RSL-1895 epoxy resins were in short supply. The B10 systems were therefore not used to make thicker panels for use in short block compression or short beam shear tests. Thinner panels of E-glass\ RSL-1895 were

not made to compare impact properties with E-glass\ Derakane composites. With additional supplies of these resins now available, a logical next step would be to fill these gaps in the test matrix. Other tests to be considered might include interlaminar shear with toughened cyanate ester, or injection of Derakane at elevated temperatures with the E-glass and graphite fabrics.

The fiber volume fraction and void measurement methods were seen to work well. Good agreement between fiber volume fraction methods was obtained for low void content panels. The void measurements were checked by inspection of photomicro-graphs and found to be reasonably accurate. Although a quantitative measurement of void content appeared acceptable in some cases, in most cases the method seems to be best suited to detecting qualitative changes in void volume between samples. In carbon fiber composites, variations of as little as 0.3% void volume could be reliably detected by the method. Using this technique, future work could include mapping of fiber volume fraction and void content in composite panels. A panel could be divided into a grid of specimens to be used for void content measurement only. These specimens could be measured for void content by the density method more quickly, easily, and reliably than by image analysis of micrographs, or other destructive tests, such as acid digestion.

Void measurement of fiberglass composites was somewhat less accurate than void content measurements of carbon fabric composites. Although the method was still reasonably capable of detecting the qualitative change in void content, direct measurement was off by at least 1%. A void free panel was calculated to have a negative

void content of 1.2%, while one containing a large number of voids was calculated to be nearly void free. Material properties of the resins and fibers were generated from multiple measurements, all of which were in agreement. Open porosity may be a more significant factor with the E-glass fabric than was originally thought, with the result being skewed void results. Further study of this problem is needed, including a closer look at open voids. It is also recommended that the fiberglass preform be directly weighed before loading the mold, to reduce any errors from assuming a uniform areal weight.

Mechanical tests results for the three basic resin systems showed a clear trend. The Shell RSL-1895 epoxy performed much better than Derakane vinyl ester composites in compression and both inplane and interlaminar shear tests. This trend was seen in materials with both carbon and glass reinforcements. Composites made from the RSL-1895 and Derakane 441-400 resins suffered similar amounts of damage in impact tests. Compression after impact tests indicated that AS-4 fabric composites with RSL-1895 retained a lower percentage of its strength in a damaged condition than the sized AS-4 composites with Derakane. However, the absolute strengths for these composites are about the same for similar impact energies. The sized AS-4 fabric composites with RSL-1895 resin also had a higher compression after impact strength for a given damage area than Derakane resin composites with sized AS-4.

Undamaged compression testing of AroCy B10 composites with sized AS-4 indicated strengths higher than AS-4 composites with both the RSL-1895 and Derakane

resin systems. Iosipescu shear tests showed a similar trend. Further, the sized AS-4 and B10 composites suffered less damage from impact than either the epoxy or vinyl ester systems. Impact damage to AS-4 fabric composites with B10 cyanate ester resin was lower even than Derakane composites with 162 E-glass at higher impact energies. Both relative and absolute compression strengths after impact were higher for sized AS-4 composites with B10 resin than with either Derakane or RSL-1895 resin systems. These tests indicate that B10 resin composites offer superior performance over composites made with the other resin systems in all tests considered. Future work should look at manufacture of a thicker B10 panel, and subjecting B10 composites to short block compression and interlaminar shear with the carbon fabric.

Toughened versions of the B10 cyanate ester resin offered even better normalized residual strengths and suffered less damage due to impact than their untoughened counterparts. Normalized residual strengths increase with toughener content of the matrix, but undamaged strengths for composites made with the toughened resin systems were lower than composites with untoughened B10 resin. As a result, absolute compression strengths after impact do not vary significantly among composites with various B10 cyanate ester resins. Iosipescu shear tests were also conducted on samples of AS-4 fabric composites with VTUFF 1525 and B10. The shear strengths and moduli of the VTUFF1525 composite are lower than those of the untoughened resin composite. VTUFF 1525 composites had shear performance slightly below that of AS-4 fabric composites with RSL-1895.

Several composite panels were manufactured using the Derakane vinyl ester resin and an unsized AS-4 fabric. This fabric, considerably more frail and difficult to work with than standard "W"-sized fiber, was used to investigate the interaction between the fiber sizing and preform infiltration. Generally vinyl ester composites with or without sizing infiltrated similarly, with comparable injection times. On average, void contents were slightly lower in unsized fiber composites. Mechanical tests showed a clear difference in the materials, however. Compression testing turned out in favor of the sized fiber composites, with higher strengths from both the short block and undamaged CAI specimens. Results of inplane shear testing indicated similar performance from the two materials. A small increase in apparent shear strength for the unsized fiber was noted in short beam shear tests. Unsized fabric composites appeared to perform much better in impact as well, having lower damage areas and higher normalized residual strengths for all impact energies. With the lower undamaged strength, however, the absolute strengths for the two materials turned out to be very similar with respect to impact energy, though the unsized composites still incurred less damage. The sizing therefore appears to be a slight detriment to the graphite / vinyl ester composite. Although the compression strengths dropped, possibly due to flaws in the fabric, the unsized material retained more of its strength under impact than the sized fiber composite. Unsized fiber appears to produce a better bond to the resin than fibers with sizings.

Three RSL-1895 panels made with sized AS-4 were injected at 10°C increments

and subjected to similar testing. Fiber volume fractions for the three panels were very close, but void measurement showed that fewer voids formed in panels injected at higher temperatures. Short block compression likewise showed a slight increase in strength with increasing injection temperature. However, both interlaminar shear and four point flexure tests indicated highest strengths at the middle temperature, 75°C. No explanation has been found for this. Although the panels appeared to improve in void content and also in compression with increasing temperature, bending and interlaminar properties seem to reach a maximum and then fall off slightly. It is recommended that future studies include a wider range of injection temperatures, including very low temperatures if needed. One purpose of this would be to find a lower limit to injection temperature. Below this temperature the void content of the panel may be too high, or the mechanical performance may drop to unacceptable levels. Higher injection temperatures may also determine if mechanical properties continue to fall off or if they level out with increasing injection temperatures.

The variation of injection temperature appears to have a minor effect on the void content of an RTM composite, and a small effect on mechanical properties. Reduction of injection pressure was shown to reduce the void volume fraction of the composite, but no significant improvement in mechanical properties was seen as a result. Additional trial injections at lower pressures might be attempted, to determine if void contents continue to decrease.

This research has shown that it is possible to produce high-quality, high fiber

volume fraction composites from many materials by resin transfer molding. Using resin transfer molding, high performance composites can be made quickly and consistently. Fabric preforms having high fiber volume fraction and low permeability can be successfully infiltrated with low resulting void contents. Many combinations of injection temperature and pressure were used in this investigation, resulting in small variations in void contents and mechanical properties. Lower injection pressures and higher injection temperatures result in a lower final void content in the composite.

Sized AS-4 carbon fabric was successfully used in the manufacture of composites with many resin systems. Many comparisons were made in the processing and mechanical properties of composites with vinyl ester, epoxy and cyanate ester resins. The vinyl ester, while easy to process at room temperature, had the worst performance in compression, inplane shear and interlaminar shear. The epoxy matrix composites had higher strengths in all of these categories. Compression and inplane shear tests indicated that cyanate ester resin composites were stronger than the epoxy matrix composites. Cyanate ester resin composites had compression strengths of about 540 MPa, as compared with about 500 MPa for epoxy matrix composites, or 400 MPa for vinyl ester composites. The vinyl ester resin composites had higher impact damage tolerance, and similar damage resistance, as compared to sized AS-4 composites with epoxy resin. The cyanate ester composites, however, had better impact resistance and tolerance than either vinyl ester or epoxy systems. The cyanate ester system had the best mechanical performance in all tests conducted. This resin, when heated, is also very easy

to infiltrate even high fiber volume fraction carbon preforms.

Comparisons of thermoplastic toughened cyanate esters indicated that impact properties did improve, but at the expense of static properties. While composites made with untoughened cyanate ester resin had a compression strength of about 542 MPa, composites made with 25% toughened resin had a compression strength of only 507 MPa. However, impact damage to composites made with the toughened resin was significantly lower than to composites with untoughened resin. The cyanate ester resin composite's performance, even without the toughener added, surpasses the other systems considered and is far easier to process. Aside from controlling damage area, there would be little advantage to toughening the cyanate ester system.

The use of unsized fiber in vinyl ester resin composites has similar results. Impact performance of the composites is improved, but static compression strength is lower. Compression strengths for the unsized fiber composites are about 350 MPa, as compared with about 400 MPa for sized fiber composites. The improved damage resistance and impact tolerance of the unsized fiber composites is tempered by the fact that undamaged strengths are lower. There is no discernable difference in injection time between the two fabrics, but the unsized material is more difficult to cut and load into the mold. While the unsized fiber adds slightly to the impact performance of the vinyl ester composites, it would not affect a major improvement in mechanical properties.

# References


[ 1 ] Fowler, G. and Phifer, S., "Resin Transfer Molding for High Fiber/ Low Void Content." *Proceedings of the 38th International SAMPE Symposium*, May 10-13, 1993, pp. 471-476.

[ 2 ] Carroll, E. A. and Cochran, R., "Characterization of High Fiber Volume Fraction RTM Panels." *Proceedings of the 25th International SAMPE Technical Conference*, October 26-28, 1993, pp. 222-232.

[ 3 ] Hamada, H., Ikegawa, N., and Meakawa, Z., "Structural Resin Transfer Molding With Twin Injection System." *49th Annual Conference, Composites Institute, The Society of the Plastics Industry*, February 7-9, 1994, Session 10-A.

[ 4 ] Lundström, T. S., Gebart, B. R., and Lundemo, C. Y., "Void Formation in RTM." *Journal of Reinforced Plastics and Composites*, Vol. 12, December 1993, pp. 1339-1349.

[ 5 ] Haque, A., Mahfuz, H., Yu, T. X., and Jeelani, S., "Effect of Processing Parameters on Property Changes of Resin Transfer Molded Materials." *Proceedings of the 25th International SAMPE Technical Conference*, October 26-28, 1993, pp. 305-317.

[ 6 ] Ghiorse, S. H., "Effect of Void Content on the Mechanical Properties of Carbon/Epoxy Laminates." *SAMPE Quarterly*, Vol. 24, January 1993.

[ 7 ] ASTM D2734 - 91, *Annual Book of ASTM Standards*, 1991.

[ 8 ] Hwang, K. H., Kim, Y. R., Lee, J. W., Jung, M. J., and Rew, Y., "Effects of Processing Conditions on the Formation of Voids During Advanced RTM Processes." *49th Annual Conference, Composites Institute, The Society of the Plastics Industry*, February 7-9, 1994, Session 4-F.

[ 9 ] Stabler, W. R., Tatterson, G. B., Sadler, R. L., and El-Shiekh, A. H. M., "Void Minimization in the Manufacture of Carbon Fiber Composites by Resin Transfer Molding." *SAMPE Quarterly*, Vol. 23, January 1993.

[ 10 ] Palmese, G. R., and Karbhari, V. M., "Effects of Sizings on Microscopic Flow encountered in RTM Processing." *Proceedings of the 25th International SAMPE Technical Conference*, October 26-28, 1993, pp. 254-264.

[ 11 ] Dahlbäck, L. M., and Lundström, T.S., "A Method to Measure Wetting Between Resin and Reinforcement." *Proceedings of the Tenth International Conference on Composite Materials*, August 14-18, 1995, pp. 293-300.

[ 12 ] Hammani, A., Gauvin, R., Trochu, F., Tauret, O., and Ferland, P., "Analysis of the Edge Effect on Flow Patterns in Liquid Composite Molding.", *Proceedings of the Tenth International Conference on Composite Materials*, August 14-18, 1995, pp.277-284.

[ 13 ] Leek, R., Carpenter, G., Rubel, A., and Donnellan, T., "Simulation of Edge Flow Effects in Resin Transfer Molding.", *Proceedings of the 25th International SAMPE Technical Conference*, October 26-29, 1993, pp. 233-245.

[ 14 ] Salem, A. J. and Parnas, R. S., "The Unidirectional and Radial In-Plane Flow of Fluids Through Woven Composite Reinforcements." *Proceedings of the American Society for Composites Sixth Technical Conference*, October 7-9, 1991, pp. 1012-1021.

[ 15 ] Karbhari, V. M. and Wilkins, D.A., "Effect of Preform Architecture and Injection Strategies on the Robustness of RTM Parts." *Advanced Composite Materials: New Developments and Applications Conference Proceedings,* September 30-October 3, 1991, pp. 91-103.

[ 16 ] Bretz, G. T., Houston, D. Q., Sullivan, J. L., Hagerman, E., and Kakarala, N., "Discussion of Test Procedure Involving Iosipescu Shear Testing." *Proceedings of the 8th ASM Advanced Composites Conference*, November 2-5, 1992.

[ 17 ] Hayward, J.B. and Harris, B. "Effect of Process Variables on the Quality of RTM Mouldings." *SAMPE Journal,* Vol. 26, May 1993, pp. 39-46.

[ 18 ] Carroll, E.A. and Cochran, R., "Characterization of RTM Panels with Woven Preforms." Proceedings of the 34th International SAMPE Symposium, May 8-11, 1989, pp.97-107.

[ 19 ] Chan, A. W. and Morgan, R. J., "Resin Impregnation and Void Formation in Enhanced Resin Transfer Molding Scheme." *Proceedings of the 8th Annual ASM Advanced Composites Conference*, November 2-5, 1992, pp. 69-73.

[ 20 ] Kuttenkeuler, J. and Grenestedt, J. L., "Influence of Process Parameters on Mechanical Behavior of RTM Moldings." *Proceedings of the 10th International Conference on Composite Materials*, August 14-18 1995, pp. 261-268.

[ 21 ] Stockton, J. E., "Structural Resin Transfer Molding of High Temperature Composites." *Proceedings of the 34th International SAMPE Symposium*, May 8-11, 1989, pp. 1032-1040.

[ 22 ] Rhône-Poulenc, Performance Resins and Coatings Division, Technical Bulletin, AroCy B-10 Cyanate Ester Monomer.

[ 23 ] Rau, A. V., unpublished work.

[ 24 ] Minguet, P., Fedro, M., and Gunther, C., "Test Methods for Textile Composites." *NASA Contractor Report No. 4609*, July 1994.

[ 25 ] Hackett, S. J. and Griebling, P.C., "Unique Advanced Materials with High Performance and Resin Transfer Molding Characteristics." *Advanced Materials, Cost Effectiveness, Quality Control, Health and Environment*, May 28-30, 1991.

[ 26 ] Weideman, M. H., Loos, A. C., Dexter, H. B., and Hasko, G. H., "An Infiltration/ Cure Model for Manufacture of Fabric Composites by the Resin Infusion Process." *Virginia Tech Center for Composite Materials and Structures, Report No. CCMS-92-05*, 1992.

[ 27 ] MacRae, J. D., Loos, A. C., Dexter, H. B., Deaton, J. W., and Hasko, G. H., "Development and Verification of a Resin Film Infusion/ Resin Transfer Molding Simulation Model for Fabrication of Advanced Textile Composites." *Virginia Tech Center for Composite Materials and Structures, Report No. CCMS-95-01*, 1994.

[ 28 ] Hammond, V.H., Loos, A. C., Dexter, H.B. and Hasko, G.H., "Verification of a Two-Dimensional Infiltration Model for the Resin Transfer Molding Process." *Virginia Tech Center for Composite Materials and Structures, Report No. CCMS-93-15*, 1993.

[ 29 ] The Dow Chemical Company, Thermoset Applications Industry Group, Technical Product Information, "DERAKANE Epoxy Vinyl Ester Resins".

# Appendix: Physical Measurements of Specimens

This appendix contains the physical data generated for each specimen used in this investigation. All specimens were measured for size, density, fiber volume fraction and void content.

The physical measurements are in tabular form. Each row corresponds to a single mechanical specimen, whose panel designation can be found in the first column. The second column indicates the specimen number. The remaining columns in the table, from left to right, indicate:

- Thickness, width, and length of the specimen in mm.
- Weight of the specimen in air, grams.
- Weight of the specimen suspended in Isopropyl Alcohol (IPA), grams.
- Calculated density of the composite specimen, based on weights in air and IPA.
- Resin used in the composite and its density, (g/cc). The densities for the resins were measured values.
- Fiber used in the composite, its density (g/cc), the number of plies "n", and Areal Weight ($g/m^2$). The densities used for glass fibers were measured, while the literature values were used for carbon.
- Fiber volume fraction, based on the areal weight and thickness calculation.
- Fiber volume fraction, based on the density method
- Void volume fraction, based on the technique described in Chapter 2.

| | | mm | mm | mm | grams | grams | g/cc | | g/cc | | g/cc | g/m² | | | | |
|---|---|---|---|---|---|---|---|---|---|---|---|---|---|---|---|---|
| Panel | Spec | Thick | Width | Length | Wt. in Air | Wt. in IPA | Density | Resin | Density | Fiber | Density | Areal Wt | n | Vf Areal | Vfdensity | Vvoid |
| 02 | 02A | 6.350 | 44.60 | 38.08 | 20.619 | 12.182 | 1.919 | DK | 1.173 | 162e | 2.565 | 391.8 | 23 | 0.553 | 0.536 | 0.020 |
| 02 | 02B | 6.350 | 44.55 | 38.22 | 20.659 | 12.18 | 1.914 | DK | 1.173 | 162e | 2.565 | 391.8 | 23 | 0.553 | 0.532 | 0.025 |
| 02 | 02C | 6.350 | 44.54 | 38.16 | 20.648 | 12.187 | 1.917 | DK | 1.173 | 162e | 2.565 | 391.8 | 23 | 0.553 | 0.534 | 0.023 |
| 02 | 02X | 6.325 | 44.52 | 38.15 | 20.652 | 12.204 | 1.920 | DK | 1.173 | 162e | 2.565 | 391.8 | 23 | 0.555 | 0.537 | 0.022 |
| 02 | 02Y | 6.325 | 44.56 | 38.09 | 20.661 | 12.22 | 1.922 | DK | 1.173 | 162e | 2.565 | 391.8 | 23 | 0.555 | 0.538 | 0.020 |
| 02 | 02Z | 6.350 | 44.55 | 38.08 | 20.662 | 12.239 | 1.927 | DK | 1.173 | 162e | 2.565 | 391.8 | 23 | 0.553 | 0.541 | 0.014 |
| 04 | 04A | 6.340 | 44.50 | 38.16 | 21.159 | 12.726 | 1.971 | RSL | 1.186 | 162e | 2.565 | 391.8 | 23 | 0.554 | 0.569 | -0.017 |
| 04 | 04B | 6.370 | 44.45 | 38.15 | 21.218 | 12.744 | 1.967 | RSL | 1.186 | 162e | 2.565 | 391.8 | 23 | 0.552 | 0.566 | -0.017 |
| 04 | 04C | 6.320 | 44.48 | 38.12 | 21.138 | 12.738 | 1.976 | RSL | 1.186 | 162e | 2.565 | 391.8 | 23 | 0.556 | 0.573 | -0.020 |
| 04 | 04X | 6.375 | 44.45 | 38.12 | 21.18 | 12.652 | 1.951 | RSL | 1.186 | 162e | 2.565 | 391.8 | 23 | 0.551 | 0.554 | -0.004 |
| 04 | 04Y | 6.350 | 44.49 | 38.11 | 21.177 | 12.68 | 1.957 | RSL | 1.186 | 162e | 2.565 | 391.8 | 23 | 0.553 | 0.559 | -0.007 |
| 04 | 04Z | 6.350 | 44.49 | 38.09 | 21.129 | 12.663 | 1.960 | RSL | 1.186 | 162e | 2.565 | 391.8 | 23 | 0.553 | 0.561 | -0.009 |
| 1 | 1A | 6.280 | 44.54 | 38.17 | 16.333 | 7.942 | 1.529 | DK | 1.173 | AS4/S | 1.800 | 193 | 36 | 0.615 | 0.567 | 0.025 |
| 1 | 1B | 6.300 | 44.49 | 38.09 | 16.417 | 7.978 | 1.528 | DK | 1.173 | AS4/S | 1.800 | 193 | 36 | 0.613 | 0.566 | 0.025 |
| 1 | 1C | 6.310 | 44.51 | 38.12 | 16.422 | 7.988 | 1.529 | DK | 1.173 | AS4/S | 1.800 | 193 | 36 | 0.612 | 0.568 | 0.023 |
| 1 | 1X | 6.260 | 44.57 | 38.13 | 16.334 | 7.945 | 1.529 | DK | 1.173 | AS4/S | 1.800 | 193 | 36 | 0.617 | 0.568 | 0.026 |
| 1 | 1Y | 6.350 | 44.56 | 38.26 | 16.429 | 7.973 | 1.526 | DK | 1.173 | AS4/S | 1.800 | 193 | 36 | 0.608 | 0.563 | 0.024 |
| 1 | 1Z | 6.310 | 44.53 | 38.15 | 16.454 | 8.008 | 1.530 | DK | 1.173 | AS4/S | 1.800 | 193 | 36 | 0.612 | 0.569 | 0.023 |
| 1 | 1 S1 | 6.420 | 6.35 | 38.12 | 2.3857 | 1.164 | 1.534 | DK | 1.173 | AS4/S | 1.800 | 193 | 36 | 0.601 | 0.575 | 0.014 |
| 1 | 1 S2 | 6.430 | 6.35 | 38.13 | 2.3844 | 1.165 | 1.536 | DK | 1.173 | AS4/S | 1.800 | 193 | 36 | 0.600 | 0.579 | 0.012 |
| 1 | 1 S3 | 6.430 | 6.27 | 38.09 | 2.3519 | 1.148 | 1.534 | DK | 1.173 | AS4/S | 1.800 | 193 | 36 | 0.600 | 0.576 | 0.013 |
| 1 | 1 S4 | 6.420 | 6.36 | 38.09 | 2.3821 | 1.162 | 1.533 | DK | 1.173 | AS4/S | 1.800 | 193 | 36 | 0.601 | 0.575 | 0.014 |
| 1 | 1 S5 | 6.410 | 6.34 | 37.99 | 2.3671 | 1.158 | 1.538 | DK | 1.173 | AS4/S | 1.800 | 193 | 36 | 0.602 | 0.582 | 0.011 |
| 1 | 1 S6 | 6.390 | 6.35 | 38.09 | 2.3655 | 1.157 | 1.537 | DK | 1.173 | AS4/S | 1.800 | 193 | 36 | 0.604 | 0.581 | 0.012 |
| 2 | 2A | 3.388 | 65.05 | 65.05 | 21.8658 | 10.646 | 1.531 | DK | 1.173 | AS4/S | 1.800 | 193 | 18 | 0.570 | 0.570 | -0.000 |
| 2 | 2B | 3.368 | 65.05 | 65.04 | 21.7104 | 10.585 | 1.533 | DK | 1.173 | AS4/S | 1.800 | 193 | 18 | 0.573 | 0.574 | -0.000 |
| 2 | 2C | 3.371 | 65.02 | 65.02 | 21.7335 | 10.604 | 1.534 | DK | 1.173 | AS4/S | 1.800 | 193 | 18 | 0.573 | 0.575 | -0.001 |
| 2 | 2D | 3.366 | 65.02 | 65.02 | 21.7306 | 10.343 | 1.499 | DK | 1.173 | AS4/S | 1.800 | 193 | 18 | 0.573 | 0.520 | 0.029 |
| 4 | 4A | 3.411 | 65.00 | 64.99 | 21.6293 | 10.439 | 1.518 | DK | 1.173 | AS4/U | 1.800 | 193 | 18 | 0.566 | 0.550 | 0.008 |
| 4 | 4B | 3.366 | 65.00 | 64.99 | 21.3632 | 10.321 | 1.520 | DK | 1.173 | AS4/U | 1.800 | 193 | 18 | 0.573 | 0.553 | 0.011 |
| 4 | 4C | 3.373 | 64.99 | 65.01 | 21.4673 | 10.393 | 1.522 | DK | 1.173 | AS4/U | 1.800 | 193 | 18 | 0.572 | 0.557 | 0.008 |
| 4 | 4D | 3.343 | 65.00 | 65.01 | 21.2363 | 10.255 | 1.519 | DK | 1.173 | AS4/U | 1.800 | 193 | 18 | 0.577 | 0.552 | 0.014 |
| 5 | 5A | 3.358 | 65.00 | 64.95 | 21.5016 | 10.427 | 1.525 | B10 | 1.22 | AS4/S | 1.800 | 193 | 18 | 0.575 | 0.526 | 0.023 |
| 5 | 5B | 3.332 | 65.02 | 65.02 | 21.3932 | 10.557 | 1.551 | B10 | 1.22 | AS4/S | 1.800 | 193 | 18 | 0.579 | 0.570 | 0.004 |

| | | mm | mm | mm | grams | grams | g/cc | | g/cc | | g/cc | g/m² | | | | |
|---|---|---|---|---|---|---|---|---|---|---|---|---|---|---|---|---|
| Panel | Spec | Thick | Width | Length | Wt. in Air | Wt. in IPA | Density | Resin | Density | Fiber | Density | Areal Wt | n | Vf Areal | Vf density | Vvoid |
| 5 | 5C | 3.312 | 64.99 | 65.04 | 21.3259 | 10.409 | 1.534 | B10 | 1.22 | AS4/S | 1.800 | 193 | 18 | 0.583 | 0.542 | 0.019 |
| 5 | 5D | 3.299 | 64.97 | 64.97 | 21.2639 | 10.389 | 1.536 | B10 | 1.22 | AS4/S | 1.800 | 193 | 18 | 0.585 | 0.544 | 0.019 |
| 6 | 6A | 3.254 | 65.04 | 65.02 | 20.9472 | 10.237 | 1.536 | Vt25 | 1.22 | AS4/S | 1.800 | 193 | 18 | 0.593 | 0.545 | 0.023 |
| 6 | 6B | 3.266 | 65.02 | 65.02 | 20.8486 | 10.139 | 1.529 | Vt25 | 1.22 | AS4/S | 1.800 | 193 | 18 | 0.591 | 0.533 | 0.028 |
| 8 | 8A | 3.205 | 65.04 | 65.05 | 20.643 | 10.07 | 1.533 | RSL | 1.186 | AS4/S | 1.800 | 193 | 18 | 0.602 | 0.566 | 0.019 |
| 8 | 8B | 3.205 | 65.05 | 65.02 | 20.6109 | 10.03 | 1.530 | RSL | 1.186 | AS4/S | 1.800 | 193 | 18 | 0.602 | 0.560 | 0.022 |
| 8 | 8C | 3.183 | 65.02 | 65.01 | 20.5133 | 10.019 | 1.535 | RSL | 1.186 | AS4/S | 1.800 | 193 | 18 | 0.606 | 0.569 | 0.019 |
| 8 | 8D | 3.195 | 65.01 | 65.02 | 20.5174 | 9.985 | 1.530 | RSL | 1.186 | AS4/S | 1.800 | 193 | 18 | 0.604 | 0.560 | 0.023 |
| 11 | 11I | 3.120 | 76.21 | 19.05 | 6.821 | 3.346 | 1.542 | DK | 1.173 | AS4/U | 1.800 | 193 | 18 | 0.619 | 0.588 | 0.016 |
| 11 | 11J | 3.140 | 76.22 | 19.08 | 6.876 | 3.376 | 1.543 | DK | 1.173 | AS4/U | 1.800 | 193 | 18 | 0.615 | 0.590 | 0.013 |
| 11 | 11K | 3.150 | 76.22 | 19.04 | 6.913 | 3.396 | 1.544 | DK | 1.173 | AS4/U | 1.800 | 193 | 18 | 0.613 | 0.591 | 0.011 |
| 11 | 11R | 3.160 | 51.98 | 25.41 | 6.443 | 3.157 | 1.540 | DK | 1.173 | AS4/U | 1.800 | 193 | 18 | 0.611 | 0.585 | 0.014 |
| 12 | 12I | 3.160 | 76.21 | 89.56 | 6.81 | 3.301 | 1.524 | DK | 1.173 | AS4/S | 1.800 | 193 | 18 | 0.611 | 0.560 | 0.027 |
| 12 | 12J | 3.160 | 76.21 | 19.04 | 6.851 | 3.377 | 1.549 | DK | 1.173 | AS4/S | 1.800 | 193 | 18 | 0.611 | 0.599 | 0.006 |
| 12 | 12K | 3.170 | 76.30 | 19.06 | 6.871 | 3.34 | 1.528 | DK | 1.173 | AS4/S | 1.800 | 193 | 18 | 0.609 | 0.567 | 0.023 |
| 12 | 12R | 3.180 | 52.00 | 25.40 | 6.433 | 3.124 | 1.527 | DK | 1.173 | AS4/S | 1.800 | 193 | 18 | 0.607 | 0.564 | 0.023 |
| 14 | 14IC | 3.510 | 64.92 | 64.98 | 22.543 | 10.887 | 1.519 | Vt25 | 1.22 | AS4/S | 1.800 | 193 | 18 | 0.550 | 0.515 | 0.016 |
| 14 | 14ID | 3.470 | 64.92 | 64.95 | 22.419 | 10.847 | 1.522 | Vt25 | 1.22 | AS4/S | 1.800 | 193 | 18 | 0.556 | 0.520 | 0.017 |
| 14 | 14I | 3.460 | 76.18 | 19.35 | 7.459 | 3.616 | 1.524 | Vt25 | 1.22 | AS4/S | 1.800 | 193 | 18 | 0.558 | 0.525 | 0.016 |
| 14 | 14J | 3.460 | 76.20 | 19.03 | 7.479 | 3.626 | 1.525 | Vt25 | 1.22 | AS4/S | 1.800 | 193 | 18 | 0.558 | 0.525 | 0.016 |
| 14 | 14K | 3.460 | 76.18 | 19.04 | 7.476 | 3.623 | 1.524 | Vt25 | 1.22 | AS4/S | 1.800 | 193 | 18 | 0.558 | 0.524 | 0.016 |
| 14 | 14R | 3.460 | 51.98 | 25.45 | 6.91 | 3.36 | 1.529 | Vt25 | 1.22 | AS4/S | 1.800 | 193 | 18 | 0.558 | 0.532 | 0.012 |
| 15 | 15I | 3.290 | 76.21 | 19.05 | 7.136 | 3.451 | 1.521 | RSL | 1.186 | AS4/S | 1.800 | 193 | 18 | 0.587 | 0.545 | 0.021 |
| 15 | 15J | 3.300 | 76.19 | 19.03 | 7.153 | 3.464 | 1.523 | RSL | 1.186 | AS4/S | 1.800 | 193 | 18 | 0.585 | 0.549 | 0.019 |
| 15 | 15K | 3.300 | 76.21 | 19.04 | 7.172 | 3.468 | 1.521 | RSL | 1.186 | AS4/S | 1.800 | 193 | 18 | 0.585 | 0.545 | 0.021 |
| 15 | 15R | 3.340 | 51.98 | 24.41 | 6.717 | 3.239 | 1.517 | RSL | 1.186 | AS4/S | 1.800 | 193 | 18 | 0.578 | 0.539 | 0.020 |
| 16 | 16A | 6.370 | 44.55 | 38.07 | 16.571 | 8.06 | 1.529 | RSL | 1.186 | AS4/S | 1.800 | 193 | 36 | 0.606 | 0.559 | 0.024 |
| 16 | 16B | 6.360 | 44.52 | 38.08 | 16.594 | 8.088 | 1.532 | RSL | 1.186 | AS4/S | 1.800 | 193 | 36 | 0.607 | 0.564 | 0.022 |
| 16 | 16C | 6.350 | 44.50 | 38.09 | 16.535 | 8.046 | 1.530 | RSL | 1.186 | AS4/S | 1.800 | 193 | 36 | 0.608 | 0.560 | 0.025 |
| 16 | 16X | 6.380 | 44.52 | 38.15 | 16.594 | 8.09 | 1.533 | RSL | 1.186 | AS4/S | 1.800 | 193 | 36 | 0.605 | 0.564 | 0.021 |
| 16 | 16Y | 6.380 | 44.51 | 38.11 | 16.67 | 8.125 | 1.532 | RSL | 1.186 | AS4/S | 1.800 | 193 | 36 | 0.605 | 0.564 | 0.021 |
| 16 | 16Z | 6.370 | 44.50 | 38.08 | 16.654 | 8.153 | 1.539 | RSL | 1.186 | AS4/S | 1.800 | 193 | 36 | 0.606 | 0.574 | 0.016 |
| 16 | 16 S1 | 6.380 | 6.34 | 38.20 | 2.3971 | 1.181 | 1.548 | RSL | 1.186 | AS4/S | 1.800 | 193 | 36 | 0.605 | 0.590 | 0.008 |
| 16 | 16 S2 | 6.380 | 6.35 | 38.20 | 2.3956 | 1.179 | 1.547 | RSL | 1.186 | AS4/S | 1.800 | 193 | 36 | 0.605 | 0.587 | 0.009 |

| | | mm | mm | mm | grams | grams | g/cc | | g/cc | | g/cc | g/m² | | | | |
|---|---|---|---|---|---|---|---|---|---|---|---|---|---|---|---|---|
| **Panel** | **Spec** | **Thick** | **Width** | **Length** | **Wt. in Air** | **Wt. in IPA** | **Density** | **Resin** | **Density** | **Fiber** | **Density** | **Areal Wt** | **n** | **Vf Areal** | **Vf density** | **Vvoid** |
| 16 | 16 S3 | 6.300 | 6.34 | 38.20 | 2.4003 | 1.183 | 1.549 | RSL | 1.186 | AS4/S | 1.800 | 193 | 36 | 0.613 | 0.591 | 0.011 |
| 16 | 16 S4 | 6.390 | 6.34 | 38.20 | 2.3946 | 1.179 | 1.547 | RSL | 1.186 | AS4/S | 1.800 | 193 | 36 | 0.604 | 0.588 | 0.008 |
| 16 | 16 S5 | 6.390 | 6.34 | 38.20 | 2.3946 | 1.179 | 1.547 | RSL | 1.186 | AS4/S | 1.800 | 193 | 36 | 0.604 | 0.588 | 0.008 |
| 16 | 16 S6 | 6.390 | 6.35 | 38.19 | 2.4024 | 1.186 | 1.551 | RSL | 1.186 | AS4/S | 1.800 | 193 | 36 | 0.604 | 0.595 | 0.005 |
| 18 | 18A | 6.500 | 44.49 | 38.09 | 16.553 | 8.104 | 1.539 | DK | 1.173 | AS4/U | 1.800 | 193 | 36 | 0.594 | 0.583 | 0.006 |
| 18 | 18B | 6.300 | 44.49 | 38.11 | 16.551 | 8.142 | 1.546 | DK | 1.173 | AS4/U | 1.800 | 193 | 36 | 0.613 | 0.595 | 0.010 |
| 18 | 18C | 6.280 | 44.55 | 38.14 | 16.491 | 8.11 | 1.545 | DK | 1.173 | AS4/U | 1.800 | 193 | 36 | 0.615 | 0.594 | 0.011 |
| 18 | 18X | 6.460 | 44.50 | 38.10 | 16.723 | 8.153 | 1.533 | DK | 1.173 | AS4/U | 1.800 | 193 | 36 | 0.598 | 0.573 | 0.013 |
| 18 | 18Y | 6.460 | 44.49 | 38.10 | 16.719 | 8.165 | 1.535 | DK | 1.173 | AS4/U | 1.800 | 193 | 36 | 0.598 | 0.577 | 0.011 |
| 18 | 18Z | 6.310 | 44.51 | 38.11 | 16.568 | 8.14 | 1.544 | DK | 1.173 | AS4/U | 1.800 | 193 | 36 | 0.612 | 0.592 | 0.011 |
| 18 | 18 S1 | 6.330 | 6.35 | 38.12 | 2.3743 | 1.171 | 1.550 | DK | 1.173 | AS4/U | 1.800 | 193 | 36 | 0.610 | 0.601 | 0.005 |
| 18 | 18 S2 | 6.340 | 6.36 | 38.14 | 2.3782 | 1.173 | 1.550 | DK | 1.173 | AS4/U | 1.800 | 193 | 36 | 0.609 | 0.601 | 0.004 |
| 18 | 18 S3 | 6.330 | 6.35 | 38.11 | 2.3802 | 1.176 | 1.552 | DK | 1.173 | AS4/U | 1.800 | 193 | 36 | 0.610 | 0.605 | 0.003 |
| 18 | 18 S4 | 6.340 | 6.35 | 38.11 | 2.3751 | 1.172 | 1.550 | DK | 1.173 | AS4/U | 1.800 | 193 | 36 | 0.609 | 0.602 | 0.004 |
| 18 | 18 S5 | 6.330 | 6.36 | 38.12 | 2.3863 | 1.172 | 1.543 | DK | 1.173 | AS4/U | 1.800 | 193 | 36 | 0.610 | 0.591 | 0.010 |
| 18 | 18 S6 | 6.330 | 6.36 | 38.11 | 2.3772 | 1.174 | 1.552 | DK | 1.173 | AS4/U | 1.800 | 193 | 36 | 0.610 | 0.604 | 0.003 |
| 19 | 19R2 | 3.175 | 50.72 | 25.44 | 6.3371 | 3.146 | 1.560 | B10 | 1.22 | AS4/S | 1.800 | 193 | 18 | 0.608 | 0.586 | 0.011 |
| 19 | 19R3 | 3.190 | 52.02 | 25.43 | 6.5291 | 3.239 | 1.559 | B10 | 1.22 | AS4/S | 1.800 | 193 | 18 | 0.605 | 0.584 | 0.010 |
| 20 | 20A | 3.302 | 64.72 | 65.07 | 21.28 | 10.448 | 1.543 | Vt20 | 1.22 | AS4/S | 1.800 | 193 | 18 | 0.584 | 0.557 | 0.013 |
| 20 | 20B | 3.251 | 65.00 | 65.07 | 21.158 | 10.397 | 1.544 | Vt20 | 1.22 | AS4/S | 1.800 | 193 | 18 | 0.594 | 0.559 | 0.016 |
| 20 | 20C | 3.302 | 64.85 | 65.07 | 21.39 | 10.463 | 1.537 | Vt20 | 1.22 | AS4/S | 1.800 | 193 | 18 | 0.584 | 0.547 | 0.018 |
| 20 | 20D | 3.277 | 64.74 | 65.07 | 21.203 | 10.41 | 1.543 | Vt20 | 1.22 | AS4/S | 1.800 | 193 | 18 | 0.589 | 0.557 | 0.015 |
| 21 | 21A | 3.393 | 64.97 | 64.96 | 27.1428 | 15.989 | 1.911 | DK | 1.173 | 162e | 2.565 | 391.8 | 12 | 0.540 | 0.530 | 0.012 |
| 21 | 21B | 3.393 | 65.00 | 64.97 | 27.1693 | 16.029 | 1.915 | DK | 1.173 | 162e | 2.565 | 391.8 | 12 | 0.540 | 0.533 | 0.008 |
| 21 | 21C | 3.396 | 65.01 | 65.02 | 27.2461 | 16.075 | 1.916 | DK | 1.173 | 162e | 2.565 | 391.8 | 12 | 0.540 | 0.533 | 0.007 |
| 21 | 21D | 3.368 | 64.99 | 64.97 | 27.0394 | 15.969 | 1.918 | DK | 1.173 | 162e | 2.565 | 391.8 | 12 | 0.544 | 0.535 | 0.010 |
| 24 | 24R1 | 3.353 | 51.77 | 25.45 | 8.4831 | 5.048 | 1.940 | DK | 1.173 | 162e | 2.565 | 391.8 | 12 | 0.547 | 0.551 | -0.005 |
| 24 | 24R2 | 3.383 | 51.97 | 25.43 | 8.512 | 5.04 | 1.925 | DK | 1.173 | 162e | 2.565 | 391.8 | 12 | 0.542 | 0.541 | 0.001 |
| 24 | 24R3 | 3.405 | 51.73 | 25.44 | 8.512 | 5.029 | 1.919 | DK | 1.173 | 162e | 2.565 | 391.8 | 12 | 0.538 | 0.536 | 0.002 |
| 25 | 25R1 | 3.327 | 51.93 | 25.43 | 6.7548 | 3.384 | 1.574 | Vt1520 | 1.22 | AS4/S | 1.800 | 193 | 18 | 0.580 | 0.610 | -0.014 |
| 25 | 25R2 | 3.315 | 51.75 | 25.46 | 6.7518 | 3.341 | 1.555 | Vt1520 | 1.22 | AS4/S | 1.800 | 193 | 18 | 0.582 | 0.577 | 0.002 |
| 25 | 25R3 | 3.299 | 51.49 | 25.45 | 6.6953 | 3.36 | 1.577 | Vt1520 | 1.22 | AS4/S | 1.800 | 193 | 18 | 0.585 | 0.615 | -0.014 |
| 27 | 27IA | 3.350 | 65.05 | 65.00 | 21.3735 | 10.402 | 1.530 | Vt1525 | 1.22 | AS4/S | 1.800 | 193 | 18 | 0.576 | 0.535 | 0.020 |
| 27 | 27IB | 3.363 | 65.02 | 65.19 | 21.5598 | 10.52 | 1.534 | Vt1525 | 1.22 | AS4/S | 1.800 | 193 | 18 | 0.574 | 0.541 | 0.016 |

| | | mm | mm | mm | grams | grams | g/cc | | g/cc | | g/cc | g/m² | | | | |
|---|---|---|---|---|---|---|---|---|---|---|---|---|---|---|---|---|
| Panel | Spec | Thick | Width | Length | Wt. in Air | Wt. in IPA | Density | Resin | Density | Fiber | Density | Areal Wt | n | Vf Areal | Vf density | Vvoid |
| 27 | 27R1 | 3.322 | 52.02 | 25.43 | 6.704 | 3.25 | 1.524 | Vt1525 | 1.22 | AS4/S | 1.800 | 193 | 18 | 0.581 | 0.525 | 0.027 |
| 27 | 27R2 | 3.294 | 52.02 | 25.43 | 6.6992 | 3.293 | 1.545 | Vt1525 | 1.22 | AS4/S | 1.800 | 193 | 18 | 0.586 | 0.560 | 0.012 |
| 31 | 31A | 6.390 | 38.12 | 44.43 | 16.7068 | 8.214 | 1.545 | RSL | 1.186 | AS4/S | 1.800 | 193 | 36 | 0.604 | 0.585 | 0.010 |
| 31 | 31B | 6.380 | 38.09 | 44.46 | 16.5095 | 8.039 | 1.531 | RSL | 1.186 | AS4/S | 1.800 | 193 | 36 | 0.605 | 0.562 | 0.023 |
| 31 | 31C | 6.370 | 38.09 | 44.46 | 16.6576 | 8.185 | 1.544 | RSL | 1.186 | AS4/S | 1.800 | 193 | 36 | 0.606 | 0.583 | 0.012 |
| 31 | 31 S1 | 6.390 | 6.33 | 38.06 | 2.3682 | 1.164 | 1.545 | RSL | 1.186 | AS4/S | 1.800 | 193 | 36 | 0.604 | 0.584 | 0.010 |
| 31 | 31 S2 | 6.390 | 6.34 | 38.08 | 2.3837 | 1.171 | 1.544 | RSL | 1.186 | AS4/S | 1.800 | 193 | 36 | 0.604 | 0.583 | 0.011 |
| 31 | 31 S3 | 6.390 | 6.33 | 38.08 | 2.3852 | 1.173 | 1.545 | RSL | 1.186 | AS4/S | 1.800 | 193 | 36 | 0.604 | 0.585 | 0.010 |
| 31 | 31 S4 | 6.380 | 6.33 | 37.98 | 2.3797 | 1.174 | 1.550 | RSL | 1.186 | AS4/S | 1.800 | 193 | 36 | 0.605 | 0.593 | 0.006 |
| 31 | 31 S5 | 6.380 | 6.33 | 38.03 | 2.3751 | 1.167 | 1.544 | RSL | 1.186 | AS4/S | 1.800 | 193 | 36 | 0.605 | 0.583 | 0.011 |
| 31 | 31 S6 | 6.370 | 6.32 | 38.05 | 2.3653 | 1.161 | 1.543 | RSL | 1.186 | AS4/S | 1.800 | 193 | 36 | 0.606 | 0.581 | 0.013 |
| 31 | 31 F1 | 6.400 | 12.70 | ******* | 15.9222 | 7.838 | 1.547 | RSL | 1.186 | AS4/S | 1.800 | 193 | 36 | 0.603 | 0.588 | 0.008 |
| 31 | 31 F2 | 6.390 | 12.70 | | 15.8861 | 7.815 | 1.546 | RSL | 1.186 | AS4/S | 1.800 | 193 | 36 | 0.604 | 0.586 | 0.009 |
| 31 | 31 F3 | 6.390 | 12.70 | | 15.8935 | 7.811 | 1.544 | RSL | 1.186 | AS4/S | 1.800 | 193 | 36 | 0.604 | 0.584 | 0.011 |
| 31 | 31 F4 | 6.400 | 12.70 | | 15.82 | 7.729 | 1.536 | RSL | 1.186 | AS4/S | 1.800 | 193 | 36 | 0.603 | 0.569 | 0.017 |
| 31 | 31 F5 | 6.420 | 12.70 | | 15.6885 | 7.595 | 1.522 | RSL | 1.186 | AS4/S | 1.800 | 193 | 36 | 0.601 | 0.548 | 0.028 |
| 32 | 32A | 6.410 | 38.09 | 44.48 | 16.751 | 8.225 | 1.543 | RSL | 1.186 | AS4/S | 1.800 | 193 | 36 | 0.602 | 0.582 | 0.011 |
| 32 | 32B | 6.380 | 38.13 | 44.49 | 16.6517 | 8.176 | 1.543 | RSL | 1.186 | AS4/S | 1.800 | 193 | 36 | 0.605 | 0.581 | 0.012 |
| 32 | 32C | 6.370 | 38.10 | 44.44 | 16.6337 | 8.181 | 1.546 | RSL | 1.186 | AS4/S | 1.800 | 193 | 36 | 0.606 | 0.586 | 0.011 |
| 32 | 32 S1 | 6.360 | 6.35 | 38.06 | 2.38 | 1.171 | 1.546 | RSL | 1.186 | AS4/S | 1.800 | 193 | 36 | 0.607 | 0.587 | 0.011 |
| 32 | 32 S2 | 6.360 | 6.33 | 38.11 | 2.3763 | 1.172 | 1.550 | RSL | 1.186 | AS4/S | 1.800 | 193 | 36 | 0.607 | 0.592 | 0.008 |
| 32 | 32 S3 | 6.360 | 6.32 | 38.12 | 2.3784 | 1.173 | 1.550 | RSL | 1.186 | AS4/S | 1.800 | 193 | 36 | 0.607 | 0.592 | 0.008 |
| 32 | 32 S4 | 6.370 | 6.32 | 38.11 | 2.3771 | 1.175 | 1.553 | RSL | 1.186 | AS4/S | 1.800 | 193 | 36 | 0.606 | 0.598 | 0.004 |
| 32 | 32 S5 | 6.360 | 6.32 | 38.12 | 2.3713 | 1.169 | 1.549 | RSL | 1.186 | AS4/S | 1.800 | 193 | 36 | 0.607 | 0.591 | 0.008 |
| 32 | 32 S6 | 6.360 | 6.32 | 38.13 | 2.3552 | 1.153 | 1.539 | RSL | 1.186 | AS4/S | 1.800 | 193 | 36 | 0.607 | 0.574 | 0.017 |
| 32 | 32 F1 | 6.390 | 12.70 | ******* | 15.9104 | 7.82 | 1.545 | RSL | 1.186 | AS4/S | 1.800 | 193 | 36 | 0.604 | 0.584 | 0.010 |
| 32 | 32 F2 | 6.400 | 12.69 | | 15.9513 | 7.852 | 1.547 | RSL | 1.186 | AS4/S | 1.800 | 193 | 36 | 0.603 | 0.588 | 0.008 |
| 32 | 32 F3 | 6.400 | 12.70 | | 15.9418 | 7.832 | 1.544 | RSL | 1.186 | AS4/S | 1.800 | 193 | 36 | 0.603 | 0.583 | 0.010 |
| 32 | 32 F4 | 6.390 | 12.71 | | 15.9528 | 7.83 | 1.542 | RSL | 1.186 | AS4/S | 1.800 | 193 | 36 | 0.604 | 0.581 | 0.012 |
| 32 | 32 F5 | 6.410 | 12.71 | | 15.885 | 7.764 | 1.536 | RSL | 1.186 | AS4/S | 1.800 | 193 | 36 | 0.602 | 0.570 | 0.016 |
| 33 | 33A | 6.410 | 38.10 | 44.43 | 16.74 | 8.226 | 1.544 | RSL | 1.186 | AS4/S | 1.800 | 193 | 36 | 0.602 | 0.583 | 0.010 |
| 33 | 33B | 6.410 | 38.09 | 44.45 | 16.564 | 8.079 | 1.533 | RSL | 1.186 | AS4/S | 1.800 | 193 | 36 | 0.602 | 0.566 | 0.019 |
| 33 | 33C | 6.410 | 38.09 | 44.45 | 16.7477 | 8.243 | 1.547 | RSL | 1.186 | AS4/S | 1.800 | 193 | 36 | 0.602 | 0.587 | 0.008 |
| 33 | 33 S1 | 6.430 | 6.35 | 38.20 | 2.4021 | 1.184 | 1.549 | RSL | 1.186 | AS4/S | 1.800 | 193 | 36 | 0.600 | 0.591 | 0.005 |

| | | mm | mm | mm | grams | grams | g/cc | | g/cc | | g/cc | g/m² | | | | |
|---|---|---|---|---|---|---|---|---|---|---|---|---|---|---|---|---|
| **Panel** | **Spec** | **Thick** | **Width** | **Length** | **Wt. in Air** | **Wt. in IPA** | **Density** | **Resin** | **Density** | **Fiber** | **Density** | **Areal Wt** | **n** | **Vf Areal** | **Vf density** | **Vvoid** |
| 33 | 33 S2 | 6.420 | 6.35 | 38.17 | 2.4058 | 1.181 | 1.543 | RSL | 1.186 | AS4/S | 1.800 | 193 | 36 | 0.601 | 0.581 | 0.010 |
| 33 | 33 S3 | 6.420 | 6.35 | 38.18 | 2.407 | 1.18 | 1.541 | RSL | 1.186 | AS4/S | 1.800 | 193 | 36 | 0.601 | 0.578 | 0.012 |
| 33 | 33 S4 | 6.430 | 6.35 | 38.15 | 2.4055 | 1.183 | 1.545 | RSL | 1.186 | AS4/S | 1.800 | 193 | 36 | 0.600 | 0.585 | 0.008 |
| 33 | 33 S5 | 6.410 | 6.35 | 38.18 | 2.4059 | 1.184 | 1.546 | RSL | 1.186 | AS4/S | 1.800 | 193 | 36 | 0.602 | 0.587 | 0.008 |
| 33 | 33 S6 | 6.410 | 6.35 | 38.15 | 2.3986 | 1.179 | 1.545 | RSL | 1.186 | AS4/S | 1.800 | 193 | 36 | 0.602 | 0.584 | 0.009 |
| 33 | 33 F1 | 6.410 | 12.58 | ******* | 15.7833 | 7.76 | 1.545 | RSL | 1.186 | AS4/S | 1.800 | 193 | 36 | 0.602 | 0.585 | 0.009 |
| 33 | 33 F2 | 6.410 | 12.70 | | 15.9392 | 7.906 | 1.558 | RSL | 1.186 | AS4/S | 1.800 | 193 | 36 | 0.602 | 0.606 | -0.002 |
| 33 | 33 F3 | 6.390 | 12.00 | | 15.9026 | 7.813 | 1.544 | RSL | 1.186 | AS4/S | 1.800 | 193 | 36 | 0.604 | 0.583 | 0.011 |
| 33 | 33 F4 | 6.390 | 12.70 | | 15.8833 | 7.803 | 1.544 | RSL | 1.186 | AS4/S | 1.800 | 193 | 36 | 0.604 | 0.583 | 0.011 |
| 33 | 33 F5 | 6.400 | 12.69 | | 15.5676 | 7.504 | 1.516 | RSL | 1.186 | AS4/S | 1.800 | 193 | 36 | 0.603 | 0.538 | 0.034 |

# Vita

Robert John Demaree was born on June 22, 1971 in Lubec, Maine. The son of an engineer, Robert spent time living in Maine, New York, and New Jersey. Robert graduated from Cinnaminson High School in Cinnaminson, New Jersey in June of 1989, and enrolled at Virginia Tech in August of that year. While an undergraduate, Robert spent two years as a member of the Virginia Tech solar car team. He graduated from Virginia Tech in May of 1993 with a B.S. in Mechanical Engineering.

Robert entered graduate school in the fall of 1993. He enrolled in the Department of Materials Science and Engineering, to study processing of composite materials. In the course of his graduate carrer, Robert participated in the development of a polymer properties laboratory course, and taught this class for two years. He was also able to train for and receive his private pilot's license.